PAUL SCHERRER INSTITUT

PSI

u^b

b
UNIVERSITÄT
BERN

LABOR FÜR RADIO- UND UMWELTCHEMIE
DER UNIVERSITÄT BERN UND
DES PAUL SCHERRER INSTITUTS

Annual Report 2012

COVER:

The Near Ambient Pressure
Photoemission (NAPP) end-
station set up at SLS allows
electron spectroscopic
analysis of solid-air, liquid-
air and solid-liquid inter-
faces at sample pressures
up to 20 mbar and will
therefore be an ideal tool
also for environmental
chemistry studies. The NAPP
project is a collaboration
between PSI and ETH Zurich
and supported by the Swiss
National Science Foundation
(R'Equip) and the Center of
Competence in Energy and
Mobility (CCEM). The picture
shows the NAPP endstation
hooked up at the PHOENIX
beamline. The horizontally
mounted electrostatic lens
system is in the center, the
electron analyzer to the left
and the sample chamber to
the right. The X-ray beam
hits the sample from the
backside in the center of
the chamber in front of the
conically shaped entrance
cone into the lens system.

Annual Report 2012

Editors: A. Türler
M. Schwikowski
A. Blattmann

TABLE OF CONTENTS

Analytical Chemistry

Radwaste Analytics

Radionuclide Development

Environmental Radionuclides Universität Bern

EDITORIAL

Our unit continues to thrive and thus I am very pleased to present the next issue of our traditional annual report.

In 2012, all our large scale projects have matured to the point of producing first results.

As the photograph on this years title page shows, the new, near ambient pressure photoelectron spectrometer, a joint initiative of the surface chemistry group of Markus Ammann and the heterogeneous catalysis group of Jeroen van Bokhoven, was successfully commissioned this year (pp 21-23). First experiments off-line and on-line at the SLS were conducted and surpassed expectations. This instrument ideally complements other tools already available to investigate gas phase-surface interactions at conditions relevant for processes occurring on aerosol particles in the atmosphere.

The assembly of the MICADAS at the Laboratory of Ion Beam Physics (LIP) at ETHZ has been completed and the instrument was thoroughly tested, so that first ^{14}C measurements could be conducted (p 53). The MICADAS is scheduled to arrive at Bern University mid February 2013 and the official inauguration of the instrument will take place on May 3 in the framework of a half-day symposium. Meanwhile, the LARA (Laboratory for Radiocarbon Analysis) under the direction of Sönke Szidat has already been founded and all the participating research groups are eagerly waiting to get their samples analyzed in Bern.

The new joint radionuclide development group between LCH and ZRW suffered from a set-back, since the group leader, Konstantin Zhernosekov, left us for a new position in industry. This gave us the chance to slightly reorganise the activities in Bern and at PSI. Therefore, I am very happy to introduce Josue Moreno as new manager of the R&D radiopharmaceutical laboratory in Bern. Josue Moreno is a former employee of the Institute of Radiochemistry in Munich and a radiochemist with more than ten years of experience in the production of radionuclides for radiopharmaceutical applications. Under his guidance, we are confident to produce first diagnostic and therapeutic radiopharmaceuticals for patients of the Insel hospital in 2013. The position of group leader radionuclide development at PSI is currently vacant, but I am very optimistic to present the successor of Konstantin in next years annual report. Nevertheless, our collaboration with the Centre of Radiopharmaceutical

Sciences at PSI has already resulted in first, high ranking publications (p. 52).

All groups of LCH continue to successfully publish their results in renowned journals and special results are highlighted with media releases, such as the reconstruction of atmospheric lead concentrations in Russia since 1680, a contribution of Margit Schwikowski's analytical chemistry group.

LCH also excelled again at the SOLA Stafette. A team of avid runners exclusively staffed with members of LCH finished as 83rd team out of 860 participating teams, an all time record which will be hard to beat.

Also this years social event combined educational aspects with a fun outing. First we visited the company MB Microtec in Niederwangen which produces tritium powered light sources for watch dials, aircraft instruments and other applications. We were greeted with coffee and sweets and immediately felt at home scientifically. Afterwards, muscle power was asked for, when we rented human powered rail-cycles that brought us along an abandoned railroad track to a barbecuing area, where we spent a relaxing afternoon in the late autumn sun.

We concluded the year with a guided tour on foot through nearby Brugg and Windisch, where we followed the archaeological sites that our Roman ancestors had left nearly 2000 years ago. To heat up from the bitter cold we met in the "Rösti Farm" to replenish the missing calories. To be honest actually more than just that, because this was an "all you can eat" offer.

The year 2013 started with very sad news. Our PhD student Alexander Zapf was killed by an avalanche while backcountry skiing. We lost a skilled and enthusiastic young researcher, a great colleague, and a good friend and we painfully miss him.

Andreas Türler

PREDICTION OF THERMAL RELEASE RATES OF SUPERHEAVY ELEMENTS

D. Wittwer, R. Eichler, H.W. Gäggeler (Univ. Bern & PSI)

INTRODUCTION

One promising connection between vacuum chromatography and an accelerator based production setup for superheavy elements is vacuum implantation of recoiling nuclear reaction products and their fast in-situ thermal release. Therefore, it is crucial to have knowledge about the thermal release rates of superheavy elements (SHE) from high-melting metallic matrices. The release rates are expected to vary regarding the nature of interaction of the SHE with the catcher metal matrix. Investigation of radiation damage enhanced diffusion (RDED) velocities of various tracer/host element combinations were performed [1] allowing a preselection of the possible host materials. Additional data were obtained from literature [2,3]. Release rates of SHE can be predicted on an extrapolative basis. Here, the principle and the results of these predictions are shown.

RESULTS

The release rate strongly depends on two kinetic mechanisms: solid state diffusion and desorption from the host surface. Predictions of diffusion properties of SHE were made using a Miedema [4] based principle refined by Bakker [5]. The volume of tracer atoms dissolved in a host metal at infinite dilution is taken as a criterion for the diffusion velocity of the tracer. Desorption times of volatile elements, such as SHE with $Z \geq 112$, from metal surfaces at the high release temperatures are mostly negligible [1]. Therefore, it can be stated that the diffusion of the tracer from the bulk to the surface is the rate determining step of the release process. An example of an extrapolative prediction is shown in Fig.1. D_{Trac} and D_{Host} are the diffusion coefficients of the tracers in the host matrix and the self diffusion coefficient of the host matrix, respectively. V_{Trac} and V_{Host} are the molar volumes of the tracers in a solid host matrix solution at infinite dilution and of the host matrix atoms in the solid state. On the basis of these extrapolated diffusion properties, using volume data of SHE collected in [6], it was possible to predict release rates of SHE. The principle to calculate release rates from diffusion data was established by Crank [7]:

$$F[\%] = 100 - \frac{800}{\pi^2} \sum_{n=0}^{\infty} \frac{1}{(2n+1)^2} \times \exp\left[-\frac{(2n+1)^2 \pi^2 Dt}{d^2}\right],$$

with D being the diffusion coefficient, d the thickness of the host matrix and t the annealing time. From the release values it was determined that Zr appears to be the best performing material in terms of release and operation time at reasonably low annealing temperatures, see Fig. 2. At higher temperatures (>2500 K) W is a valid candidate as well. Re is also predicted to be a suitable high temperature release matrix candidate.
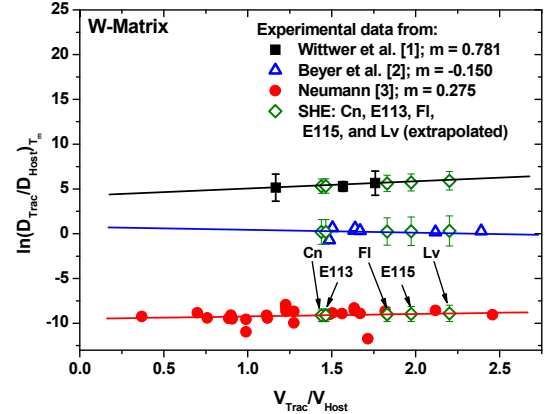
Fig. 1: The volume approach from Bakker [5] as $\ln(D_{Trac}/D_{Self})$ versus V_{Trac}/V_{Host} given for tungsten as host material at its melting temperature ($\theta = 1.00$). The plot includes literature data [1,2,3]. The hollow rectangles with the error bars (1σ) are calculated values for the SHE with $112 \leq Z \leq 116$. m: slope of the linear regressions.
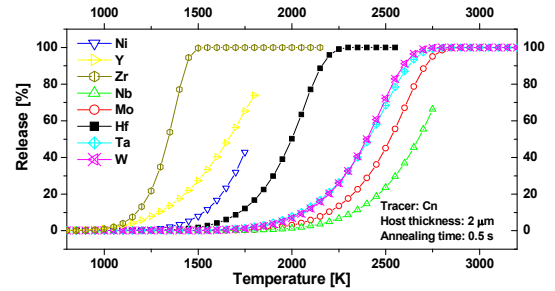
Fig. 2: Calculated release yield of Cn out of 2 μm thick catching material at 0.5 s annealing time versus the annealing temperature.

ACKNOWLEDGEMENT

REFERENCES

[1] D. Wittwer et al., Nucl. Instrum. Meth. Phys. Res. B, in press.

[2] G. Beyer et al., Nucl. Instrum. Meth. Phys. Res. B, **204**, 225 (2003).

[3] G. Neumann et al. in „Self-diffusion and Impurity Diffusion in Pure Metals", Pergamon Materials Series (2008).

[4] A. R. Miedema, J. Less-Common Met., **45** 237 (1976).

[5] H. Bakker, J. Less-Common Met., **105**, 129 (1985).

[6] D. Wittwer et al., Radiochim. Acta, accepted.

[7] J. Crank in "Mathematics of Diffusion". Oxford Univ. Press (1975).

PREPARATION AND IRRADIATION TESTS OF INTERMETALLIC ^{243}Am/Pd HEAVY ION PRODUCTION TARGETS

I. Usoltsev, R. Eichler, A. Türler (Univ. Bern & PSI), D. Piguet (PSI),
G.K. Vostokin, A.V. Sabel'nikov, O.V. Petrushkin, S.N. Dmitriev (FLNR Dubna)

INTRODUCTION

A preparation method for Pd-based intermetallic targets developed here at PSI [1] has been successfully applied to produce two stationary ^{243}Am/Pd targets at the Flerov Laboratory of Nuclear Reactions (FLNR) Dubna, Russia. Test irradiations of these targets have been performed at the FLNR's U-400 cyclotron using high intensity beams (up to 15 μA_{electr}) of ^{48}Ca^{18+}. Both targets were characterized by alpha-particle spectroscopy and by light microscopy before and after the irradiation. For comparison and for test experiments a ^{nat}Nd/Pd intermetallic target and a solely electroplated ^{243}Am/Ti target were prepared, irradiated, and characterized as well.

EXPERIMENTAL

The target material (^{243}Am with traces of ^{nat}Nd) was quantitatively electroplated stepwise from nitrate solution in isopropanol on a previously polished 3 μm Pd foil. The electrochemical cell used for the electrodeposition is depicted in Fig. 1.
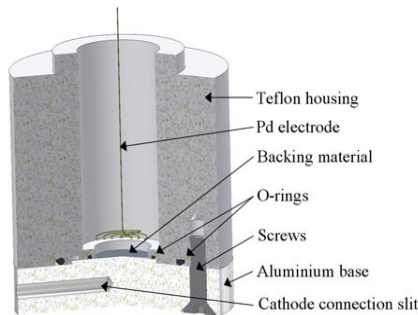
Fig. 1: Electrodeposition cell.

Afterwards, the electroplated target was heated up in a quartz apparatus on an alumina support slab in a flow of pure hydrogen reducing the target material in a so called "coupled reduction" process. Alpha-particle measurements allowed for quantification of the material loss after irradiation. Overall stability of the targets was additionally monitored by means of light microscopy.

RESULTS AND CONCLUSIONS

In Table 1, irradiation parameters are summarized for all ^{243}Am targets. The stability of the targets was evaluated by measuring the target material loss after irradiation by alpha spectrometry. From this measurement all the investigated targets appeared to be rather stable. Although the ^{243}Am/Ti target experienced a three times higher integral beam dose it showed a similar stability. A direct comparison between the targets is still possible due to the fact that the higher beam dose is counterbalanced by a factor

of 1.5 higher maximum beam intensities applied to the intermetallic targets.

Tab. 1: Irradiation parameters and measured stability for the investigated targets.

Target	^{48}Ca^{18+} beam dose	Max. beam current, μA_{electr}	Stability
^{243}Am/Pd 0.85 mg/cm^2	1.1×10^{18}	15	95%
^{243}Am/Pd 1.7 mg/cm^2	6×10^{17}	14	97%
^{243}Am/Ti 1.4 mg/cm^2	3.2×10^{18}	10	95%

Additional information on target stability came from the nuclear reaction product yields. ^{185}Hg produced in the ^{nat}Nd(^{48}Ca,xn) fusion reaction and ^{220}Rn from ^{243}Am(^{48}Ca) transfer reactions were measured in a gas chromatographic setup connected to the target chamber. Intermetallic targets showed constant production rates, whereas the ^{243}AmO$_2$/Ti target showed a considerable decline of production yields starting approximately six days after the begin of the irradiation. Microphotographs of the ^{243}Am/Ti target after irradiation (Fig. 2) indicate that a significant part of the target backing material (Ti) is missing. Hence a considerable part of all the reaction products are implanted into the walls of the target chamber – an effect that jeopardises moth-long transactinide experiments [2]. The described method of target preparation will be applied to ^{242}Pu and ^{244}Pu isotopes in future chemical investigations of element 114 (Fl) in spring 2013 at FLNR in Dubna.
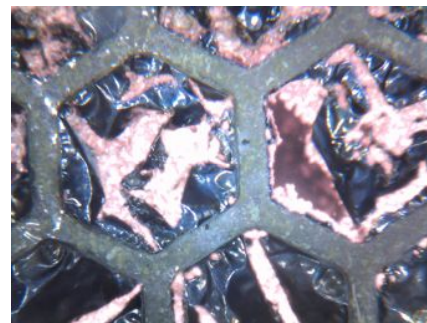
Fig. 2: Optical microscopy image of the ^{243}Am/Ti target after irradiation.

ACKNOWLEDGEMENT

REFERENCES

[1] I. Usoltsev et al., Nucl. Instrum. Meth. Phys. Res. A, **691**, 5 (2012).
[2] I. Usoltsev et al., Nucl. Instrum. Meth. Phys. Res. A, (in preparation).

ATTEMPTS TO PRODUCE Rh-BASED INTERMETALLIC TARGETS FOR HEAVY ION IRRADIATIONS

I. Usoltsev, R. Eichler, A. Türler (Univ. Bern & PSI), D. Piguet (PSI)

INTRODUCTION

Up to now, the electrodeposition method proved to be the only adequate approach towards an effective preparation of actinide targets [1]. Quantitative deposition yields of often very expensive isotopes and sufficient homogeneity of the obtained target material layer thickness are crucial advantages of the molecular plating procedure. Intrinsic disadvantage of the method, however, is that the obtained layer of the target material is deposited in the form of an oxide. Besides poor electrical and thermal conductivity, the oxide layer proved to be an aggressive agent towards the widely used titanium backings. Therefore, we suggested intermatallic actinide targets based on high melting, noble metal backings [2]. The high atomic number of platinum prevents its use as a backing material due to the unacceptably high attenuation of the incident beam and the production of undesired fusion products. The stability of Pd based intermetallic targets is still limited due to the relatively low melting point [3]. The best alternative to Pd could be its neighbour in the periodic table – Rh, which is also known to form stable intermetallic alloys with actinide metals [4]. Lower atomic number, outstanding chemical stability and higher melting point make Rh superior to Pd, and therefore an attractive candidate as backing material for high intensity production targets. However, the high inertness of Rh is a serious obstacle when it comes to the reduction of the actinide oxide material in hydrogen atmosphere. Sometimes temperatures of up to 1550°C are required to complete the reduction in two- to three days [4].

EXPERIMENTAL

Several thin layers of an actinide/lanthanide target material were stepwise electroplated from nitrate solutions in isopropanol on previously polished 2 or 12 μm Rh foils. Afterwards, the electroplated target was heated up in a quartz apparatus in a flow of pure hydrogen either on an alumina support slab in a standard resistance oven or on a Ta susceptor 'brick' by means of RF induction source (NovaStar® 3LW, Ameritherm Inc.). Alpha-particle measurements allowed the characterisation of the target material distribution in the Rh backing after the reduction step.

RESULTS AND CONCLUSIONS

Due to the simplicity and quickness of operation, first experiments were conducted with the induction heating source. A 0.73 mg/cm^2 Eu target with ^{241}Am tracer on 2.2 μm Rh backing was reduced within 15 h at ~1300°C. The final distribution of the target material after the reduction was deduced from the corresponding alpha-particle spectra, taken from both sides of the target (Fig. 1). The segregation enthalpy of Am in Rh matrix was calculated as -60 kJ/mole using Miedema's model. This explains the observed segregation of ^{241}Am towards the surface of the Rh backing foil. Unclear, however, remains the ratio of Am activity between the front side (where the electrodeposition took place) and the back side, with a two times higher alpha-particle count rate on the back side.
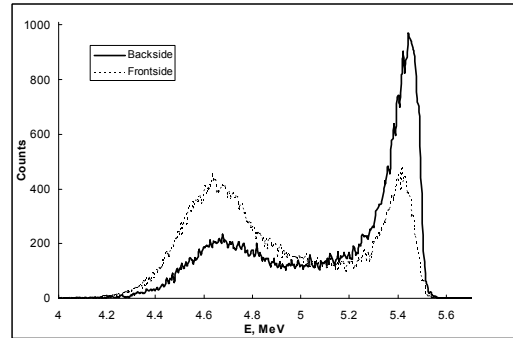
Fig. 1: Alpha-particle spectrum of ^{241}Am/Rh target.

Furthermore, in contrast to Pd [2], the quartz apparatus used at temperatures higher than 1000°C appeared to have a deteriorating effect on the integrity of the Rh foils. So-called hydrogen induced embrittlement (HIE) of the Rh backing is caused in this case by volatile Si-containing compounds, formed at high temperatures in hydrogen atmosphere. Therefore, we conclude that by avoiding silicon containing materials or/and by keeping them colder than 1000°C the desired reduction with Rh foil becomes feasible. Different approaches have been tried to preclude HIE with no success: shielding of the sample with Pd and Pt membranes, and pre- and post-annealing in vacuum and He. Finally, a boron nitride slab was chosen as support material for the target and the quartz apparatus was replaced with a nickel one. This combination of materials allows using temperatures up to 1300°C. Despite being effective against HIE, the described approach failed due to the interdiffusion process between BN and the Rh foil, which takes place even at temperatures lower than 1300°C. Therefore, further investigations are needed to optimize the reduction process.

ACKNOWLEDGEMENT

REFERENCES

[1] W. Parker et al., Nucl. Instrum. Methods **26**, 61 (1964).

[2] I. Usoltsev et al., Nucl. Instrum. Meth. Phys. Res. A, **691**, 5 (2012).

[3] I. Usoltsev et al., Nucl. Instrum. Meth. Phys. Res. A, (in preparation).

[4] B. Erdmann, Kernforschungszentrum Karlsruhe, Bericht (1971) KFK 1444.

PRELIMINARY STUDIES WITH A DIAMOND DETECTOR FOR ISOTHERMAL VACUUM CHROMATOGRAPHY EXPERIMENTS

P. Steinegger, R. Eichler, A. Türler (Univ. Bern & PSI), R. Dressler (PSI)

INTRODUCTION

Standard silicon PIN-diodes or PIPS-detectors are broadly used for α-spectroscopic measurements. The small band gap of Si, which is only 1.1 eV prevents their operation under the influence of incident IR, visible and UV light or at ambient temperatures above 40°C. Therefore, their use for high temperature gas chromatographic investigations or their operation in the vicinity of heat sources is limited. Alternatives are needed to perform experiments at elevated temperatures. Diamond, as a large band gap material (5.5 eV), is regarded as a quasi-semiconductor [1]. Single-crystal chemical vapour deposition (CVD) diamonds are commercially available. Due to their electronic characteristics, diamonds allow spectroscopic measurements under broad daylight conditions and elevated temperatures of theoretically up to 1000°C. High purity single crystals e.g. ultra nitrogen-pure grade (< 50 ppb [2]) are required for achieving a reasonable α-spectroscopic resolution. Especially, vacuum chromatography setups would profit from this detector development.

HEATING STUDIES

Fig. 1 shows a possible coupling of a diamond detector to a high temperature isothermal vacuum chromatography. It is of utmost importance to place the detector as close to the column exit as possible in order to reach a high deposition efficiency. In this rather harsh environment, the detector gets heated up by IR radiation emitted from the end of the isothermal oven.
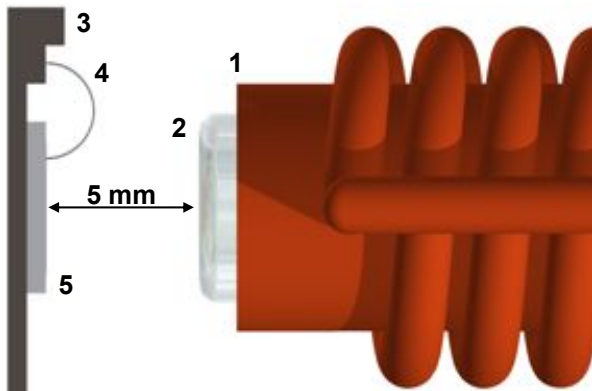
Fig. 1: Test setup for isothermal vacuum chromatography with carrier-free ^{211}Pb; **1** isothermal oven, **2** quartz column exit, **3** ceramic carrier, **4** wire bonds, **5** CVD diamond detector.

Test runs without a thermal shield showed that the temperatures exceeded 300°C at the detector position, requiring all included parts to be resistant to these high temperatures. Former investigations [3] showed that even direct heating of the detector up to 200°C had no severe effects on the quality of the spectroscopy. In order to simulate a more realistic situa-

tion in a vacuum chromatography experiment, we tested the spectroscopic behaviour of a diamond detector in vacuum close to a resistively heated Ta wire (T_{wire} > 1000°C) and compared the recorded spectrum under these conditions to the reference spectrum measured at room temperature (see Fig. 2).
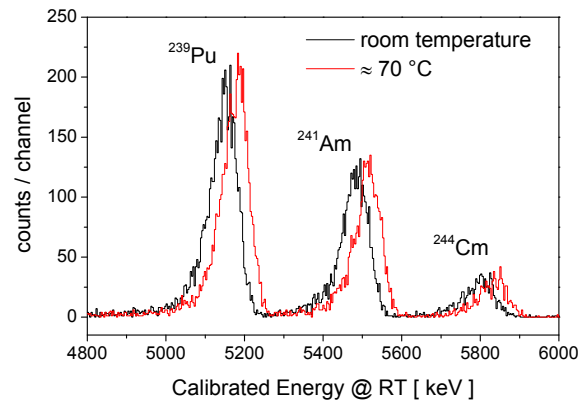
Fig. 2: α-spectra of a three-line source at room temperature and with a resistively heated Ta wire in 10 cm distance (T_{wire} > 1000°C, T_{det} ≈ 70°C); the energy resolution remained at ≈ 80 keV (FWHM).

The shift of the α-peaks towards higher energies in case of the measurement recorded under thermal irradiation was tentatively attributed to a temperature dependent kinetic effect in the charge collection process. To further investigate this effect, these measurements will be repeated including a ^{148}Gd source with a 3.4 MeV α-line at different temperatures.

CONCLUSION AND OUTLOOK

This study showed that the immediate vicinity of a heat source does not affect the spectroscopic behaviour of a diamond detector, which is consistent with earlier observations [3]. We achieved a satisfying energy resolution of 80 keV in a rather harsh environment. In a next step, we will proceed with isothermal vacuum chromatography experiments of carrier-free ^{211}Pb. Furthermore, a diamond detector assembly has to be designed that provides higher detection efficiencies for future studies with super heavy elements.

ACKNOWLEDGEMENT

REFERENCES

[1] Pomorski et al., Phys. Stat. Sol. **203**, 12 (2006).
[2] http://www.e6cvd.com
[3] Steinegger et al., Ann. Rep. Lab. of Radio- & Environ. Chem., Univ. Bern & PSI p. 6 (2011).

DECOMPOSITION STUDIES OF TRANSITION METAL CARBONYLS AT A Cf-252 SPONTANEOUS FISSION SOURCE

I. Usoltsev, R. Eichler, A. Türler (Univ. Bern & PSI)

INTRODUCTION

Metal carbonyls are compounds consisting of a transition metal atom coordinated by several CO molecules. It was shown recently at the TRIGA reactor of Mainz University, Germany, that carbonyls can be rather easily produced under ambient conditions simply by flushing a CO/N_2 mixture (4:1) through the recoil chamber of a Cf-249 fission source at a flow rate of 500 ml/min [1]. This allowed the measurment of adsorption enthalpies (ΔH_{ads}) of the corresponding carbonyl species of Mo, Tc, Ru, and Rh on quartz surface in gas adsorption chromatographic investigations. Further experiments at the TASCA separator at GSI Darmstadt, Germany, observed efficient carbonyl formation also for W and Os. Within the limits of uncertainty the carbonyls $Mo(CO)_6$, $W(CO)_6$, and $Os(CO)_5$ were found to have the same ΔH_{ads} on quartz. In investigations of relativistic effects, it would be desirable to design a chemical experiment that can discriminate homologues in a group of the periodic table. Therefore, we propose another approach involving the investigation of the thermal stability of transition metal carbonyls.

EXPERIMENTAL

In Fig. 1 a scheme of the experimental setup used for production and decomposition of carbonyls is shown. A CO/He (1:1) mixture was flushed through the recoil chamber of the "Ms. Piggy" ^{252}Cf SF source at Bern University at a flow rate of 1.5 l/min. The formed transition metal carbonyls are transported afterwards trough the decomposition column and finally reach a charcoal trap. The decomposition column (1 m) with exchangeable inner surface was heated up by means of a self-made resistance oven and its temperature was controlled with a K-type thermocouple. By performing a gamma spectrometric measurement of the charcoal trap decomposition curves were obtained (See Fig. 2).
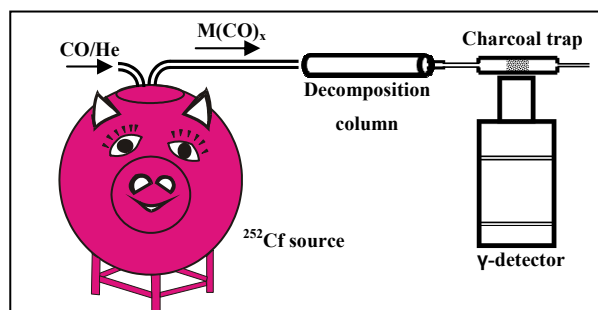
Fig. 1: Experimental setup for carbonyl decomposition studies.

RESULTS AND CONCLUSIONS

Four transition metal isotopes forming carbonyls were particularly interesting ^{104}Mo, ^{108}Tc, ^{109}Ru, and ^{111}Rh. Having only short-lived precursors, the detected γ-lines relate only to the behaviour of the corresponding carbonyls. The decomposition of metal carbonyls on hydroxylated surfaces (SiO_2, Al_2O_3) is accompanied by side reactions e.g. formation of different oxides. Inert (Teflon® PFA) or metal (Au, Ag, Pd) surfaces minimize possible side reactions. A steel surface was found to be reactive towards metal carbonyls. Therefore, all steel parts in the setup were replaced with polymeric materials and a PFA Teflon® column held at room temperature was used as a 100% reference for all the performed measurements. As follows from Fig. 2, a PFA Teflon® column cannot be used for decomposition studies, since 100% of the carbonyls stay intact up to 300°C - the m.p. of the material. On a gold surface, already 40% of ^{104}Mo carbonyl is decomposed at ambient conditions; the other carbonyls are decomposed completely. Complete decomposition of ^{108}Tc, ^{109}Ru, and ^{111}Rh carbonyls at room temperature was observed as well on Ag and Pd surfaces. Tc and Rh carbonyls ($M(CO)_5$) have an unpaired electron and for that reason might be much more reactive than Mo. Monomeric carbonyls are also not characteristic for Ru normally forming carbonyl clusters. Mo forms obviously the most stable $Mo(CO)_6$ carbonyl decomposing only at elevated temperatures. The apparent differences between the examined surfaces can be further explained by surface coverage with CO (carrier gas). The adsorption of CO on both PFA Teflon® and Ag surfaces is weak with $-\Delta H_{ads}\sim 20$ kJ/mol. Thus Ag appears as an extension of the PFA Teflon® curve. Pd and Au surfaces are partially covered with CO at 25°C and are thus interfering with the decomposition by superimposed adsorption and desorption of CO. We conclude that silver is the most appropriate surface for future decomposition studies of group 6 element carbonyls including $Sg(CO)_6$.
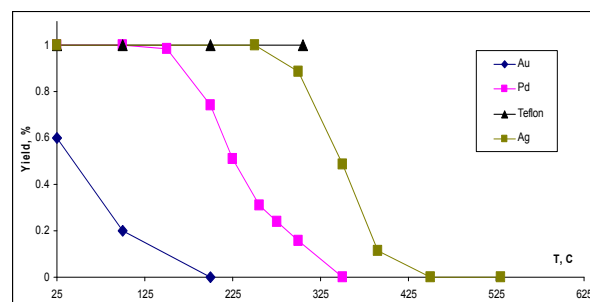
Fig. 2: Decomposition curves for ^{104}Mo carbonyl on different surfaces.

REFERENCE

[1] J. Even et al., Inorg. Chem. **51**, 6431 (2012).

GAS PHASE CHEMISTRY OF W AND Os CARBONYL COMPLEXES FORMED AT A HEAVY ION ACCELERATOR WITHOUT PRESEPARATION

Y. Wang, Z. Qin, F.-L. Fan, F.-Y. Fan, S.-W. Cao, X.-L. Wu, X. Zhang, J. Bai, X.-J. Yin, L.-L. Tian, L. Zhao, W. Tian, Z. Li, C.-M. Tan, J.-S. Guo (IMP), H.W. Gäggeler (PSI)

INTRODUCTION

Formation of carbonyls in hot atom reactions has recently been pioneered as a powerful tool for future study of some transactinide elements [1]. It was postulated that synthesis of carbonyls at heavy ion accelerators is only possible behind a preseparator. In this study we have investigated carbonyl formation at a heavy ion accelerator without any preseparator, hence, by adding carbon monoxide directly to a carrier gas in which the products were stopped (gas-jet technique).

EXPERIMENTAL

Fig. 1 depicts the set-up used at the IMP sector field cyclotron for our study. Tb or Ho targets of about 0.7 mg/cm^2 thickness on a 19 µm Be foil were bombarded by a cot 101 MeV ^{19}F^{7+} beam with about 450 nA (corresponding to 64 pnA) intensity. At the exit of the chamber the volatile products were transported with the carrier gas through a 5 m long Teflon capillary to an isothermal chromatography device. In this device 2 m long and 2 mm dia. Teflon columns could be kept at temperatures between 0°C and -80°C. Behind the column the products were transported along a 1 m long Teflon capillary to an activated charcoal trap positioned in front of a HPGe detector to assay γ-decaying nuclides.
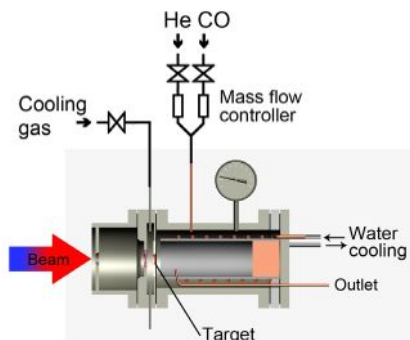
Fig. 1: Set-up used for the synthesis and transport of carbonyls at the IMP cyclotron.

RESULTS

Fig. 2 shows the yield of ^{173}W as a function of beam intensity. Clearly, a saturation is observed at an intensity of about 1 µA (equivalent to 143 pnA). It was then decided to run the experiments with about 450 nA.
Fig. 3 shows the yield curve for ^{173}W as a function of temperature along the Teflon chromatography column. Fig. 4 shows a similar chromatogram for ^{174}Os using a ^{nat}Ho target. The resulting adsorption enthalpies deduced from the measured breakthrough curves resulted in -47±2 kJ/mol and -43±2 kJ/mol, for W(CO)$_6$ and Os(CO)$_4$, respectively.
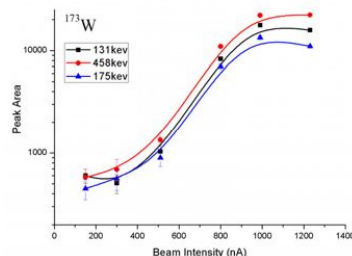
Fig. 2: Yield of ^{173}W, formed in the ^{19}F + ^{nat}Tb reaction as a function of beam intensity.
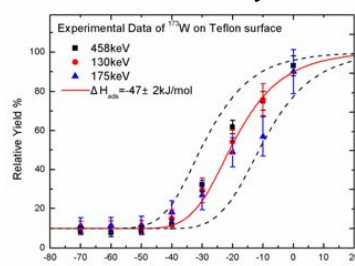
Fig. 3: Yield curve for ^{173}W in an isothermal Teflon column.
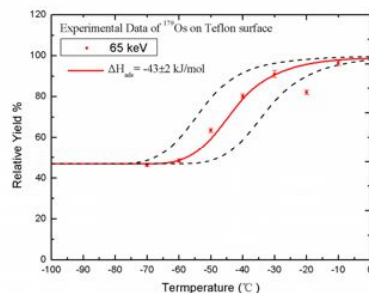
Fig. 4: Yield curve for ^{174}Os in an isothermal Teflon column

It is important to note, that the yield curves do not drop to 0% at low temperatures but to about 10% and 50%, respectively. We interpret this observation by aerosol transport of ^{173}W and ^{174}Os by carbon clusters formed via interaction of the beam with CO in the collection chamber or according to the Boudouard equilibrium. The higher break through in the case of the ^{174}Os curve may be caused by an increased contamination of the recoil chamber with black carbon in the later experiment with Os. To conclude, though model studies with carbonyls seem possible with the gas jet technique, the clear drawback is the aerosol formation and the beam limitation that prevents application of this approach for studying transctinide carbonyls.

REFERENCE

[1] J. Even et al., Inorg. Chem. **51**, 6431 (2012).

STABILITY OF CHEMICAL COMPOUNDS OF THE SUPERHEAVY ELEMENTS Cn AND Fl

N.M. Chiera, R. Eichler, A. Türler (Univ. Bern & PSI)

Since the 1960's several successful experiments demonstrated that transactinide elements behave chemically similar to their lighter homologues in the corresponding group of the periodic table [1]. However, with increasing nuclear charges, the influence of relativistic effects on the electron structure causes deviations from the periodicity of chemical properties [1]. Gas adsorption experiments of ^{283}Cn on a noble metal surface such as gold, revealed its noble metallic behaviour, similar to the nearest lighter homologue Hg, but, due to relativistic effects and spin-orbit coupling, Cn revealed also high volatility almost like a noble gas, and a higher chemical inertness than mercury [2]. For Flerovium, modern relativistic calculation methods predict higher chemical inertness compared to Pb, the lighter homologue, but still pronounced metallic properties [3]. Since these superheavy elements are characterized by short half-lives and low production rates, their chemical behavior has to be explored on a single atomic scale. For this purpose gas chromatography is used, allowing for efficient studies of the interaction of volatile gas-phase species with stationary surfaces [1,2,4]. In preparation and design of such experiments extrapolative predictions of the expected transactinide behavior in various simple chemical systems are possible by correlating thermochemical state functions mutually [1]. Figures 1-3 show correlations of the standard formation enthalpies, $\Delta_f H_g^{298}(M)$, of the monoatomic gaseous elements with the standard formation enthalpies of their oxides, hydrides and sulfides in gaseous or solid states, $\Delta_f H_{g,s}^{298}(MO/ MH_x/ MS)$ [5,6].
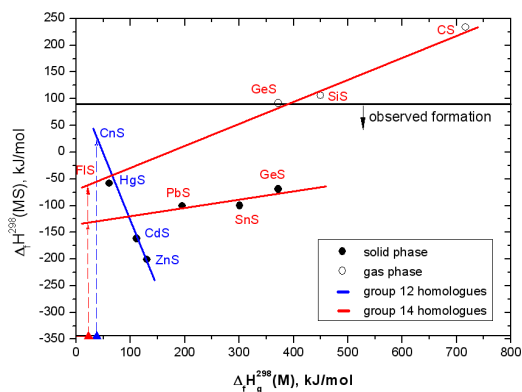
Fig. 1: Stability trends for group 12 and 14 sulfides.

In contrast to oxide and hydride formation the decreasing enthalpy of sulfide formation along the homologues of group 14 permit us to predict that element 114, Fl, may form stable sulfides. For Cn the formation enthalpies of sulfides, hydrides, and oxides are higher than those of the homologues. However, even if the formation of $\Delta_f H_s^{298}(CnS)$ is endothermic, its stability is higher than $\Delta_f H_g^{298}(GeS)$, which has been observed experimentally [7].
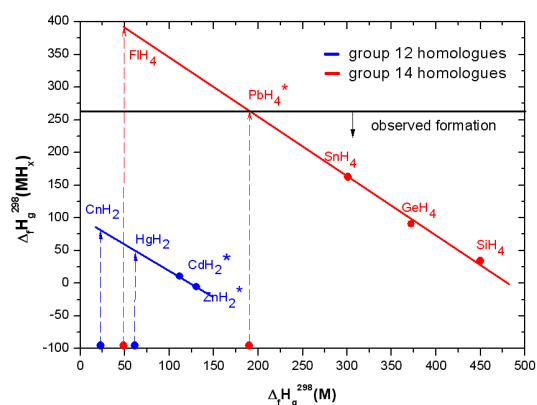
Fig. 2: Stability trends for group 12 and 14 hydrides.
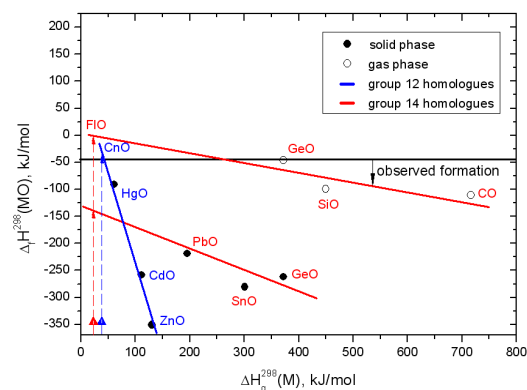
Fig. 3: Stability trends for group 12 and 14 oxides.

The affinity of mercury towards sulfur is well known, and the formation of $HgS_{(s)}$ is thermodynamically favored [8]. Therefore, first model experiments are envisaged concerning the investigation of the kinetics and thermodynamics of the adsorption and reactive interaction of elemental Hg with sulfur surfaces. This model will prepare further chemical investigations of the superheavy elements Cn and Fl.

REFERENCES

[1] M. Schädel ed. "The Chemistry of Superheavy Elements". Dordrecht, Kluwer Academic Publishers (2003).

[2] R. Eichler et al., Nature **447**, 72 (2007).

[3] V. Pershina, et al., J. Chem. Phys. **127**, 134310 (2007).

[4] R. Eichler et al., Radiochim. Acta **98**, 133 (2010).

[5] http://www.hbcpnetbase.com/

[6] I. Barin "Thermochemical data of pure substances" Weinheim, New York (1995).

[7] P. Hassanzadeh, J. Phys. Chem. **96**, 6181 (1992).

[8] M. Svensonn, Sci. Tot. Env. **368**, 418 (2006).

BROADENING THE DYNAMIC RANGE IN PGAA

S. Söllradl, A. Türler (Univ. Bern & PSI),
L. Canella, P. Kudejova, Z. Revay (Forschungsneutronenquelle Heinz Maier-Leibnitz), H. Lührs (Univ. Bremen)

INTRODUCTION

Prompt Gamma Activation Analysis (PGAA) is a nuclear analytical technique, which allows the non-destructive, simultaneous measurement of most chemical elements. PGAA is insensitive to the form and the shape of samples. It is highly sensitive for elements with high cross sections like boron. However, if boron is present in the sample on the percent level, the high count rate and the self-shielding become significant. Our sample contained approximately 8% boron (σ = 763 barn [1] emitting a single γ–ray with an energy of 478 keV) in a matrix of oxides of aluminium (σ = 0.231 barn [1]) and silicon (σ = 0.172 barn [1]). The strongest γ peaks of Si are emitted at 3.5 MeV and 4.9 MeV, while Al has its strongest peaks above the γ energies of 1.7 MeV.

The count rate of a γ peak in a spectrum is determined by its partial γ–ray production cross-section σ_γ, the neutron flux, the efficiency of the detection system and the mass of the element in the activated sample. In our case, boron gives the dominating part of the recorded spectrum, leading to a count rate almost saturating the detector. To lower the counting efficiency in the low-energy part of the spectrum, lead sheets were introduced in front of the detector.

METHODOLOGY

The sample is a mixture of Al_2O_3 (59.62%$_{mol}$), SiO_2 (32.69%$_{mol}$), and H_3BO_3 (7.69%$_{mol}$). It was milled for one week resulting in a fine, homogeneous, white powder. It was irradiated in the cold neutron beam at the PGAA facility at FRM II in Garching with a flux of 4×10^9 cm^{-2} s^{-1}. To modify the low-energy efficiency of the detection system, the experiment was performed with 0 mm (no attenuator), 5 mm, and 10 mm of Pb in front of the HPGe-detector to selectively attenuate the low-energy γ–rays (Fig. 1). The PGAA spectra, which were acquired using different-thicknesses of attenuators, are shown in Fig. 2.
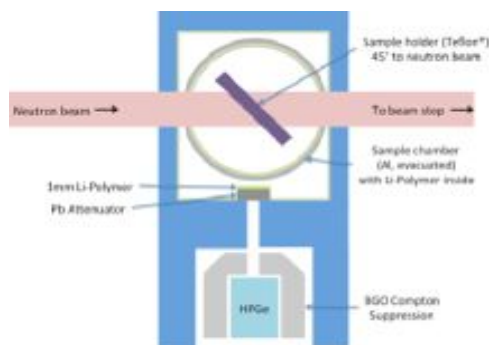
Fig. 1: Schematic view of the used PGAA setup

RESULTS
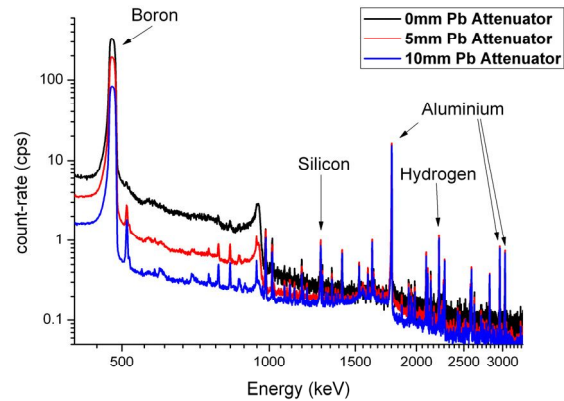
Fig. 2: Low-energy part of the measured PGAA spectra

The count rates were significantly reduced for the energy range around the boron peak, whereas the γ peaks with energies above 1.5 MeV were less attenuated. The ratios of the count rates for the 478 keV boron peak and of the 3033-keV aluminium peak were found as follows:

- Without attenuator: 1346 ± 3.2%

- Using 5 mm Pb: 680 ± 1.3 %

- Using 10 mm Pb: 343 ± 1.1 %

Comparing peaks at different energies with attenuation to those without it, a function could be derived, which agreed well with the attenuation curve.

CONCLUSION

The experiment has proven that modification of the counting efficiency using lead attenuators broadens the dynamic range of PGAA measurements.

REFERENCES

[1] L. Molnár ed. "Handbook of Prompt Gamma Activation Analysis", Dordrecht, Kluwer Academic Publishers (2004).

ADSORPTION OF HNO$_3$ ON ICE

S. Schreiber (ETHZ & PSI), M. Ammann (PSI)

INTRODUCTION

Nitric acid (HNO$_3$) is an important reservoir species for reactive nitrogen oxides in the upper troposphere and is the carrier of removal of nitrogen oxides via wet deposition. Yet, global atmospheric chemistry models tend to overestimate the HNO$_3$ abundance, which implies a missing sink. Aircraft based field measurements have shown that a significant fraction of HNO$_3$ partitions to cirrus cloud ice particles [1], yet the nature of the ice uptake and its influence on upper tropospheric NO$_x$ and ozone is not well understood.

EXPERIMENTAL

We used a Knudsen cell flow reactor in combination with the short lived radioactive tracer ^{13}N (decay constant λ=0.0011s^{-1}) [2]. The tracers are produced at the PROTRAC facility at PSI [3] and transported to the lab in the form of NO. HNO$_3$ is synthesized online in the lab. The molecules are fed into a reaction chamber that is kept at free molecular flow conditions, where they can either interact with the ice sample, or leave the reactor through a calibrated orifice. These molecules are collected in a chemical trap afterwards. We have two pairs of scintillation detectors in coincident counting geometry that detect the decays of HNO$_3$ in the reaction chamber (and thus on the ice) and in the trap. These count rates are denoted as R$_{KC}$ and R$_{trap}$. After allowing the tracer molecules into the reactor for a distinct time, we can calculate the net probability that a ^{13}N labelled HNO$_3$ molecule is lost to the ice surface upon collision, γ_{13N}, from the ratio of R$_{KC}$ and R$_{trap}$.

RESULTS

After correction for wall uptake, we have found γ_{13N} = 0.03 for HNO$_3$ at 205 K. This value needs careful interpretation, because the radioactive decay is an additional loss process in the experiment that prevents a direct extrapolation of γ_{13N} to the real atmosphere.

Assuming Langmuir adsorption [4] and low surface coverage, the steady state uptake of labelled molecules is a function of the surface accommodation coefficient α_s and the desorption rate constant k_d:

$$\gamma_{13N} = \frac{\lambda \alpha_s}{\lambda + k_d} \qquad (1)$$

Though our experiment is sensitive in determining the tracer uptake γ_{13N}, no distinct values for the kinetic parameters can be obtained from Eq. (1) alone. This problem can be addressed by considering the response of the detector signal R$_{KC}$ to changes in the tracer flow. This response is approximately exponential exp(-λ_{eff}t) with

$$\lambda_{eff} = \lambda + \frac{k_d A}{\alpha_s A + A_{esc}}. \qquad (2)$$

Here, A and A_{esc} are the geometric areas of the ice sample and the escape orifice. Combining the information about γ_{13N} and λ_{eff} now allows retrieving the kinetic parameters and also the surface partitioning coefficient $K_{lin,C} = \alpha_s \omega / 4 k_d$, where ω is the mean thermal velocity. This is demonstrated in Fig 1.
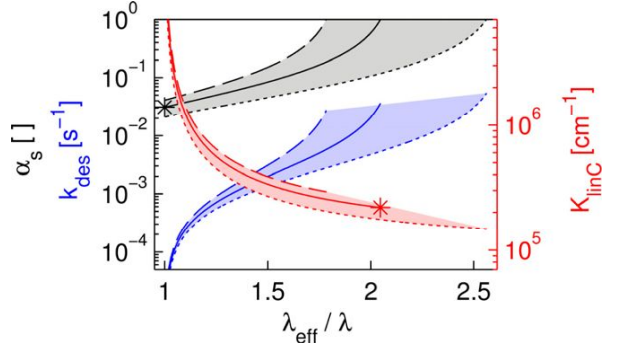
Fig. 1: Interpretation of γ_{13N}. For the measured value γ_{13N} =0.03, the accessible parameter space is shown. For example, if the effective response was λ_{eff} =1.5 λ, α_s =0.08, k_d=2×10^{-3} s^{-1} and, calculated from these, $K_{lin,C}$=3×10^5 cm^{-1}. The shaded areas represent the uncertainty in γ_{13N}.

In our HNO$_3$ experiments, we see that R$_{KC}$ decreases with λ_{eff} even slightly more slowly than λ after the tracer flow to the reactor was stopped. This slow response could be caused by delayed HNO$_3$ transport into the reactor (after switching off) and desorption from the walls. We therefore cannot specify a value for λ_{eff}. Despite that, we can specify a lower limit for α_s=0.03, an upper limit for k_d=4×10^{-2} s^{-1} and a lower limit for $K_{lin,C}$=2×10^5 cm^{-1}. With changes in reactor geometry (A and A_{esc}) and less wall uptake, one would become more sensitive to λ_{eff}.

ACKNOWLEDGEMENT

REFERENCES

[1] C. Voigt et al., Geophys. Res. Lett., **33**, L05803 (2006).
[2] S. Schreiber et al., in preparation for Rev. Sci. Instr. (2013).
[3] M. Ammann, Radiochim. Acta, **89**, 831 (2001).
[4] R.A. Cox et al., Phys. Chem. Chem. Phys., **7**, 3434 (2005).

DOES H$_2$O$_2$ DIFFUSE INTO ICE?

T. Ulrich (PSI & Univ. Bern), M. Ammann (PSI), S. Leutwyler (Univ. Bern), T. Bartels-Rausch (PSI)

INTRODUCTION

The exchange of atmospheric trace gases with the cryosphere can significantly alter the concentration of contaminants both in snow or ice and in the air [1]. H$_2$O$_2$ is of particular concern as it is a powerful oxidant both in the atmosphere and in surface snow or ice [2]. Here we discuss results from laboratory-based experiments about the exchange of gas-phase H$_2$O$_2$ with ice.

RESULT: DIFFUSIVE LOSS

The experiments were done in ice-coated wall flow tubes (CWFT). Upon exposure to the ice surface at 258 K, the H$_2$O$_2$ gas-phase concentration drops, as the ice takes up the molecules (Fig. 1). Then, it starts to recover as the uptake equilibrium is approached. Notable is that the gas-phase concentration of H$_2$O$_2$ does not return to its initial level within 1h. Other trace gases, such as HNO$_4$, have shown a complete recovery in similar experiments [3].
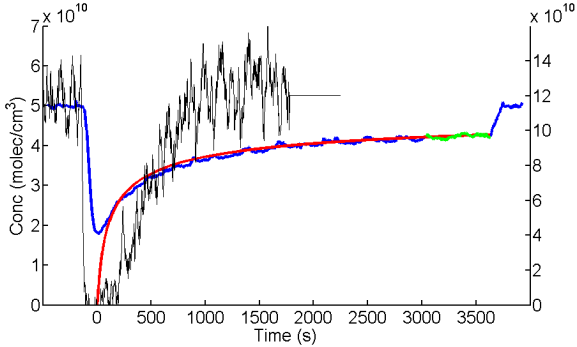
Fig. 1: Gas phase concentration of H$_2$O$_2$ (blue line, left axis) and HNO$_4$ (black line, right axis) with time. Between $t = 0$ s and 3560 s the H$_2$O$_2$ is passed over the ice. Also shown is an asymptotic fit (red line) to the later part of the uptake data (green line) for H$_2$O$_2$.

$$\left[H_2O_2\right](t) = \left[H_2O_2\right]_{initial} \cdot \exp\left(A_{exp} \cdot H \sqrt{\frac{D}{\pi \cdot t}} \right) \quad \text{(Eq 1)}$$

Fig. 1 shows a fit to the data at long interaction times based on Eq. 1 that parameterizes the uptake as diffusion in the ice with time (t) and experimental parameters (A_{exp}). The excellent fit to the data indicates that slow diffusion might limit the uptake of H$_2$O$_2$ to ice in this experiment. This fit also gives a value of 0.92 cm s$^{1/2}$ for the term $H \cdot D^{1/2}$ that combines solubility (H) with diffusivity (D).

DISCUSSION: RESERVOIR IN THE ICE

This diffusive uptake can occur into two reservoirs: into the ice crystal and into the grain boundaries (GBs) [2]. Here, we will discuss the feasibility of both.

Diffusion of impurities into the ice crystal is slow and diffusivities are typically ~10^{-11} cm^2 s [2]. With this diffusivity and the experimentally derived $H \cdot D^{1/2}$, a solubility of H$_2$O$_2$ in the ice crystal, similar to other trace gases, is derived (Table 1). This would indicate that diffusion of H$_2$O$_2$ into the ice crystal explains our observations. However, this

rough calculation and the fit in Fig. 1 do not take the volume of the ice into account. Further calculations that consider volume-limited capacity show that the amount that diffuses into the ice is much smaller than the observed loss. Thus diffusion into the ice crystals is not the dominating process.

Diffusion into GBs is more uncertain, as neither solubility nor diffusivity is well known. Based on values for the diffusivity of water in GBs [4] and a GB fraction of 0.4 vol-‰, reasonable solubilities are derived (Tab. 1). However, for GBs the diffusion is too fast, so they would be saturated too early to explain the observed long-lasting uptake. This rough estimate thus rules out diffusion into GBs as dominating process. Clearly, the volume of grain boundaries needs to be precisely known to derive sound conclusions.

In summary, diffusion into the ice crystal does not explain our observations. Diffusion into GBs needs further investigation.

Tab. 1: Solubilities (H) and diffusivities (D) in ice crystals (sc), GBs and water (liq). Results from this study (*) and literature values [#] are compared.

		D (cm^2/s)		H (M/M)	
H$_2$O$_2$	sc	2.30·10^{-11}	[5]	1.84·10^5	*
H$_2$O$_2$	GB	2.00·10^{-9}	[4]	9.95·10^5	*
HCl	sc	-		8.31·10^5	[5]
H$_2$O$_2$	liq	-		1.75·10^7	[6]

REFERENCES

[1] T. Bartels-Rausch et al., Rev. Mod. Phys., **84**, 885 (2012).
[2] T. Bartels-Rausch et al., Atmos. Chem. Phys., under review (2012).
[3] Th. Ulrich et al., Atmos. Chem. Phys., **12**, 1833 (2012).
[4] H. Lu et al., J. Chem. Phys., **130**, 054501 (2009).
[5] E. Thibert et al., J. Phys. Chem. B, **101**, 3554 (1997).
[6] H. Hwang et al., Environ. Sci. Technol., **19**, 255 (1985).

A DRILLED FLOW-TUBE TO STUDY THE ROLE OF GRAIN BOUNDARIES ON THE AIR-ICE EXCHANGE OF TRACE GASES

E.S. Thomson, J.B.C. Pettersson (Univ. Gothenburg), F. Riche, M. Schneebeli (SLF),
M. Ammann, T. Bartels-Rausch (PSI)

GRAIN BOUNDARIES IN SNOW

In winter, snow covers substantial parts of the land surface. This cryosphere is a highly dynamic medium that impacts fluxes of chemicals between the atmosphere and the subnival ecosystem [1].

A current question in cryospheric and atmospheric science is the role that grain boundaries, and snow/ice microstructure in general, play as reservoirs for impurities during transport through the snow and for chemical reactions on timescales that matter for exchange processes [2].

Here we present results from an on-going collaboration between PSI, SLF, and the University of Gothenburg that resulted in a new approach to study the impact of grain boundaries on chemistry and transport processes.

A UNIQUE FLOW TUBE

Two approaches are widely used to derive kinetic and thermodynamic information of trace gas - ice interactions in controlled laboratory studies. Coated wall flow tubes offer the advantage that trace gases are exclusively exposed to ice surfaces and thus the results are not disturbed by interactions with the wall material of the sample holder. Alternatively, in sample holders, planar ice samples can be exposed to trace gases and ice thin sections can be cut and analysed for their crystal structure.
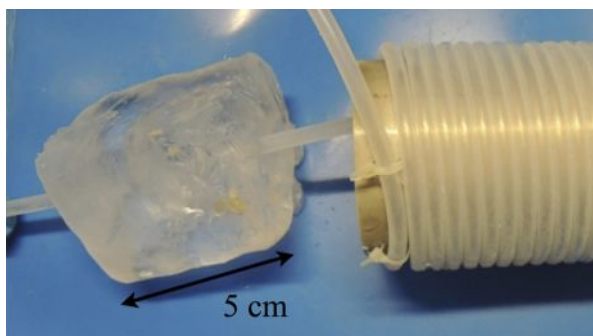
Fig. 1: The new ice flow tube shown with the precooling loop attached.

Figure 1 shows a new set-up that combines the advantages of both approaches. A flow tube is drilled into an ice block and directly attached to the gas delivery system. In this set-up the trace gas is only in contact with ice, and inert sample tubes. The ice tubes can be analysed for their grain structure and boundary area under a polarized microscope (Figs. 2 and 3)[3].

CONTROL OF GRAIN BOUNDARIES

At SLF the production of two types of such flow tubes has been developed. By soaking ice powder with cold water under low pressure, highly ploycrystalline ice samples can be grown (Fig. 2). Slowly freezing water results in single crystalline ice blocks (Fig. 3).
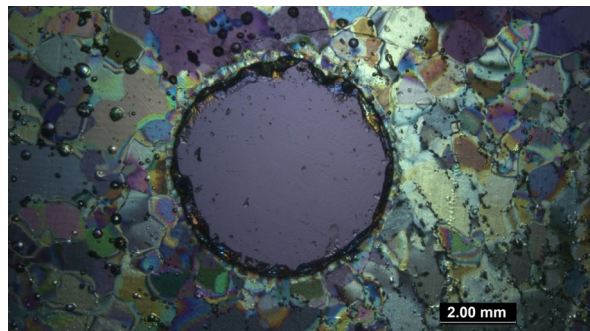
Fig. 2: A flow tube (blue-grey circle) drilled in to a polycrystalline ice block.
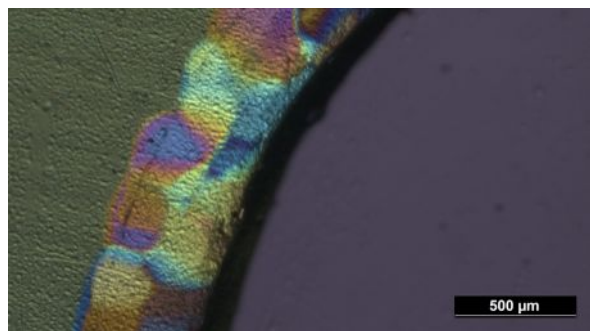
Fig. 3: The edge of a flow tube (blue-grey) drilled into a single crystalline ice block (greenish).

STATUS AND FUTURE WORK

The interaction of H_2O_2 with ice in a single crystal ice block was successfully probed in a preliminary experiment. Currently, the production of single crystal ice blocks is being optimized to prevent small grain nucleation from drilling damage at the ice's edge (Fig. 3).

ACKNOWLEDGEMENT

REFERENCES

[1] T. Bartels-Rausch et al., Rev. Mod. Phys., **84**, 885–944 (2012).
[2] T. Bartels-Rausch et al., Atmos. Chem. Phys., under review (2012).
[3] Riche, F., et al., J. Glaciol., **58**, 815–817 (2012).

IDENTIFYING INERT MATERIALS FOR LABORATORY EXPERIMENTS WITH ICE

T. Ulrich (PSI & Univ. Bern), M. Ammann (PSI), S. Leutwyler (Univ. Bern), T. Bartels-Rausch (PSI)

INTRODUCTION

Heterogeneous chemistry and surface adsorption are of great interest in atmospheric science, as these processes can significantly alter the environmental fate of pollutants and of greenhouse gases [1]. In the laboratory, these processes are commonly investigated by exposing a gas of interest to a solid sample. To unambiguously assign observed changes in the gas-phase concentration to processes on the sample surface, it is crucial that interactions with the walls of the sample holder can be neglected. This is of particular concern when interactions with ice surfaces are investigated, as wall interactions tend to increase at lower temperatures.

In this study we tested several fluorinated polymers with respect to their uptake of common trace gases to find the most inert and thus best suited material.

RESULT
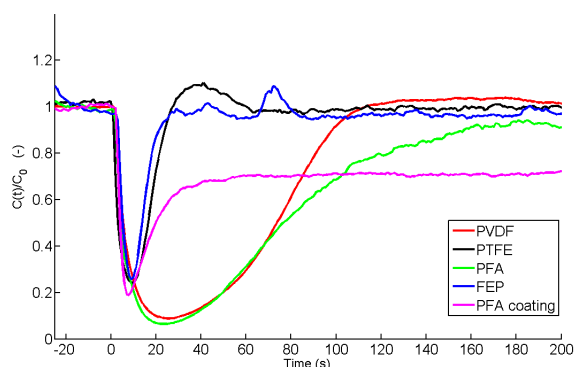
Fig. 1: Relative gas-phase concentration of acetic acid with time upon exposure to different fluorinated polymers. At t=0s the trace gas was exposed to the sample at 223 K.

Figure 1 shows how the gas-phase concentration of acetic acid in a flow of nitrogen drops when the trace gas is exposed to a 80 cm long 0.4 cm inner diameter tube of different types of fluorinated polymers. Fluorinated ethylene propylene (FEP) and polytetrafluoroethylene (PTFE) show an ideal behaviour with a very fast recovery. Perfluoroalkoxy copolymer (PFA) and polyvinylidene difluoride (PVDF) adsorb significantly more acetic acid and are thus less suited as sample holder for experiments with this organic acid. Figure 1 also shows that the processing of fluorinated polymers is critical, as a coating made from PFA powder shows an infinite uptake, very different from tubes used for the other experiments.

In summary, FEP showed little uptake of acetic acid. In Fig. 2 the uptake of other trace gases to FEP is compared at low temperatures. Clearly, FEP does not

significantly adsorb hydrogen peroxide (H_2O_2) at 242 K, nitrous acid (HONO) at 253 K, methanol, acetic acid, nor acetone at 223 K.
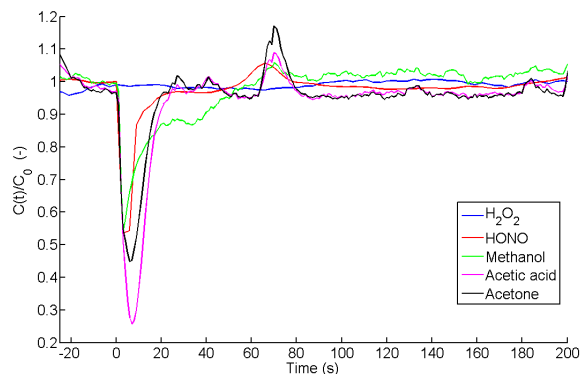
Fig. 2: Relative gas-phase concentration of various trace gases with time upon exposure to fluorinated ethylene propylene (FEP). At t=0s low concentrations of the sample gas were exposed to fluorinated polymers at 223 K to 253 K.

In summary, FEP is very inert to several trace gases of atmospheric relevance. This becomes particularly evident, when the uptake behaviour to the polymers is compared to the uptake to ice. Figure 3 shows that the uptake of H_2O_2 to ice continues for hours.
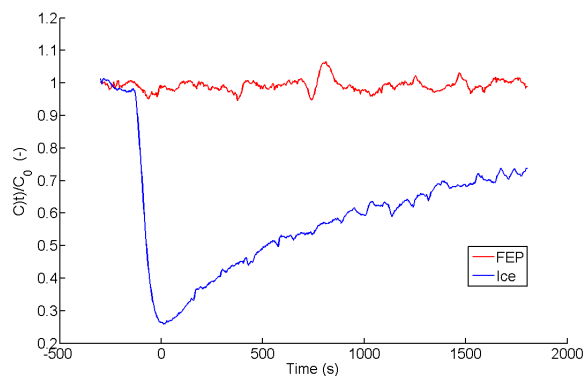
Fig. 3: Comparison of the uptake to ice and FEP. At t=0 traces of H_2O_2 were exposed to the samples at 243 K.

ACKNOWLEDGEMENT

REFERENCE

[1] Bartels-Rausch et al., Rev. Mod. Phys., **84**, 885 (2012).

VISIBLE LIGHT INDUCED DECOMPOSITION OF NITRATED PROTEINS AND PRODUCTION OF NITROUS ACID

Y.F. Cheng, Y. Elshorbany (MPIC), T. Bartels-Rausch (PSI), K. Selzle,
J. Lelieveld (MPIC), M. Ammann (PSI), U. Pöschl, H. Su (MPIC)

INTRODUCTION

Proteins have long been recognized as important compounds in the biogeochemical cycles of terrestrial ecosystems. Airborne proteins account for up to ~5% of urban particulate matter, and soil proteins provide a source of nitrogen for plants and soil microorganisms. Proteins can be nitrated by NO_2 and O_3 during their residence or exposure in the atmosphere. The airborne nitrated-proteins have been proposed as an explanation for the promotion of allergies by traffic related air pollution, which was supported by immunological experiments with cells, mice, and human sera [1]. Though the formation of nitrated-protein has been intensively studied, there are very few studies looking at their fate, i.e. transformation processes.

In this study, we investigated the reaction of nitrated-proteins in the presence of visible light. The results show a clear light induced decomposition of nitrated-proteins with nitrous acid as the main product, which suggests a shortening of the lifetime of nitrated proteins during daytime. Through HONO, an important OH precursor, nitrated-proteins on aerosol and ground surfaces may also influence the atmospheric chemistry and oxidation capacity.

EXPERIMENTS

The decomposition of nitrated proteins was analyzed by online and offline analytical methods in a flow tube experiment [2]. The nitrated proteins were prepared by mixing Ovalbumin (OVA) with a liquid solution of tetranitromethane (TNM) in methanol and by cleaning using size exclusion chromatography. The sample was dried with a freeze-dryer.

The nitration degree was 1.57 nitrated tyrosine residues per protein molecule, as analyzed by liquid chromatography (LC-DAD) [3]. Each OVA consists of 10 tyrosine residues. The nitrated OVA was used to coat the quartz flow tube (~0.5 m), typically with ~2-3 mg nitrated OVA on each tube.

We exposed the nitrated-protein coated tubes with visible light of variable intensity, both in absence and in presence of 15 ppb gaseous NO_2. The gas-phase NO_2 and HONO concentrations at the exit of the flow tube were measured continuously during the experiment. After each experiment, the reacted proteins were extracted from the tube by deionized water (Milli-Q) and the nitration degree was analyzed by the LC-DAD system.

RESULTS

Figure 1 shows the observed HONO emissions from one typical sample. Clearly, HONO emission from nitrated-proteins was only observed in the presence of light and the resulting HONO concentration is proportional to the light intensity.
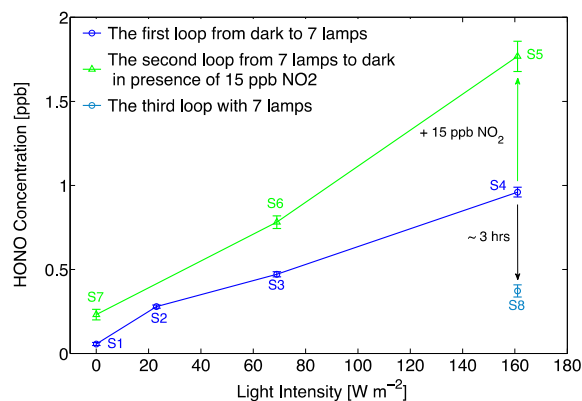
Fig. 1: HONO emission from nitrated OVA. The S1 to S8 represent results on the same sample: S1, dark condition; S2, 1 lamp on; S3, 3 lamps on; S4, 7 lamps on; S5, 7 lamps on + NO_2; S6, 3 lamps on + NO_2; S7, dark condition + NO_2; and S8, 7 lamps on.

This indicates a light induced decomposition of nitrated proteins. In presence of both NO_2 and light, the HONO formation is additionally increased. Finally, we found a significant decay of HONO production with time, implying significant loss of nitrated proteins through light induced decomposition. This is also confirmed by LC-DAD results, showing reduced nitration degree for proteins taken from the end of the experiments.

Our results indicate that the decomposition of nitrated proteins is enhanced by light exposure. Additionally, HONO was identified as one of the major products of the decomposition.

ACKNOWLEDGEMENT

REFERENCES

[1] T. Franze et al., Analyst, **128**, 824 (2003).
[2] K. Stemmler et al., Nature, **440**, 195 (2006).
[3] H. Yang et al., Anal. Bioanal. Chem., **397**, 879 (2010).

WATER UPTAKE TO A SINGLE SHIKIMIC ACID PARTICLE

S. Steimer (ETHZ & PSI), A. Huisman, U. Krieger, C. Marcolli, T. Peter (ETHZ), M. Ammann (PSI)

INTRODUCTION

It has recently been shown that organic particles are capable of forming amorphous solids or semi-solids under atmospheric conditions [1]. Since water acts as a plasticizer, changes in relative humidity can alter the physical state of the particle. In turn, water uptake and diffusion are heavily influenced by the physical state. Shikimic acid is a plant metabolite and a possible component of biomass burning aerosol [2]. In the following study, water uptake by single shikimic acid particles was studied using an electrodynamic balance (EDB) to determine physical state and particle radius as well as concentration as a function of humidity.

EXPERIMENTAL

The shikimic acid particle was generated from a 2.5 wt-% solution of shikimic acid in Milli_Q water via injection with an ink jet cartridge. The charged particle is levitated in the electric field of the EDB (Fig. 1), with the balancing DC voltage being proportional to the mass to charge ratio of the particle. Changes in particle mass are therefore reflected by an accompanying change in DC voltage. The particle is illuminated by a HeNe laser, with its image detected by CCD 1 and its phase function by CCD 2. The latter can be used to monitor physical state and give an estimate of size changes. A more precise size measurement can be obtained from the Mie backscatter spectra of a LED point source [3]. A bulk measurement of water activity and density of a 20.0 wt-% shikimic acid solution helped in parameterizing the concentration dependence of water activity and density using the size data obtained by Mie scattering.
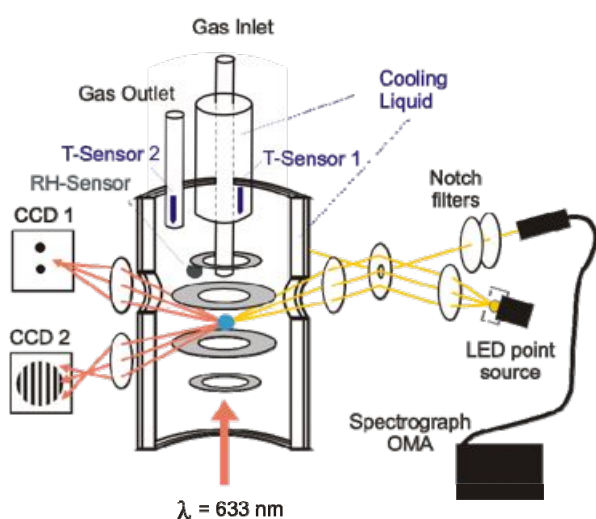
Fig. 1: Electrodynamic balance

RESULTS

The particle was found to stay spherical throughout the measurement, indicating that no crystallization occurred at any humidity. At low humidity levels (<32% RH), the particle is not in thermodynamic equilibrium anymore as hysteresis loops are apparent when cycling RH, see Fig. 2. This suggests the formation of a semi-solid or glassy state, with strong impedance to water uptake and release. Over the complete humidity range, the particle grows from 8.3 µm for the dry particle to 10.2 µm at 90 % RH. Accordingly, the concentration ranges from 8.6 M to 4.8 M.
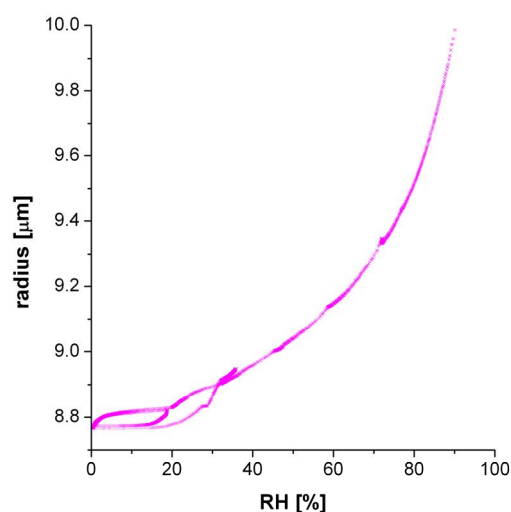
Fig. 2: Shikimic acid humidogram (measured EDB data). The particle is in thermodynamic equilibrium above ~32 %RH.

OUTLOOK

A kinetic transport model will be used to calculate water diffusion coefficients from the obtained data.

ACKNOWLEDGEMENT

REFERENCES

[1]   A. Virtanen et al., Nature, **467,** 824 (2010).
[2]   P. M. Medeiros et al., Environ. Sci. Technol., **42**, 8310 (2008).
[3]   A. A. Zardini et al., Opt. Express **14,** 6951 (2006).

PROCESSING OF SHIKIMIC ACID PARTICLES CAUGHT IN THE ACT VIA MICROSPECTROSCOPY

S. Steimer (ETHZ & PSI), A. Huisman, U. Krieger, C. Marcolli, T. Peter (ETHZ), E. Coz (CIEMAT), G. Grzinic (Univ. Bern & PSI), M. Lampimäki, M. Ammann (PSI)

INTRODUCTION

It has been shown that organic compounds may become solid or semi-solid under atmospheric conditions [1]. The chemical aging of aerosols changes their physical and chemical properties and therefore their environmental impact [2]. It is therefore important to understand how the physical state of aerosol compounds might affect chemical ageing. Shikimic acid is a plant metabolite, which has been found to be present in biomass burning aerosol [3]. In the present work we study the chemical aging of shikimic acid particles. Their reaction with ozone was investigated at four different humidity levels. The process was monitored in situ using scanning transmission X-ray microscopy (STXM) and near edge X-ray absorption fine structure spectroscopy (NEXAFS).

EXPERIMENTAL

Shikimic acid particles were generated from shikimic acid solution via ultrasonic nebulisation. The particles were dried with a diffusion drier, and a differential mobility analyzer (DMA) was used to select particles of a specific electrical mobility. These were then impacted on a silicon nitride membrane. A temperature controlled environmental micro reactor [4] was used to adjust relative humidity during the experiment (13%-83% RH) and facilitate in situ exposure to ozone. All STXM and NEXAFS experiments were conducted at the Pollux beamline at the SLS.

RESULTS

The carbon K-edge spectra for shikimic acid particles before and after oxidation show a clear decrease of the optical density (OD) at 284.5 eV for oxidized particles. This peak is associated with the carbon double bond of shikimic acid. As can be seen in Figure 1, the oxidation depends on humidity, with particles showing increased oxidation at higher humidity levels. Considering that water acts as a plasticizer for shikimic acid, this result can be seen as an indication of the relation of physical state and chemical ageing. Chemical maps however, show that the oxidation proceeds homogeneously at all humidity levels; no gradient is observed in response to increasing viscosity at higher humidity levels. This either indicates that a gradient being formed is below the spatial resolution of the microscope, or that no radial gradient is formed. Combined with the size dependence of the oxidation (Figure 2) this points to either a shallow gradient or a surface limited process.
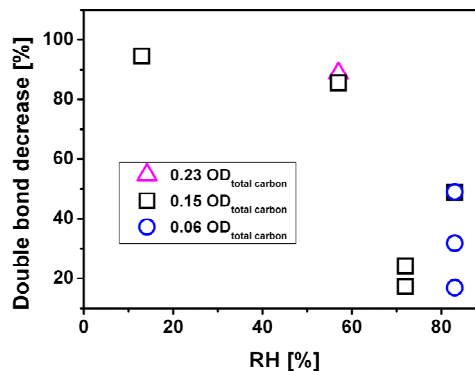
Fig. 1: Humidity dependence of the progress of oxidation after 211 min exposure to 2.5 ppm ozone. Different symbols mark particles of different total carbon optical density, which is a measure of particle thickness.
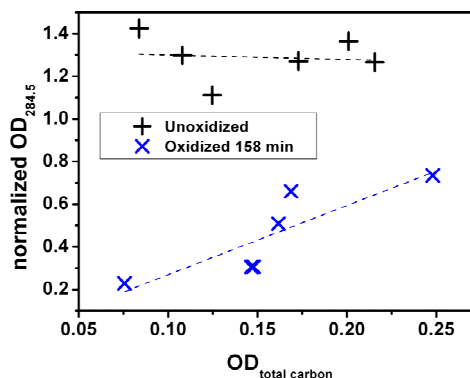
Fig. 2: Size dependence of the double bond peak height at 72% before (black crosses) and after (blue x) oxidation with 2.5 ppm ozone. The optical density of total carbon (310-320 eV) is a measure of particle thickness.

ACKNOWLEDGEMENTS

REFERENCES

[1] A. Virtanen et al., Nature, **467**, 824 (2010).
[2] Y. Rudich et al., Chem. Rev., **103**, 5097 (2003).
[3] P. M. Medeiros et al., Environ. Sci. Technol., **42**, 8310 (2008).
[4] T. Huthwelker et al., Rev. Sci. Instrum., **81**, 113706 (2010).

MICROSTRUCTURAL CHANGES OF INDIVIDUAL ORGANIC PARTICLES FROM COOKING EMISSIONS DURING ATMOSPHERIC PROCESSING

E. Coz (CIEMAT), I. El Haddad, S. Platt, J.G. Slowik, A.S.H. Prévôt (PSI/LAC), S. Steimer (ETHZ & PSI), G. Grzinic (Univ. Bern & PSI), M. Lampimäki, M. Ammann (PSI)

INTRODUCTION

Cooking activities are an important source of organic aerosols in the atmosphere frequently overlooked in source apportionment studies. The parallel development of the aerosol mass spectrometer (AMS) together with advanced laboratory facilities that simulate the photochemical degradation of particulate compounds in the atmosphere (smog chambers) in the last decade have recently provided the key to a systematic identification and quantification of sources during ambient studies [1]. The present study went further by adding a microstructural analysis of the particulate emissions during cooking, so far absent in the literature, and key to understanding atmospheric processing in detail.

EXPERIMENTAL

A set of experiments were designed and conducted at the PSI mobile smog chamber to investigate emissions from meat (chicken) grilling and vegetable boiling. All experiments were carried out in the presence of NO_X and samples were irradiated with UV light to simulate atmospheric aging. Emissions were generated from cooking inside a steel housing and injected into the smog chamber via a heated inlet system. Dilution ratios between the sample air and the chamber were determined by measuring CO_2, CO, and CH_4 concentrations in the sample air and at the chamber (cavity ring down spectrometer, Picarro). Two different samples were collected at different stages during each experiment to study the microstructural variations on the individual particles at the PolLux beamline in the Swiss Light Source. Four different types of samples were analyzed during the beamtime: vegetable boiling at a primary stage of aging and after the aging process, and primary and aged grilled chicken samples. All of them had replicas. Additional FESEM analyses were conducted on the samples to study morphological features which STXM cannot reach.

RESULTS

The analysis at the carbon edge of the fresh aerosols emitted by the boiled vegetables was associated with highly distinct particle-to-particle variations. Specific tests were done to check that these variations were not mainly a consequence of beam damage during the analyses. Furthermore, a later FESEM analysis corroborated this heterogeneity, which was mainly derived from a great variety of primary organic aerosols exhibiting very different morphologies ranging from nearly spherical to very needle-like elongated shapes. The organic particles were frequently accompanied by

nanosalts (i.e. K_2SO_4, KCl). At a higher degree of photo-oxidation, these primary features tended to be in minority and the carbon fraction was dominated by carboxylic groups.

Very different results were obtained for the experiments with grilled chicken. Particles were more homogeneous in terms of the relative contribution from different carbon functional groups and their spatial distribution within the particle microstructure. A major contribution from aromatics was found in slightly aged samples. These aromatics were nuclei for carboxylic groups produced during sample aging, which formed coatings of different thicknesses (Fig. 1). This was consistent with the results from the AMS analysis.
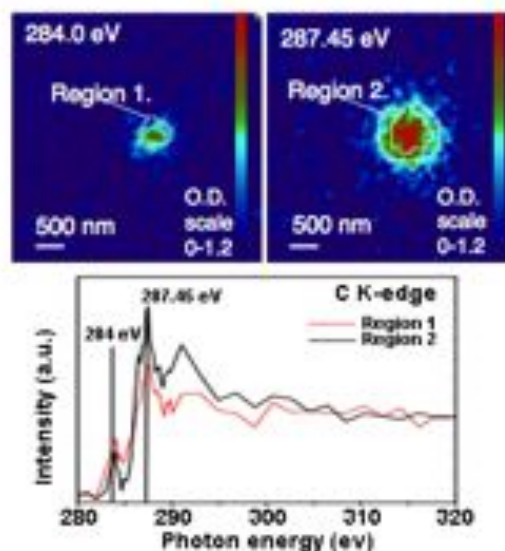
Fig. 1: Top: Optical density (O.D.) images of a particle from the sample 7 measured at 284.0 eV and 287.45 eV (images from C-stack). C K-edge spectra of the regions 1 and 2 from the same particle (bottom).

ACKNOWLEDGEMENTS

REFERENCE

[1] Mohr et al., Atmos. Chem. Phys., **12**, 1649-1665 (2012).

UPTAKE OF ^{13}N-LABELED N_2O_5 TO CITRIC ACID AEROSOL PARTICLES

G. Gržinić (Univ. Bern & PSI), T. Bartels-Rausch, M. Birrer, A. Türler, M. Ammann (PSI)

INTRODUCTION

Dinitrogen pentoxide is a significant reactive intermediate in the night time chemistry of nitrogen oxides. It can have a dual role, serving either as a NO_3 radical reservoir or as a major NO_x sink by heterogeneous hydrolysis on aerosol surfaces. It can influence tropospheric ozone production and therefore the oxidative capacity of the atmosphere [1].

EXPERIMENTAL

We used the short-lived radioactive tracer ^{13}N delivered by PSI's PROTRAC facility [2] in conjunction with an aerosol flow tube reactor in order to study N_2O_5 uptake kinetics on aerosol particles. Expanding on the setup assembled last year, improvements have been introduced in order to maximise N_2O_5 production and make the yield more reproducible. Fig. 1 shows a schematic of the new experimental setup. [13]NO is mixed with non labeled NO and O_3 in the N_2O_5 reactor where N_2O_5 is synthesized under dry conditions to prevent hydrolysis on the reactor walls. The N_2O_5 flow is then admitted into the aerosol flow tube reactor together with the humidified aerosol flow. Movable inlets allow varying the length of the aerosol flow tube. Behind the reactor a Scanning Mobility Particle Sizer (SMPS) system is used to characterize the aerosol. Alternatively a NO_x or O_3 analyzer can be plugged in instead of the SMPS. The remaining gas exiting the reactor is subsequently directed into the parallel plate diffusion denuder system, which allows for selective separation of the gaseous species. A particle filter located at the end of the denuder system is used to trap the aerosol particles. Activity of the ^{13}N labeled species can be monitored via scintillation counters placed on the denuder plates and the particle filter, respectively.
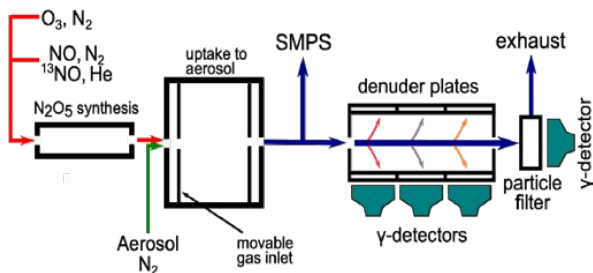
Fig. 1: The new experimental setup: separate N_2O_5 and aerosol reactors are used to allow for improved N_2O_5 production.

RESULTS

The new setup provides us with higher yields of ^{13}N-labeled gas phase N_2O_5 and allows more reproducible aerosol uptake experiments especially at higher humidity. Aerosol uptake measurements have been conducted using citric acid aerosols at different humidity levels. Fig. 2 shows a set of measurements conducted at RH=61.5%, at a fixed reaction time of around one minute, and at varying aerosol surface to volume ratio. The experimental data have been fitted with a simple first-order uptake model describing gas-particle kinetics as used in our earlier studies [3].
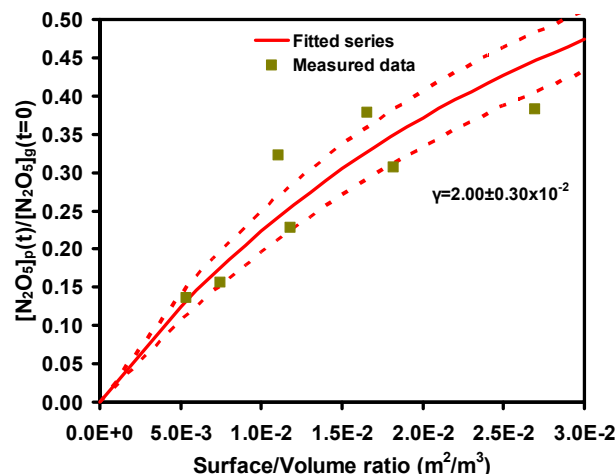
Fig. 2: Data set collected using citric acid aerosol at 61.5% RH. Green squares represent measured data points while the red curve is a fit to the data according to the kinetic model, with the dotted curve showing the error range

The results obtained have shown that the uptake coefficient increases with humidity from $1.65\pm0.3\times10^{-3}$ (~27% RH) to $1.25\pm0.3\times10^{-2}$ (45% RH) and $2.00\pm0.3\times10^{-2}$ (61.5% RH). This is comparable to some polycarboxylic acids (like malonic acid), and but higher than some others [4]. The increase is likely related to the increasing amount of water associated with citric acid at higher humidity that promotes hydrolysis of N_2O_5.

AKNOWLEDGEMENT

REFERENCES

[1] Chang, W. L., et al., Aerosol Sci. Technol., **45**, 665 (2011).
[2] Ammann, M., Radiochim. Acta, **89**, 831 (2001).
[3] Vlasenko, A., et al., Atmos. Chem. Phys., **6**, 2147–2160 (2006).
[4] IUPAC Subcommittee on Gas Kinetic Data Evaluation – Data Sheet VI.A3.8 (2009).

COATED WALL FLOW TUBE EXPERIMENTS OF OZONE UPTAKE TO MIXED SODIUM BROMIDE/CITRIC ACID FILMS AT 72% RELATIVE HUMIDITY

M.T. Lee (Univ. Bern & PSI), E. Steimle (Univ. D'orleans), A. Türler (Univ. Bern & PSI),
T. Bartels-Rausch, M. Ammann (PSI)

INTRODUCTION

The reaction of ozone (O_3) with bromide is of interest in the context of formation of photolabile halogens (Br_2, $BrCl$) in the marine boundary layer. Recent experiments have suggested that the bromide oxidation rate is related to the surface concentration of bromide [1] and inversely related to the gas phase concentration of O_3, an indication for a precursor mediated reaction at the surface [2]. Moreover, both theoretical and experimental results demonstrated enhancement of halogenide ions at the interface [3], which may be related to the surface reaction of O_3.

So far, the effect of organics (such as those occurring at the ocean surface or in marine aerosols) on the reaction of O_3 with bromide aerosols has not been studied yet. In this study we investigate the uptake kinetics of O_3 to a mixed solution of sodium bromide (NaBr) and citric acid (CA) with a well-established coated wall flow tube technique.

EXPERIMENTAL
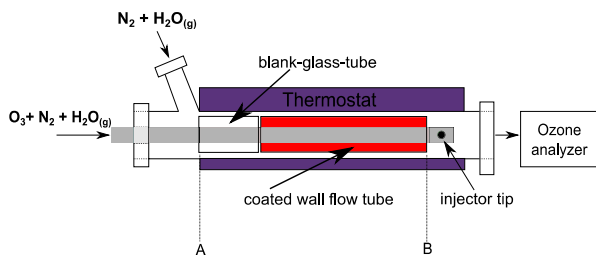
Fig. 1: A schematic diagram of the flow tube system used in O_3 uptake measurements to the coated film.

Experiments are done with a thermostated atmospheric pressure coated wall flow tube coupled to an O_3 analyzer (Fig. 1) or alternatively to a chemical ionization mass spectrometer (CIMS, not shown). A glass tube is coated with a mixed NaBr/CA solution and dried to 72% relative humidity (RH). After insertion of the tube, the sliding injector (the black spot in Fig. 1) is moved to position (B) so that its tip is reaching beyond the coating. After about 1 h of equilibrating the film at 72% RH, the injector is moved to position (A), which leads to exposure of the film to O_3, allowing the heterogeneous reaction to take place and the loss of O_3 being measured. For the mixed solutions, we used the hygroscopic properties of NaBr and CA and additivity rules to calculate the water content of the film at 72% RH [4].

RESULTS

The CIMS measurements confirmed the formation of gas-phase bromine (Br_2) from the interaction of gas-phase O_3 with the mixed NaBr/CA solution at 72% RH and 20 °C. The uptake coefficient γ, i.e., the measured loss rate of $O_3(g)$ normalized to the gas kinetic collision rate, is shown in Fig. 2 for three different NaBr to CA mixing ratios and as a function of the O_3 concentration.
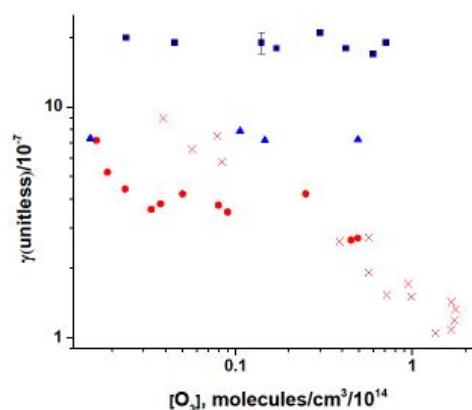
Fig. 2: Uptake coefficient γ vs. [O_3] for mixed NaBr/CA films with bromide concentrations of 4M (squares), 0.34M (triangles) and 84mM (circles), respectively, at 72% RH and 20°C. Red crosses denote data from Oldridge and Abbatt [2] (8.6mM bromide in NaCl solution).

The uptake of O_3 to the films with the two higher bromide concentrations is independent of the gas phase concentration and roughly consistent with uptake limited by reaction in the bulk. For the lowest bromide concentration, however, we observe a trend of the uptake coefficient to decrease with increasing O_3 concentration, indicating an increasing importance of a surface reaction. The latter behaviour has also been observed in sea salt solution at 0 °C with even lower bromide concentrations by Oldrige and Abbatt [2].

ACKNOWLEDGEMENT

REFERENCES

[1] Clifford and Donaldson, J. Phys. Chem. A, **111**, 9809-9814 (2007).

[2] Oldridge and Abbatt, J. Phys. Chem. A, **115**, 2590-2598 (2011).

[3] Ghosal et al., Science, **307**, 563-566 2005.

[4] Zardini et al., Atmos. Chem. Phys. **8**(18), 5589-5601 (2008).

INSTALLATION OF A NEAR-AMBIENT PRESSURE PHOTOEMISSION (NAPP) ENDSTATION

M. Ammann (PSI), M. Brown (ETHZ), J.A. van Bokhoven (PSI/ETHZ), S. Kato, M. Lampimäki, M. Birrer (PSI),
T. Huthwelker, F. Nolting, A. Kleibert (PSI/SLS)

INTRODUCTION

Electronic structure, molecular orientation and chemical composition are key in determining the chemical and physical properties of material interfaces in a wide range of scientific fields, including catalysis and environment. Ambient pressure X-ray photoelectron spectroscopy has become an emerging tool for determining electronic structure and depth resolved chemical composition at solid – gas and liquid – gas interfaces [1,2]. We have set up a mobile near ambient pressure photoemission endstation at PSI, capable of working at a large range of VUV and X-ray photon energies and at pressures from vacuum to currently 20 mbar.

THE NAPP ENDSTATION

The near ambient pressure photoemission (NAPP) endstation is based on a VG Scienta R4000-7keV HiPP analyzer, which consists of a R4000 hemispheric analyzer coupled to a differentially pumped electrostatic lens system. This analyzer is configured for kinetic energies between 0 and 7000 eV and for pressures in the analysis chamber of up to 20 mbar. The analyzer is mounted on an adjustable mobile frame so that it can be flexibly used at the SIM and PHOENIX beamlines of SLS for X-ray energies 90-2000 eV and 800 – 8000 eV, respectively, or with an offline He lamp (VG Scienta VUV 5000, with monochromator). The NAPP endstation is featuring a flexible analysis chamber concept to allow a broad range of sample systems. Currently, a liquid microjet experiment [2,3] is operational, and a chamber for in situ spectroscopy of solid surfaces is under construction.
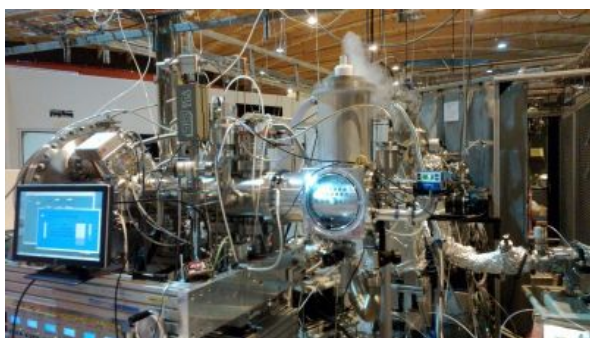
Fig. 1: The NAPP endstation hooked up at the SIM beamline at SLS, with the liquid jet chamber attached.

COMMISSIONING RESULTS

The NAPP endstation (Fig. 1) was set up during the course of 2012, and first commissioning experiments were done with the VUV lamp and at the SIM and PHOENIX beamlines. The commissioning included optimising the lens tables for the different kinetic energy ranges and analyzer modes, testing the analyzer functions over the whole sample chamber pressure range and optimising the spatial overlap of the photon beam with the liquid microjet. Fig. 2 (left) shows N1s spectra of gas phase N_2 at different N_2 pressures obtained at the SIM beamline. Fig. 2 (right) shows an Au4f spectrum obtained from a gold foil at the PHOENIX beamline. The two peaks are due to spin orbit splitting of the Au4f line. The decreasing intensity is due to the increasing loss by inelastic scattering with increasing N_2 pressure.
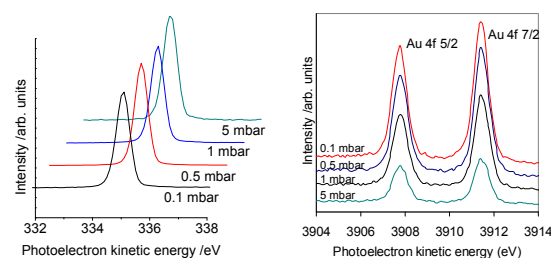
Fig. 2: Left: Normalised N1s spectra taken at 735 eV photon energy (SIM) at different gas phase N_2 pressures. The spectra are offset in x- and y-direction for clarity. Right: Au 4f spectra of a gold foil taken at 4000 eV (PHOENIX) at different N_2 pressures. The spectra are background subtracted and offset in y-direction for clarity.

The commissioning experiments demonstrated the capability of NAPP to work at low and high kinetic energies and at pressures in the sample region in the mbar range.

First experiments included investigations of nanoparticle solutions, mixed halogenide organic solutions, as well as experiments related to ceria catalyst materials under reducing and oxidising conditions. Some of these are covered by reports in this volume.

AKNOWLEDGEMENT

REFERENCES

[1] H. Bluhm, et al., Mrs. Bull., 32, 1022 (2007).
[2] D.F. Ogletree et al., Nucl. Instr. Meth. A, **601**, 151 (2009).
[3] M.A. Brown et al., J. Phys. Chem. Lett. **3**, 1754 (2012).
[4] M.A. Brown et al., J. Phys. Chem. Lett. **3**, 231 (2012).

LIQUID-JET XPS STUDY ON THE AIR-AQUEOUS INTERFACIAL COMPOSITION OF MIXED SODIUM BROMIDE / CITRIC ACID SOLUTIONS

M.T. Lee (Univ. Bern & PSI), S. Kato (PSI), M. Brown (ETHZ), J.A. van Bokhoven (PSI & ETHZ),
F. Nolting, A. Kleibert (PSI/SLS), M. Lampimäki, M. Ammann (PSI)

INTRODUCTION

Sea-salt solution – air interfaces play an important role in the chemistry of the marine boundary layer. There is direct photoelectron spectroscopy evidence that halide ion concentrations are enhanced at the aqueous solution air interface [1-2], which likely promotes surface reactions involving halogens such as bromide and iodide. Ubiquitously present organic compounds at the ocean surface may however change the composition of the interface. A first photoelectron spectroscopy study of ternary solutions of KI with butanol indicated the importance of specific interactions of the cation with the alcohol headgroup [3]. In this study we would like to go one step further and look into the effect of a more complex organic compound, citric acid, which represents highly oxidized organic compounds present in the environment.

EXPERIMENTAL

The experiments presented here made use of the new near ambient pressure photoemission (NAPP) endstation, which consists of a Scienta R4000 7keV HiPP-2 analyzer that can be coupled to flexible analysis chambers and photon sources ranging from UV to tender X-ray radiation. In this case it was coupled to a vacuum liquid microjet shown in Fig. 1. The continuously refreshed free-flowing aqueous filament under vacuum permits XPS measurements from volatile aqueous interfaces in absence of beam damage [4]. Measurements were made at the SIM beam line of the Swiss Light Source (SLS) at the Paul Scherrer Institute. The ability to tune the photon energy (150-2000 eV) is crucial to get precise component ratios as a function of photoelectron kinetic energy and thus probe depth.

RESULTS

Figure 2 shows exemplary Br 3d, Na 2s (left) and C 1s (right) photoelectron spectra taken at 450 eV and 670 eV photon energy, respectively, corresponding to about 400 eV photoelectron kinetic energy. The pass energy was 100 eV for Br 3d / Na 2s and 100 eV for the C 1s spectrum. The Br 3d peak shows the characteristic doublet structure due to spin-orbit splitting.

There are three peaks in the spectrum of the C 1s region due to the occurrence of the carbon atom in different electronic configuration, i.e., three carboxyls, one alcohol and two methyl carbons, each having distinctly different binding energy. Further analysis of these spectra at different kinetic energies allows obtaining insight into the relative enrichment of bromide at the interface as a function of the citric acid concentration in the solution.

The results are directly linked to kinetic experiments of O_3 uptake to similar solutions we are performing in our lab with a flow tube technique.
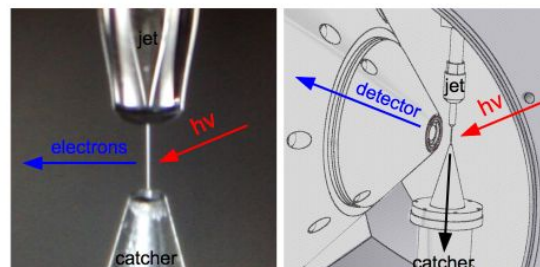
Fig. 1: Left: Photograph of the liquid-microjet in action; right: detail of the measurement configuration.
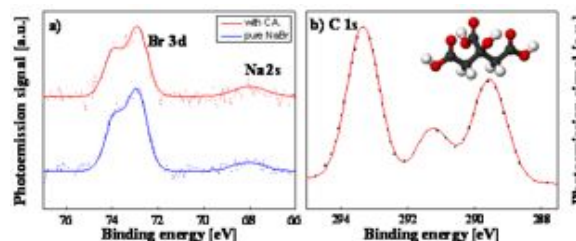
Fig. 2: a) Photoelectron spectra and their fits of aqueous 0.03 M NaBr and its mixture with 1.35 M citric acid, taken at 450 eV photon energy. b) C 1s spectrum and its fit for the same mixed solution as in a). All spectra are background subtracted and offset for clarity.

ACKNOWLEDGEMENT

REFERENCES

[1] S. Ghosal et al., Science **307**, 563 (2005).
[2] M.A. Brown et al., Phys. Chem. Chem. Phys. **10**, 4778 (2008).
[3] M. Krisch et al., J. Phys. Chem. C **111**, 13497 (2007).
[4] M.A. Brown et al., J. Phys. Chem. Lett. **3**, 231 (2012).

HARD X-RAY NEAR AMBIENT PRESSURE PHOTOEMISSION SPECTROSCOPY

S. Kato, M. Ammann (PSI), J.A. van Bokhoven, C. Paun (PSI/ETHZ), A. Redondo, M. A. Brown (ETHZ),
T. Bartels-Rausch, M. Lampimäki, M. Birrer (PSI), T. Huthwelker (PSI/SLS)

INTRODUCTION

X-ray photoelectron spectroscopy (XPS) provides information about elemental surface composition and oxidation state of elements at solid and liquid surfaces. Such surface analysis methods are generally ultrahigh vacuum (UHV) based and fail to function at higher pressure ($> 10^{-4}$ mbar) because of the decreased mean free path of electrons and the shortened lifetime of cathode filaments.

An UHV model study might be far from the reality under atmospheric conditions in terms of surface structure [1]. Therefore, near ambient pressure photoemission (NAPP) spectroscopy has great potential to reveal complex interface reactions (e.g. gas-solid, gas-liquid, liquid-solid) in various research fields such as catalysis and environmental science. We have set up a mobile NAPP endstation at the Swiss Light Source (SLS).

The sampling depth of XPS relates to the kinetic energy of the electrons excited after absorption of X-rays. The probing depth is typically a few nm when using a conventional lab X-ray source (< 1.5 keV). The advantage of using a tunable synchrotron X-ray source is the ability of varying the sampling depth. We have combined hard X-ray photoemission [2] and NAPP to obtain a depth profile *from surface to bulk* in near ambient pressure conditions. Here, we investigate gas-solid reactions in heterogeneous catalysis by using this new spectroscopic method.
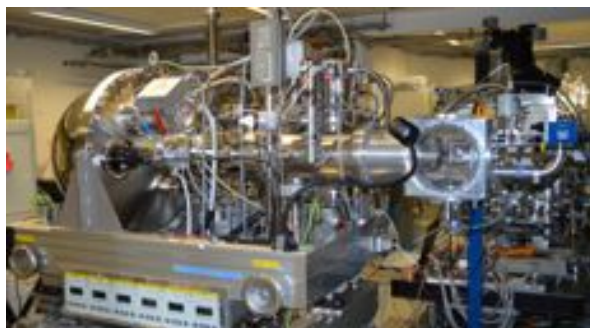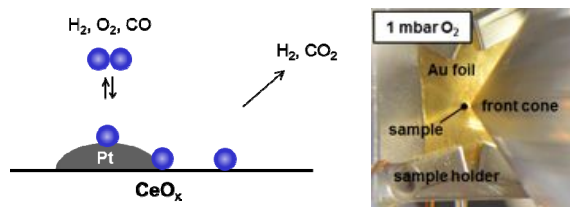
Fig. 1: Left top: Heterogeneous catalysis (Selective cleaning of H_2 from CO). Right top: Sample holder and the front cone of the electron analyser pre-lens. The NAPP endstation hooked up at the PHOENIX beamline at SLS.

EXPERIMENTAL

The basis of the NAPP endstation is a VG SCIENTA R4000 7keV HiPP analyzer with a differentially pumped electrostatic lens system. It is capable to analyse kinetic energies up to 7 keV at pressures in the analysis chamber up to currently 20 mbar (Fig. 1). The mobile NAPP endstation was installed at the PHOENIX beamline of SLS (energy range 0.8-8 keV). A solid heterogeneous catalyst (2wt%Pt/CeO$_2$) was analysed in 1 mbar atmospheres of O$_2$ (99.999%) or H$_2$ (99.999%) by using an analysis chamber developed at ETHZ otherwise used for liquid jet experiments.

RESULTS

The ceria supported Pt catalyst was exposed to the oxidizing and reducing atmospheres of 1 mbar O$_2$ or H$_2$. The hard X-ray photoemission spectra of Ce 3d were collected at 6 keV excitation energy (Fig. 2). The electron kinetic energy of 5 keV analyses the bulk state of ceria. The evolution of the ceria oxidation state under near ambient pressure conditions was probed. Changes in the XPS spectra are associated with the formation of oxygen vacancies in the ceria, which relates to the oxygen storage capacity.
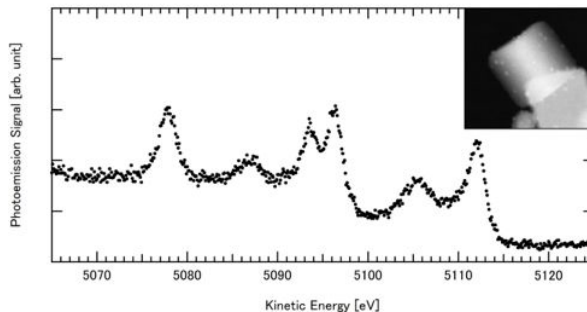
Fig. 2: Ce 3d XPS spectrum in an O$_2$ atmosphere (1.0 mbar, 298 K), taken at 6 keV photon energy. Inset: TEM image of the catalyst (2wt%Pt/CeO$_2$). The image width is 50 nm.

AKNOWLEDGEMENT

REFERENCES

[1] M. Salmeron et al., Surf. Sci. Rep. **63**, 169 (2008).
[2] K. Kobayahi et al., Nucl. Instr. Meth. Phys. Res. A, **60**, 32 (2009).

ENVIRONMENTAL PHOTOCATALYTIC STUDIES ON TiO$_2$ SURFACES USING A UV-LASER AND X-RAY PHOTOELECTRON SPECTROSCOPY

M. Lampimäki, S. Schreiber, M. Birrer (PSI), S. Axnanda, B. Mao, H. Bluhm, Z. Liu (LBNL), M. Ammann (PSI)

INTRODUCTION

Photocatalytic processes of atmospheric trace gases on the surface of TiO$_2$ containing mineral dusts may play an important role in atmospheric chemistry. UV-radiation induced electron/hole pairs can directly or indirectly (via photogenerated reactive oxygen species) affect environmental processes through the redox chemistry of atmospheric gases, such as NO$_2$, volatile organic compounds, H$_2$O and O$_2$ [1,2,3]. TiO$_2$ has been also extensively studied as an active compound in environmental photocatalytic remediation processes, for example on the surfaces of urban infrastructure [4]. Photoelectron spectroscopy provides a valuable tool to study adsorption of nitrogen oxide species and the effect of UV-radiation on metal oxide surfaces [5]. Here, we show an experimental setup including a UV-laser and ambient pressure x-ray photoelectron spectroscopy for *in situ* measurements of nitrogen oxide chemistry on a well defined TiO$_2$(110) single crystal surface.

EXPERIMENTAL

The photoelectron spectroscopy measurements were performed at the beamline 9.3.2 at the Advanced Light Source (ALS). The TiO$_2$(110) single crystal was cleaned by 1 kV Ar$^+$-ion sputtering and annealed for 10 min at 850 K in a 5×10^{-7} Torr background pressure of O$_2$. Water purified by multiple freeze-pump-thaw cycles was introduced via a leak valve into the analysis chamber. NO$_2$ from a lecture bottle containing a mixture of NO$_2$ and N$_2$O$_4$ was also admitted to the analysis chamber via a leak valve. H$_2$O and NO$_2$ concentrations were monitored by a baratron and a mass spectrometer mounted to the analyzer. O, Ti and N core-level XPS-transitions, as well as valence band regions were measured at elevated pressures.
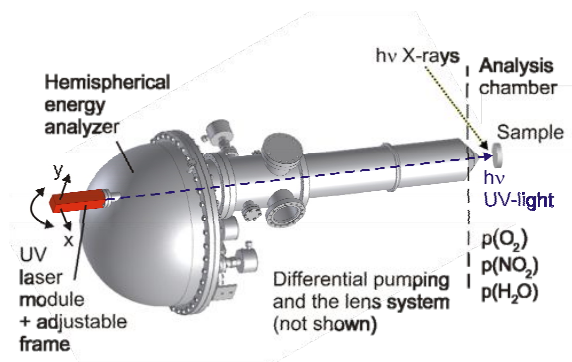
Fig. 1: Schematic presentation of the UV-laser module (λ = 375 nm) attached on the viewport of the hemispherical electron energy analyzer and aligned on the sample through the electrostatic lens system.

The sample was exposed to UV-light in situ by a laser diode module (Oxxius LBX 375) mounted on the viewport at the top of the hemispherical analyzer (Scienta R4000 HiPP) and aligned on the sample through the analyzer aperture by an adjustable frame (Fig. 1). Switching the laser on and off at the different spots on the sample allowed both, XPS measurements under illumination and reference measurements on unexposed spots on the surface.

CONCLUSION

The evolution of the surface nitrogen oxide species after exposure to O$_2$, H$_2$O, and NO$_2$ under dark and irradiated conditions is shown in Fig. 2. Preliminary results indicate small changes in the chemical state of NO$_x$ species under UV-irradiation. Further analysis of the data is in progress.
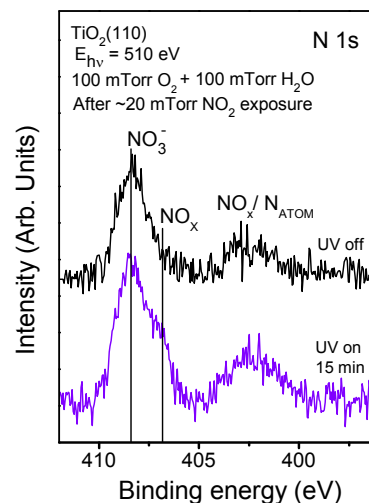
Fig. 2: Core-level spectra of the N 1s region showing nitrogen oxide species on TiO$_2$(110) under dark and UV-irradiated conditions.

REFERENCES

[1]   A. Linsebigler et al., Chem. Rev. **95,** 735 (1995).
[2]   H. Chen et al., Chem. Rev. **112,** 5919 (2012).
[3]   M. Shiraiwa et al., Nat. Chem. **3,** 291 (2011).
[4]   A. Fujishima et al., Surf. Sci. Rep. **63,** 515 (2008).
[5]   J. Baltrusaitis et al., Phys. Chem. Chem. Phys. **11,** 8295 (2009).

ICE-CORE BASED ESTIMATION OF HEAVY METAL (Cu, Zn, Cd, Sb) EMISSIONS IN THE FORMER SOVIET UNION (FSU) DURING THE PERIOD 1950-1991

A. Eichler, L. Tobler (PSI), S. Eyrikh, N. Malygina, T. Papina (IWEP), M. Schwikowski (PSI & Univ. Bern)

Anthropogenic emissions from the territory of the former Soviet Union (FSU) considerably influenced concentrations of heavy metals in the atmosphere. The share of FSU emissions to the total European heavy metal emissions is estimated to be up to 50% [1,2]. However, Pb is the only metal, with historical emission estimates for this region available (period 1955-2010 [1]), whereas for selected other metals only values for the year 1980 exist [3]. For assessing the impact of different heavy metals on the environment and human health and modelling the atmospheric transport, it is however crucial, to know historical emission data.

This is the first study presenting a trend of FSU Cu, Zn, Cd, and Sb emissions during the period 1950-91. The basis of this work are concentration records of these four metals derived from an ice core of the Belukha glacier in the Siberian Altai (Fig. 1).
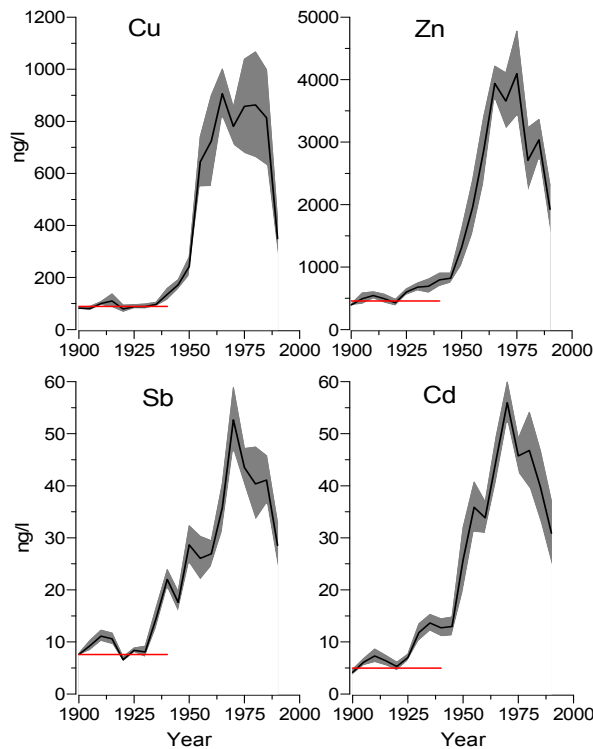
Fig. 1: Concentration records of Cu, Zn, Sb, and Cd from Belukha ice core during the period 1900-1991, given are 5-year averages (black line), the ±1σ range (gray area), and the 1850-1920 average (red).

We observed a good agreement between ice-core Pb concentrations and historical Pb emission estimates of the European part of the FSU during the period 1955-1990 [4]. Accordingly, Cu, Zn, Cd, Sb concentration records were transferred into emission values using two assumptions:

1) The concentration averages during the period 1850-1920 were set to an emission of 0 tonnes/year.
2) Emission values for the year 1980 were taken from estimates for the 12 major emission source regions in the FSU ([3] updated with [5], for Sb see e.g. [6]).

The record of Cu emissions (Tab. 1, Fig. 1) follows that of the Cu production in the FSU, increasing after World War II until the end of the 1980s and decreasing thereafter [7]. Contrary, Zn, Cd, and Sb emissions increased only until the 1970s, but dropped already at the end of the 1970s. The major emission sources of Zn and Cd in the FSU were lead-zinc and steel-iron production, whereas Sb was mainly emitted from fuel combustion, copper-nickel and steel-iron production [3]. Metal production in the FSU has strongly increased since the 1930s, peaked in the 1980s, and dropped down in 1990-91 [7] due to the economic crisis and the dissolution of the Soviet Union. Thus, the decrease in Zn, Cd, and Sb emissions at the end of the 1970s can not be explained by declining metal production. Instead we assume that the decrease is due to changes in technology for an increasing metal recovery from ores, replacement of coal by gas, and partially also to air pollution control. The total volume of pollutants from monitored stationary sources in the FSU, for instance, decreased by about 20% during the 1980s [8].

Tab. 1: Estimated anthropogenic emissions of heavy metals from the territory of the FSU (tonnes/year), given is the ±1σ range (gray area from Fig. 1).

	Cu	Zn	Cd	Sb
1950-54	1060-1720	5200-10650	280-530	170-240
1955-59	4140-5900	9800-17900	510-700	130-220
1960-64	4160-7320	17300-27200	500-630	160-210
1965-69	6530-8250	29600-34700	700-880	220-320
1970-74	5600-6900	25300-33700	920-1080	370-500
1975-79	5300-8600	27290-39900	730-870	310-380
1980-84	5160-8840	16000-25600	680-970	250-380
1985-89	4890-8220	20800-26900	540-820	270-370
1990-91	1730-3000	9980-17100	380-630	160-240

REFERENCES

[1] H. Storch et al., Sci. Tot. Env. **311**, 151 (2003).
[2] J. Pacyna, Atmos. Environ. **18**, 41 (1984).
[3] NILU Report 4/84, Norwegian Institute for Air Research, Lillestrøm, Norway (1984).
[4] A. Eichler et al., ES&T **46**, 4323 (2012).
[5] R. Boyd et al., Atmos. Environ. **43**, 1474 (2009).
[6] L. Tobler et al., this report, p. 26.
[7] http://minerals.usgs.gov/minerals/
[8] D.J. Peterson, Troubled Lands, The Legacy of Soviet Environmental Destruction (1993).

AN ICE-CORE RECORD OF ANTHROPOGENIC Sb EMISSIONS FROM EASTERN EUROPE

L. Tobler, A. Eichler (PSI), S. Eyrikh, N. Malygina, T. Papina (IWEP), M. Schwikowski (PSI & Univ. Bern)

Antimony (Sb) has been known since ancient times with a notable history in alchemy and early medicine. In recent times a large number of industrial processes and many high-technology materials, i.e flame retardants and lead-acid batteries, use and contain Sb. Dependent on its chemical state, Sb is a potentially toxic and carcinogenic trace element, and thus harmful to humans and the environment.

For Europe, there are no continuous long-term Sb emission data available. In our study we investigate Sb concentrations in an ice core from the Belukha glacier in the Siberian Altai determined by Inductively Coupled Plasma Sector Field Mass Spectrometry (ICP-SFMS) for the time period 1680-1995 (Fig.1). From an earlier study for Pb [1] it is known that this site was polluted by emissions from Eastern Europe during 1935-1995 and from the Altai in the pre-industrial period before 1935.
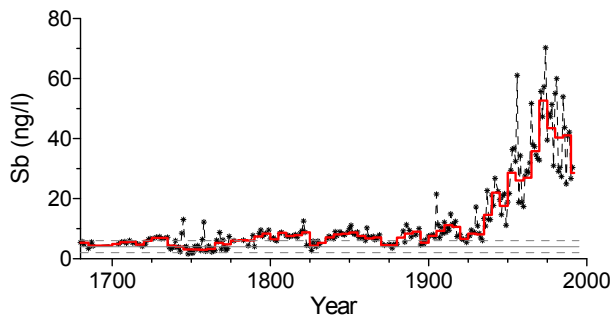
Fig. 1: Sb concentration record (annual values: black; 5-year averages: red), together with the method blank (4±2 ng/l, gray) for the period 1680-1995.

Sb emissions from mining in the Altai region before 1930 are very low and do not show a trend. Only in the period 1935-1995 Sb concentrations are enhanced, following large-scale exploitations and industrialization in the former Soviet Union (USSR) after the First Five-Year Plan (1928–32).
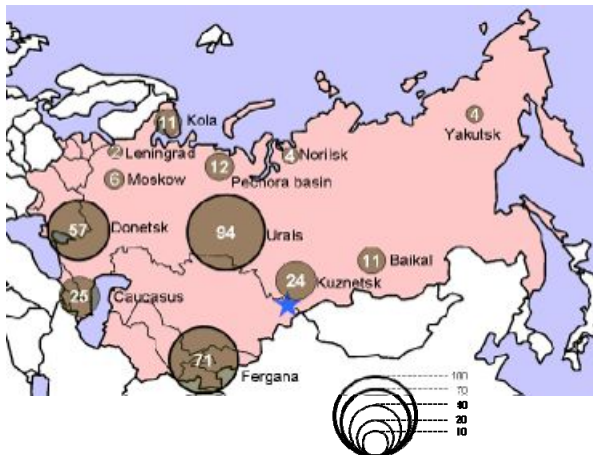
Fig. 2: Map of the former Soviet Union [2] with the location of major Sb emission regions [3,4]. Circles represent emissions of Sb in t/y for 1980. The blue star indicates the Belukha site.

Estimated major emission sources of Sb in the USSR were fossil fuel combustion (coal, oil), copper-nickel and steel-iron production [3]. The main 12 industrial regions are indicated in Figure 2, together with the estimated Sb emissions (in tonnes/year) for 1980.

Sb concentrations (5-year averages) increase from 14 ng/l in the period 1935-39 to 53 ng/l in the beginning of the 1970s. The decrease afterwards (28 ng/l in the 1990s) might be explained by the replacement of coal by gas, secondary metallurgical processes for the recovery of Sb in the copper-nickel production, the application of pollution-control technologies and the economic decline of the Soviet Union.

The comparison of the established Eastern European Sb record with other records from the Northern Hemisphere shows distinct regional differences in Sb emissions (Fig.3). Sb concentrations in an ice core from Devon Island in the Canadian High Arctic [5], representing emissions from North America, start to increase already from the beginning of the 20th century, indicating an earlier industrialization of North America. The decrease, beginning already after 1950, reflects an earlier use of dedicated filter technologies. Sb emissions from Asia, derived from an ice core from Muztagata [6], begin to rise considerably after 1975, showing the later industrialization of Asia.
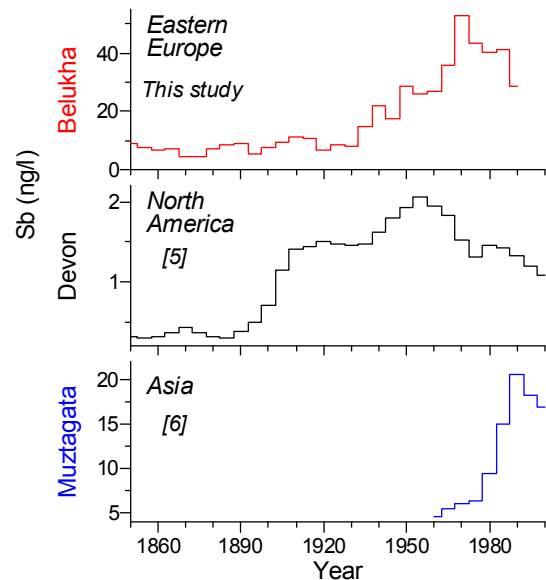
Fig. 3: Records of Sb concentrations in ice cores from different sites in the Northern Hemisphere [5,6].

REFERENCES
[1] A. Eichler et al., ES&T **46**, 4323 (2012).
[2] map from http://www.world-geograpics.com/... maps/eurasia/map_of_soviet_union_as_of_1990/
[3] NILU Report 4/84, Norwegian Institute for Air Research, Lillestrøm, Norway (1984).
[4] R. Boyd et al., Atmos. Environ. **43**, 1474 (2009).
[5] M. Krachler et al., J. Environ. Monit. **7**, 1 (2005).
[6] Y. Li et al., Ann. Glaciol. **43**, 154 (2006).

EVIDENCE FOR PRE-INKAN LEAD POLLUTION OBTAINED BY TRACE ELEMENT RECORDS FROM AN ILLIMANI ICE CORE

G. Gramlich (PSI & Univ.Bern), L. Tobler, A. Eichler (PSI), T. Kellerhals (KUP), M. Schwikowski (PSI & Univ. Bern)

A continuous, highly resolved lead record was derived by ICP-MS analysis from a well-dated ice core from Illimani, Bolivia [1], allowing detailed insight into historical atmospheric pollution in South America. Anthropogenic lead sources are e.g. mining and smeltering activities, fuel combustion or, dominating in the second half of the 20th century, leaded gasoline. The lead concentrations found in the Illimani ice-core correlate strongly with those of geogenic elements like cerium until the beginning of the 16th century, and then the records diverge significantly (see Fig. 1).
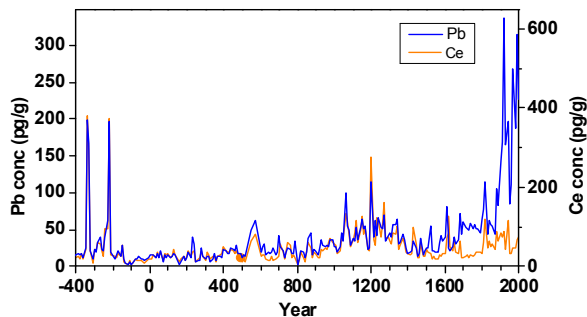
Fig. 1: Concentrations of lead (blue) and of the geogenic element cerium (orange), 10-yrs averages.

To allow a discrimination of anthropogenic lead emissions from lead originating from natural sources like soil or mineral dust a dust correction was performed. The correction is based on the individual lead to cerium ratio and a subsequent normalisation to values found in the Illimani ice core during a period with low anthropogenic influence (1500 to 100 BC) (see Eq. 1)

$$EF = \frac{[Pb/Ce]_{Sample}}{[Pb/Ce]_{Background}}$$

Eq. 1: Calculation of enrichment factors EF based on natural lead/cerium ratios.

This approach yielded specific enrichment factors of lead for a period of more than 2000 years and revealed an anthropogenic influence already centuries prior to the industrial revolution (see Fig. 2), probably mainly from extended non-ferrous metal production. Especially the eastern part of the Bolivian Altiplano is distinguished by its exceptional mineral richness of e.g. lead-, silver- or antimony-bearing ores. While it has a millennia-long history of metallurgy, for example of silver production, the reconstruction of the history of pre-Columbian "New World" metallurgy is fragmentary, partly because of extensive looting of precious metal artefacts by the conquerors [2]. In this context, the trace element records resulting from atmospheric deposition on the Illimani glacier provide invaluable information. One outcome of this work may shed additional light on the comparatively poorly documented pre-Inkan era that was influenced by the Tiwanaku culture, which evolved along the southern

shore of Lake Titicaca around 400 AD and collapsed between 900–1100 AD [3]. Enrichment factors of lead (see Fig. 2) showed significantly elevated values above natural background levels within this period.
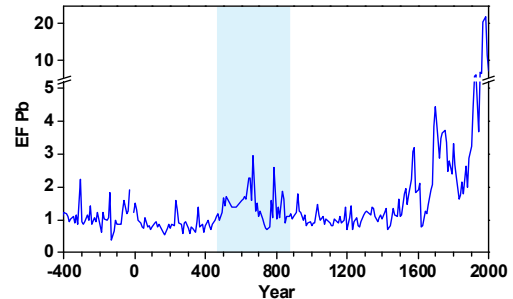
Fig. 2: Enrichment factors EF of lead (dark blue, 10-yrs median), with elevated lead levels during the time of the Tiwanaku-culture (shaded in blue).

This indication of early lead contamination corroborates the direct archaeological evidence [3] for silver production during this time span in the Lake Titicaca Basin i.e. in Puno Bay within a distance of ca. 250 km from Illimani. These archaeological finds suggest the smelting of argentiferous galena (Pb,Ag)S in furnaces similar to the wind-drafted *huayras* for silver production [2]. This indigenous technology as described by the Spanish conquerors (see Fig. 3) was traditionally used for Pb smelting until recently and might have led to excessive Pb volatilization [4]. The pre-Inkan lead enrichment found in an Illimani ice core gives further evidence for an early application of this technology.

Fig. 3: Two colonial drawings of huayras (left: end of 16th century [5], right: after Barba 1640).

ACKNOWLEDGEMENT

REFERENCES

[1] T. Kellerhals, PhD thesis, Univ. of Bern (2008).
[2] M.B. Abbott and A.P. Wolfe, Science, **301**, 1893 (2003).
[3] C. A. Schultze et al., PNAS, **106**, 17280 (2009).
[4] T. Rehren, Archaeology Int. **13**, 76 (2011).
[5] From the „Atlas of Sea Charts", courtesy of The Hispanic Society of America, New York.

THE ONSET OF NEOGLACIATION 6000 YEARS AGO IN THE MONGOLIAN ALTAI

P.-A. Herren, A. Zapf (Univ. Bern & PSI), A. Eichler, L. Tobler (PSI), H. Machguth (Univ. Zürich),
T. Papina (IWEP), M. Schwikowski (PSI & Univ. Bern)

Glacier highstands since the Last Glacial Maximum at around 25 ky BP are well documented for many regions but little is known about glacier fluctuations and low-stands during the Holocene. This lack of information is due to inaccessible dating material and the difficulty to identify minimum glacier extents. The discussion is ongoing to which degree high-mountain glaciers and ice caps have persisted throughout the Holocene [1]. A promising approach to resolve this issue is the use of high-resolution ice core records extracted from alpine glaciers. They may provide insight in former climate conditions and potentially give access to datable material in the basal ice itself or from the bedrock [2].

In July 2009 a joint Russian-Swiss expedition collected a 72 m surface-to-bedrock ice core in the Tsambagarav mountain range situated in the Mongolian Altai (4130 m asl, 48°39.338'N, 90°50.826'E). To establish a precise age-depth timescale different methods were applied [3]. Fig. 1 illustrates the final derived age-depth relation.

We interpret the basal ice age of 6000 years BP as indicative of ice-free conditions in the Tsambagarav mountain range at 4130 m asl. This age marks the transition from a mild climate, the Holocene Climate Optimum (HCO), to the colder Neoglaciation, allowing glaciers to advance. Glacier-hostile climatic conditions during the HCO caused an equilibrium line altitude (ELA) rise of at least 430 m from 3700 m asl nowadays to 4130 m asl. Extrapolating this increase in ELA to the surrounding glaciated areas results in complete degradation of the Mongolian glaciers south

of the Tsambagarav mountain range where the today altitude difference between ELA and summit is smaller than 430 m. To the north, glaciers must at least have declined severely as an ELA increase of 430 m would not be sufficient for complete disappearance under present conditions. This approach is conservative since the upper limit of the ELA-shift is defined by the elevation of Tsambagarav and might have been larger. Nevertheless the possibility remains that glaciers located on north facing slopes survived the ELA increase.

This study therefore suggests, that most of the current glaciers in the Mongolian Altai are not remnants of the Last Glacial Maximum but were formed during the second part of the Holocene.

ACKNOWLEDGEMENTS

REFERENCES

[1] Wanner et al., Quaternary Sci. Rev. **30,** 3109-3129 (2011).

[2] Jenk et al., J. Geophys. Res., **114**, D14305 (2009).

[3] P.-A. Herren et al., submitted to Quat. Sci. Rev.
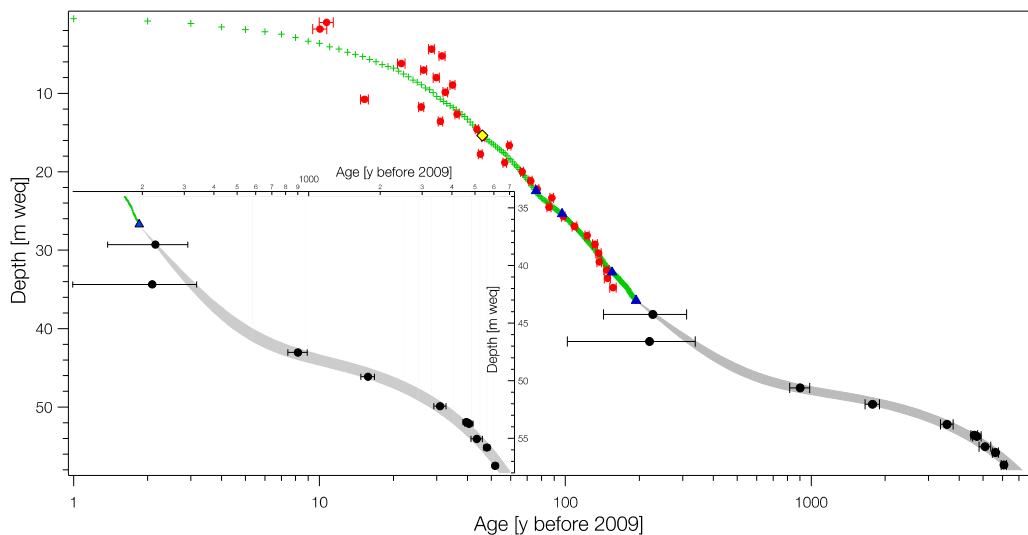
Fig. 1: Age-depth relation for the Tsambagarav ice core. Annual layer counting (green crosses), tritium peak (yellow diamond), volcanic eruptions (blue triangles), ^{210}Pb activity with analytical uncertainties (red circles), dating uncertainty for the lower part of the ice core (grey shaded area) and ^{14}C ages with the 1σ-uncertainties (black squares). Insert: magnification of the lower 36 m weq with identical symbols.

ICE CORE BASED ACCUMULATION RECONSTRUCTION FROM THE MONGOLIAN ALTAI

P.-A. Herren (Univ. Bern & PSI), A. Eichler (PSI), T. Papina (IWEP), M. Schwikowski (PSI & Univ. Bern)

For western Mongolia instrumental meteorological data is limited and spatially sparse. Here we use an ice core drilled in 2009 [1] to reconstruct precipitation in the Mongolian Altai.

TIME PERIOD AD 1815-2009

Annual accumulation rates can be reconstructed based on annual layer counting (ALC) combined with glacier flow models [2]. The accumulation was calculated from the ratio of the measured annual layer thickness (b_{ALC}) to the modelled thickness (b_{MODEL}), to correct for the nonlinear thinning, multiplied by the surface accumulation rate of 335 mm (derived from the last 10 years), see equation (1).

$$b = \frac{b_{ALC}}{b_{MODEL}} \cdot 335\, mm \quad (1)$$

According to Equation (1) the period from AD 1815 to 2009 experienced a mean net accumulation of 329 mm with a standard deviation of 91 mm (Fig 1a). The profile shows no trend although drier decades are identifiable around AD 1950 and 1910. The mean value is in good agreement with the surface accumulation of 335 mm and appears plausible in comparison with precipitation in the lowlands of less than 200 mm [3].

THE PAST 6000 YEARS

Due to strong thinning, ALC is not applicable regarding longer timescales. To reconstruct accumulation between two dated horizons (*i, j*) a different method was applied calculating the accumulation rate (b_{ij}) given by

$$b_{ij} = \frac{1}{\Delta t_{ij}} \int_{z_i}^{z_j} \left(1 - \frac{z}{H}\right)^p dz \quad (2)$$

where Δt_{ij} is the number of years between z_i and z_j. In order to describe variations in layer thinning observed in the age-depth relationship, different parameters p were used representing weak, medium, and strong thinning. The reconstructed accumulation rates differ largely with varying p yet following a similar trend. The three accumulation reconstructions were combined and are shown in Fig 1b. The past 6000 yr experienced three distinct phases of high, low, and again high accumulation rates. Lake sediment records from western Mongolia [4] showed that present conditions in central Asia are more humid relative to the past millennia, supporting the ice core derived elevated accumulation rates from AD 1815 to 2009 in Mongolia. In accordance with our accumulation reconstruction a shift of the Intertropical Convergence Zone (ITCZ) between Holocene Climate Optimum (HCO) and Neoglaciation could explain drastic changes in the precipitation pattern north of the Himalaya [5].

This is the first study reconstructing glacier accumulation in the Mongolian Altai for the last 6000 years.
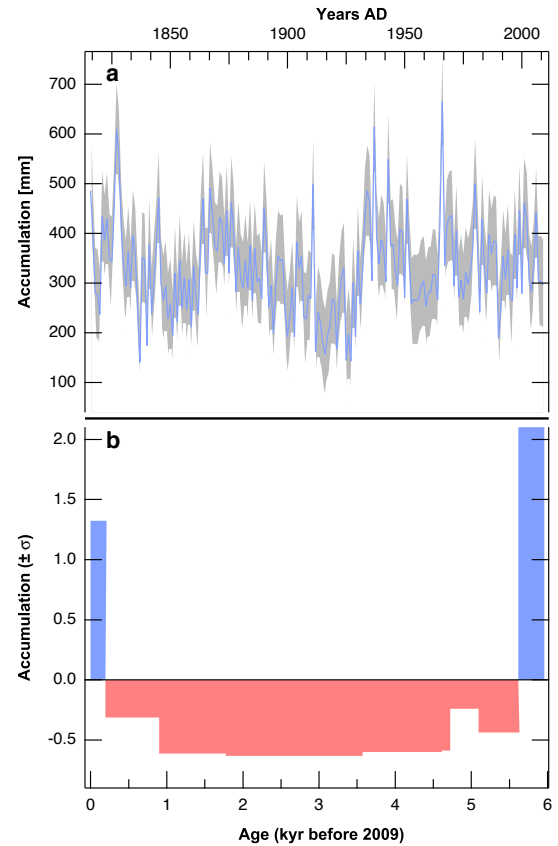
Fig. 1: (a) Accumulation profile for the period 1825 to 2009 AD in mm with 1σ uncertainties. (b) Accumulation reconstruction for the past 6000 yr. The three age-depth models representing weak, medium, and strong thinning were combined and presented as deviation from the mean.

ACKNOWLEDGEMENT

REFERENCES

[1] M. Schwikowski et al., Ann. Rep. Lab. of Radio- & Environ. Chem., Univ. Bern & PSI, p. 31. (2009),

[2] K. H. Henderson et al., J. Geophys. Res., **111**, D03104 (2006).

[3] M. Klinge et al., Erdkunde, **57**(4), 296–308 (2003).

[4] N. Rudaya et al., Quaternary Sci. Rev. **28** 540–554 (2009).

[5] Wanner et al., Quaternary Sci. Rev. **30,** 3109-3129 (2011).

MAJOR ION RECORDS FROM THE LOMONOSOVFONNA ICE CORE

I. Wendl (PSI & Univ. Bern), S. Brütsch, A. Eichler (PSI), E. Isaksson (NPI), T. Martma (Univ. Tallinn),
M. Schwikowski (PSI & Univ. Bern)

INTRODUCTION

Here, we present the full record of the water soluble major ions analysed in the 2009 Lomonosovfonna ice core. With those ions one can reconstruct climate variability and pollution back in time.

Generally, the ions can be clustered in groups, indicating different sources. Sodium, chloride, and methanesulphonic acid (MSA) are of marine origin; calcium mainly originates from terrestrial sources such as mineral dust; the main portion of nitrate is derived from anthropogenic activities; sulphate has several sources: (1) volcanic, (2) anthropogenic, and (3) marine; ammonium indicates a biogenic background; potassium and magnesium are derived from (1) marine, (2) anthropogenic or (3) terrestrial sources [1].

METHODS AND RESULTS

The ~149 m long ice core from Lomonosovfonna, Svalbard, was sampled at a resolution of 3-4 cm, with higher resolution in the lower part to account for glacial thinning towards bedrock. In total, this resulted in 3997 samples for liquid ion chromatography (Fig. 1).

The records of sodium and chloride are highly correlated ($R^2 = 0.95$) and the mean sodium to chloride ratio of 0.85 is very close to that of seawater (0.86). This indicates a common marine source. MSA, expected to peak during summer time due to a higher production rate of growing phytoplankton, shows a seasonal variation that may be used for dating purposes. The same accounts for ammonium that peaks in the springtime due to high biogenic activity. High calcium concentrations should correlate with dust layers in the ice core, indicating higher dust loadings reaching the archipelago of Svalbard. However, visible dust layers are very rare in this core. Thus, no clear correlation could be found. Nitrate, sulphate, potassium and magnesium show increased concentrations since the industrial revolution (~30 m weq). Before ~1850 AD (~60 m weq) sulphate mainly originates from marine or volcanic sources. Large volcanic eruptions can be used as time markers, such as the peak around 74.5 m weq in the sulphate record that reflects the Laki eruption that occurred 1783 AD in Iceland. Following the method described in [2] further volcanic eruptions were identified in the sulphate record: Kuwae 1459 AD and the unknown 1259 AD. Another tie point for the dating of the core is the tritium peak in a depth of ~23.2 m weq that marks the year 1963 AD. Evaluation of the preliminary dating with flow models is on-going.

REFERENCES

[1] M. Legrand & P. Mayewski, Rev. Geophys., **35**, 3 (2007).

[2] J.C. Moore et al., J. Geophys. Res., **117**, D03306 (2012).
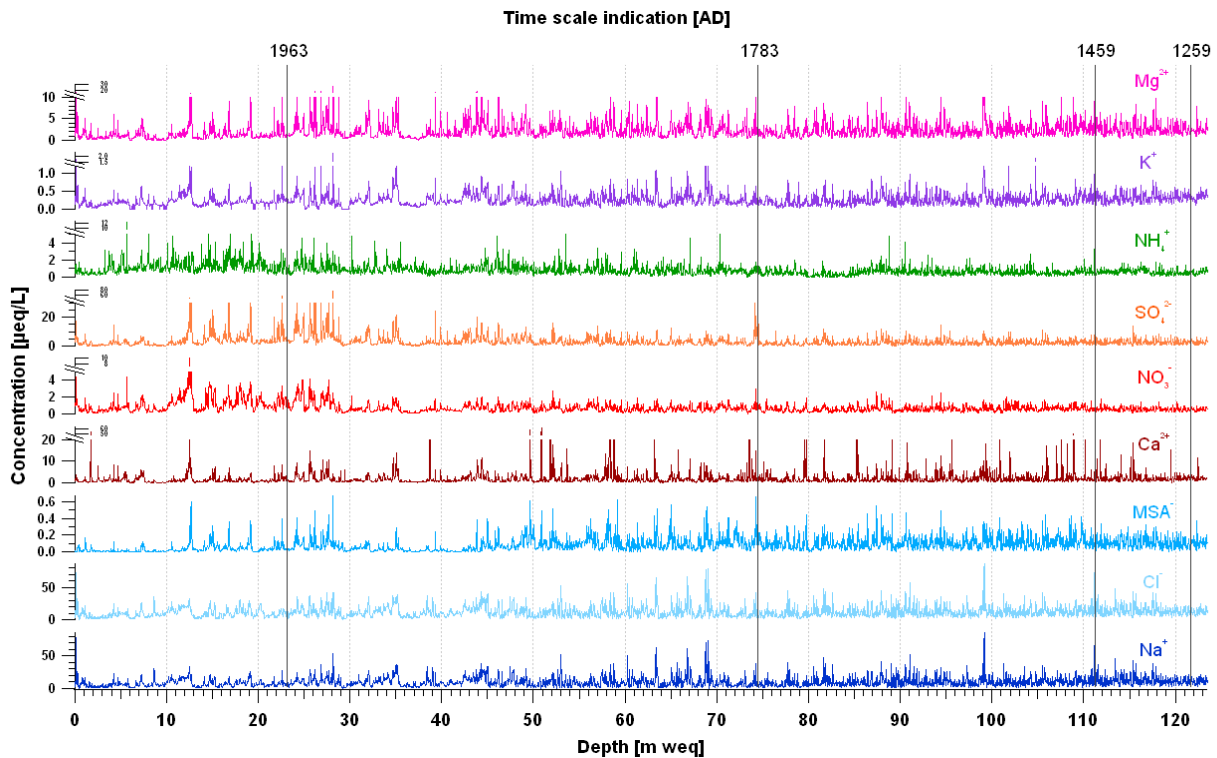
Fig. 1: Record of the major water soluble ions in the Lomonosovfonna ice core measured by ion chromatography. Preliminary dating horizons are given.

FIRST BLACK CARBON DATA FROM THE LOMONOSOVFONNA ICE CORE

I. Wendl (PSI & Univ. Bern), A. Eichler (PSI), M. Gysel, M. Laborde (PSI/LAC), I. Budde (Univ. Bern),
E. Isaksson (NPI), T. Martma (Univ. Tallinn), M. Schwikowski (PSI & Univ. Bern)

INTRODUCTION

Light-absorbing impurities in snow and ice, such as Black Carbon (BC), have a two-fold effect on the Earth's radiative balance: (1) they heat the atmosphere directly and (2) when deposited, they lower the albedo of the surface. In case of an ice or snow surface, this leads to accelerated melting and thus plays an important role, especially in the snow-covered regions such as the Arctic. The effect of BC on snow albedo was shown to be responsible for about a quarter of the observed warming by BC in total [1, 2]. In order to better understand the role of BC in the Arctic environment in the future, we need more data of the past. So far, only few studies on historical time-scales exist, including only one from the Arctic (Greenland [3]). Ice cores provide a unique opportunity to study climate relevant species on a long time-scale. With this study of BC in an ice core from Svalbard, Norway, we aim to provide further insight in the role of BC in the Arctic on historical time-scales.

MATERIAL AND METHODS

The Lomonosovfonna ice core was recovered from one of the highest glaciers in Svalbard, an archipelago north of Norway, in 2009. With a length of ~149 m it is thought to cover around 700 years of climate history.

The ice core was sampled at a resolution of 4 cm down to 108 m, further down with a resolution of 3 cm to account for glacial thinning towards bedrock. This resulted in a total of 4046 BC samples. The samples remained frozen until just prior to analysis, because refreezing or keeping them in liquid state for longer than a couple of hours resulted in BC loss [4]. After melting, the samples were sonicated for 25 min and then measured as soon as possible.

The BC mass concentration was determined with a Single Particle Soot Photometer (SP2, Droplet Measurement Technologies, Boulder, Colorado, USA) which measures BC mass on a particle-by-particle basis. A laser heats the BC particles to their boiling point (~4000 K) which then emit incandescent light. This signal is proportional to the BC mass in the particle.

Measuring liquid samples with the SP2 requires a nebulizing step because the SP2 can only measure dry aerosols. Thus the SP2 was coupled with an Apex Q jet nebulizer (High Sensitivity Sample Introduction System, Elemental Scientific Inc., USA) which showed the highest efficiency in nebulizing particles in the large range (up to ~700 nm). Those large particles contain most of the mass which is why they are important in order to study the climate effect of BC.

Calibration of the Apex Q/SP2-set-up was conducted with standards of known BC mass concentration (for further details see [4]).

RESULTS

The first 10 years of BC record from the Lomonosovfonna ice core indicate that the BC mass concentration varies with season (Fig. 1). The highest concentrations are expected to occur in late winter to early spring due to the Arctic Haze phenomenon. This is not always seen in the Lomonosovfonna record which can be explained by melting that causes a shift of the signal or by the dating uncertainty. Please note that Figure 1 includes only a preliminary dating, which will be refined soon.

The mean of 2.3 ± 2.6 ppb is in good agreement with previous BC studies on Svalbard snow [5]. The large spike in BC mass concentration around 1994 AD resembles that seen in the data of the fire markers oxalate and levoglucosan from Greenland snow, which was attributed to a known Canadian forest fire event [6].
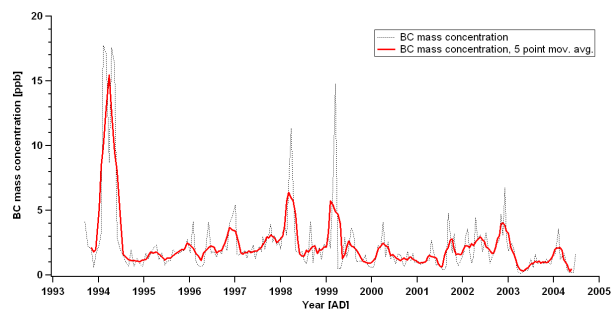
Fig. 1: BC mass concentration record for the upper part of the Lomonosovfonna ice core.

REFERENCES

[1] P. Forster et al., In: Climate Change 2007: The Physical Science Basis. Contribution of Working Group I to the Fourth Assessment Report of the Intergovernmental Panel on Climate Change [S. Solomon et al. (eds.)]. Cambridge University Press, Cambridge, United Kingdom and New York, NY, USA.

[2] J. Hansen & L. Nazarenko, PNAS, **101**, 2 (2004).

[3] J. R. McConnell et al., Science, **317**, 1381 (2007).

[4] I. Wendl et al., to be submitted.

[5] S. Forsström et al., J. Geophys. Res., **114**, D19112 (2009).

[6] N. Kehrwald et al., Tellus B, **64**, 18196 (2012).

LITTLE ICE AGE SIGNAL IN CARBONACEOUS PARTICLES FROM A BOLIVIAN ICE CORE

A. Zapf (Univ. Bern & PSI), T. Kellerhals (KUP), M. Sigl (DRI Reno), S. Szidat (Univ. Bern),
M. Schwikowski (PSI & Univ. Bern)

Organic aerosol particles in mid- to low-latitude ice cores have not been looked at in much detail in past paleoclimate studies and especially non-Alpine records are sparse. Those organic compounds include for instance primary biogenic aerosols, small particles originating from soil erosion and biomass burning as well as secondary organic aerosols that are formed in the atmosphere from volatile organic precursors. Due to the rather short atmospheric lifetime of typically few days organic aerosols directly reflect biospheric conditions at the source.

Our study presents for the first time a historical trend of particulate organic carbon (POC) and elemental carbon (EC) as recorded in the Illimani ice core (Bolivian Andes, 16°37'S, 67°46'W, 6300 m asl.). Back trajectory calculations (not shown) demonstrated that during most of the precipitation-intensive austral summer biogenic emissions from the south-western Amazon Basin reach the Illimani region. POC and EC determination was conducted as part of a method for radiocarbon dating of ice cores [1].

Carbonaceous particles occur abundantly in the investigated ice core section spanning the last 800 years. Ranging from 20 to 134 µg kg^{-1} (Fig. 1b), with an average of 73 µg kg^{-1}, POC concentrations are about twice as high as those reported for the years AD 1650 to 1940 in an ice core from the Alps [2]. Comparison of the POC record with a highly resolved temperature reconstruction from the same core (Fig. 1a) reveals consistent features during the time considered: i) the end of what is known as the medieval warm period at the beginning of the 13th century; ii) a distinct 300 year minimum/cold interval between AD 1410 and 1740, which likely corresponds to a pronounced Little Ice Age (LIA) event; iii) the sustained warming trend, which set in during the early 18th century and continued until the beginning of the 20th century. Given that, one can assume that POC emissions might largely be driven by temperature and biogenic productivity. Changes in accumulation as an alternative explanation for variations in carbonaceous aerosols are less likely considering the absence of a significant variability in accumulation-related dust tracers [4]. The EC record (Fig. 1c), a direct tracer for pre-industrial biomass burning, shows less definite characteristics. Although some of the lowest measured values occur during the LIA, the minimum is considerably less distinct.

With this study we provide another piece of evidence for a pronounced LIA interval in tropical South America and suggest POC as suitable tracer to determine trends in gross productivity of carbonaceous aerosols from regional bio-reservoirs.
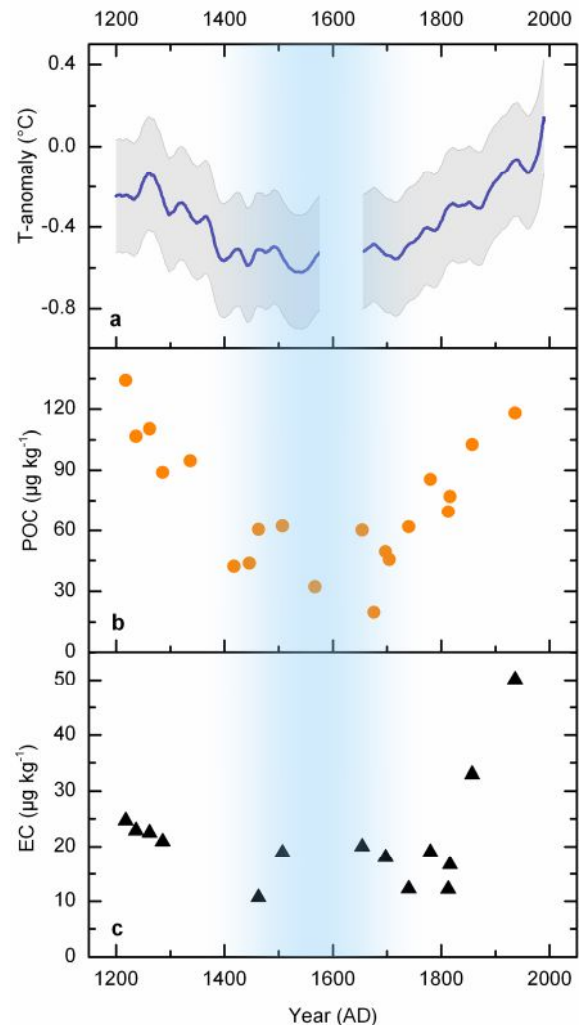
Fig. 1: 800-year records from the Illimani ice core. (a) Reconstructed tropical South American temperature anomalies (adapted from [3]). The grey shaded region envelops the ± 2σ uncertainty. (b) POC concentrations (orange circles). (c) EC concentrations (black triangles). Error bars representing the analytical uncertainty are smaller than the symbols. The blue shaded area indicates the timing of the LIA. Poor core quality precluded any chemical analysis for the time interval between AD 1580 and 1640.

REFERENCES

[1] M. Sigl et al., J. Glaciol., **55**, 194 (2009).
[2] T. Jenk et al., Atmos. Chem. Phys., **6**, 5381 (2006).
[3] T. Kellerhals et al., J. Geophys. Res., **115**, D16 (2010).
[4] S. Knüsel et al., J. Geophys. Res., **110** (2005).

FOSSIL AND NON-FOSSIL CONTRIBUTIONS TO CARBONACEOUS PARTICLES IN A FIRN CORE FROM FIESCHERHORN GLACIER

F. Cao (PSI & GIG CAS), Y.L. Zhang (Univ. Bern & PSI), S. Szidat (Univ. Bern), L. Wacker (ETHZ), M. Schwikowski (PSI & Univ. Bern)

INTRODUCTION

Carbonaceous particles which comprise organic carbon (OC) and elemental carbon (EC) are of increasing interest in climate research because of their influence on the radiation balance of the earth. The radiocarbon (^{14}C) determination of particulate OC and EC extracted from ice cores provide a powerful tool to reconstruct the historical natural and anthropogenic emissions of carbonaceous particles. A first long-term record of OC and EC concentrations along with the corresponding fraction of modern (f_M) carbon derived from radiocarbon (^{14}C) analysis in ice was published by Jenk et al. [1]. However, this ^{14}C-based source apportionment method has not been applied for the firn section due to the difficulties in decontamination. In this study, we analysed mass and ^{14}C content of OC and EC extracted from the firn section of Fiescherhorn glacier (46°33'3.2''N, 08°04'0.4''E; 3900 masl.).

METHODS

Detailed procedures on sample preparation, separation of the two fractions and applied analytical methods (AMS) can be found in [2]. In short, cutting of the firn samples and removal of possibly contaminated outer layers was performed in a cold room ($-20°$C) using a pre-cleaned stainless-steel band saw. After cutting, all parts were cleaned by chiselling to remove surface contamination. Afterwards, samples were preserved in pre-cleaned containers which were closed for melting at room temperature. The insoluble particles were extracted on quartz filters from melted firn samples by filtration, followed by acid treatment to remove carbonates. OC and EC were determined and separated by a recently developed thermal-optical method [3]. ^{14}C measurements were carried out with the MIni CArbon DAting System (MICADAS) with a gas ion source [4].

RESULTS AND OUTLOOK

The record of OC and EC apportioned by fossil and non-fossil contributions is shown in Fig. 1, covering the period from 1940-1986. In general, fossil contribution to EC was much larger than OC, indicating significant anthropogenic EC emissions due to the use of fossil fuels (coal, later oil and gasoline). From 1940 to 1960, both fossil and non-fossil OC concentrations were quite stable. In contrast to OC, fossil EC showed a sharp decrease until 1960, which is most likely due to a shift from coal burning towards liquid fuel in the residential sector. OC and EC from fossil sources increased thereafter to the maximum level in the 1970s, which was mainly driven by enhanced road traffic emissions. Decreasing concentrations in both OC and EC after 1970 are attributed to air pollution

control measures (i.e. a decrease in the emission factor of vehicle exhaust), aiming at reduction of emissions to the environment.

The remaining firn sections covering 1986-2002 will be analysed to reveal a more detailed picture of anthropogenic and natural contributions to carbonaceous particles in the most recent period.
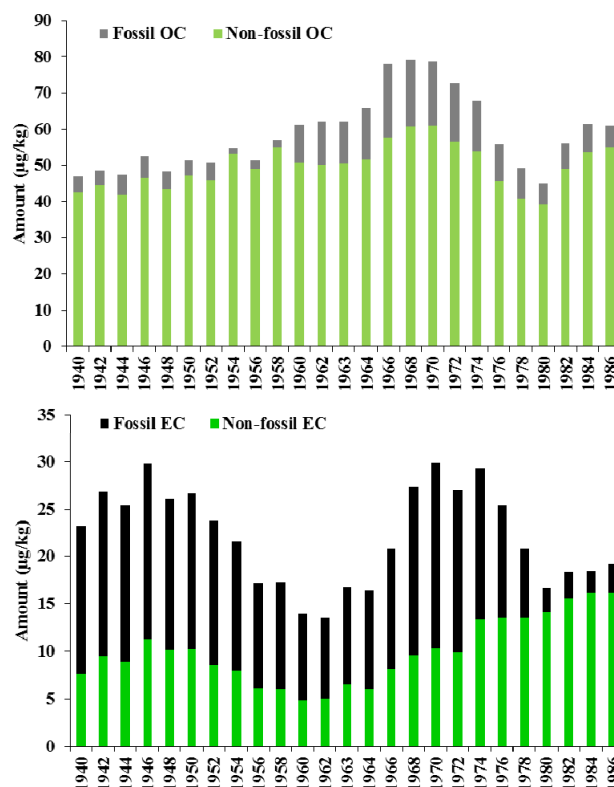
Fig. 1: Temporal changes of concentrations (µg/kg) of fossil and non-fossil OC and EC extracted from firn cores from Fiescherhorn glacier, covering 1940-1986.

ACKNOWLEDGEMENT

REFERENCES

[1] T. M. Jenk et al., Atmos. Chem. Phys., 6, 5381–5390 (2006).
[2] F. Cao et al., submitted to Radiocarbon.
[3] Y.L. Zhang et al., Atmos. Chem. Phys., 12, 10841-10856 (2012).
[4] L. Wacker et al., Nucl. Instrum. Methods B., 294, 315-319 (2013).

AN EXTRACTION SYSTEM FOR RADIOCARBON MICROANALYSES OF DISSOLVED ORGANIC CARBON (DOC)

J. Schindler (PSI & Univ. Bern), S. Szidat (Univ. Bern), M. Schwikowski (PSI & Univ. Bern)

INTRODUCTION

Glacier ice contains organic carbon (OC) which can be used for radiocarbon dating. In order to complement the well established method using the particulate organic carbon (POC) fraction [1-3], we currently assemble a setup for the extraction of dissolved organic carbon (DOC) from glacier ice. The majority of the carbon containing matter in snow and ice is present as DOC, which is, therefore, the most obvious carbon fraction for dating purposes. However, it is highly sensitive to contamination [4] and a recent study [5] did not succeed in utilising the DOC fraction for dating, suggesting artefacts of radiocarbon in-situ production in alpine glacier ice. To test this hypothesis and to gain further insight in the different OC fractions, we develop an extraction system for ultra-clean and efficient DOC extraction from glacier ice to CO_2.

SETUP

The system (Fig. 1) is designed to process up to 450 cm^3 of ice under an inert gas atmosphere. After thorough cleaning of the ice, it is melted in a glass vessel. The liquid sample is handled in an all-glass setup that is free of any carbon containing sealants or steel parts. This allows good cleaning of the entire setup and minimises blank values and memory effects. We filter the sample by vacuum filtration with a quartz fibre filter to separate the POC from the sample and transfer the filtrate to the quartz glass photo-reactor. The reactor design is similar to an existing DOC extraction system for radiocarbon dating of seawater samples [6]. In a first step, inorganic carbon is removed from the sample by acidification with H_3PO_4 and bubble degassing with helium via the central cooling finger. Afterwards, DOC is oxidised to CO_2 by external irradiation with a medium pressure UV lamp module. The sample is again purged with helium, which we use as a carrier gas for cryogenic trapping of the CO_2. A first cryogenic trap removes water vapour from the gas stream before the CO_2 is trapped at liquid nitrogen temperatures. The vacuum system (inset Fig. 1) is an adapted copy of the one used for the THEODORE combustion system at the University of Bern [7]. After trapping, the CO_2 is cleaned further from residual gas and the helium by repeated evaporation and freezing cycles. We determine its mass by manometry and sample it in glass vials for radiocarbon analyses with the AMS MICADAS system at the University of Bern.

OUTLOOK

Currently, we assemble the setup. Future work will include extensive system characterisation and blank minimisation.
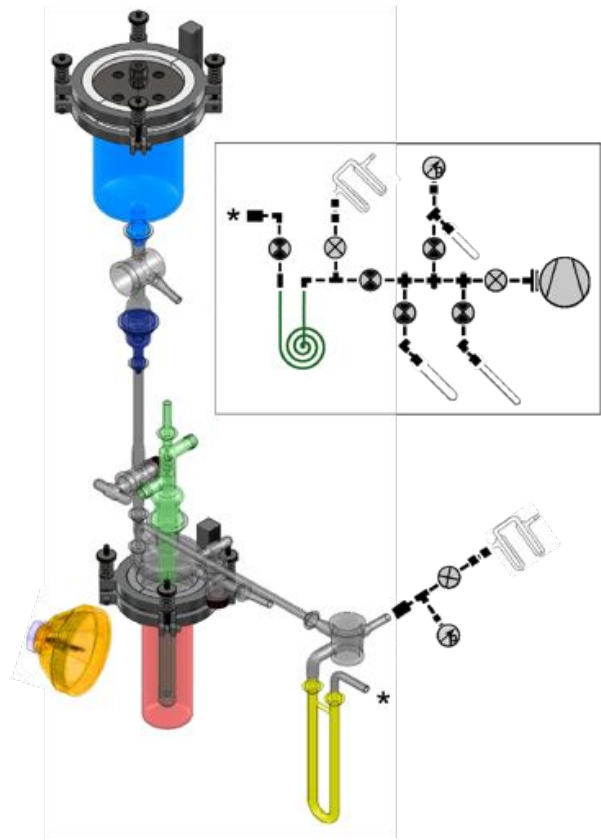
Fig. 1: The extraction setup: melting vessel (blue), filtration unit (dark blue), photo-reactor (red), UV lamp (orange), degassing and cooling finger (green) and water trap (yellow). The inset shows the vacuum line for cryogenic trapping and sampling the CO_2 from the photo-reactor, it is connected to the setup at the asterisk (dark green: CO_2 trap).

REFERENCES

[1] T. M. Jenk et al., J. Geophys. Res., **114**, D14305 (2009).
[2] M. Sigl et al., J. Glaciol., **55**, 194 (2009).
[3] I. G. M. Wientjes et al., J. Glaciol., **58**, 210 (2012).
[4] S. Preunkert et al., Environ. Sci. Technol., **45** (2011).
[5] B. May, PhD thesis, Univ. of Heidelberg (2009).
[6] S. R. Beaupré et al., Limnol. Oceanogr. Meth., **5** (2007).
[7] S. Szidat et al., Nucl. Instrum. Meth. Phys. Res. B, **223-224** (2004).

LINK BETWEEN SEASONAL ATMOSPHERIC PATTERNS AND WATER STABLE ISOTOPES FROM THE FIESCHERHORN ICE CORE OVER THE PERIOD 1978-2002

I. Mariani (Univ. Bern & PSI), A. Eichler (PSI), M. Schwikowski (PSI & Univ. Bern)

SUMMER AND WINTER PROXY

$\delta^{18}O$ in ice cores is often used as temperature proxy, and for annual layer counting, where maxima correspond to summer and minima to winter. If the seasonal cycle is well defined, and the dating uncertainty can be neglected, an investigation of the proxy on a sub-annual scale is possible. The Fiescherhorn ice core, drilled in December 2002 [1], fulfils these two requirements over the period 1978-2002 [2]. We analyzed its $\delta^{18}O$ maxima and minima, and the corresponding deuterium excess as a moisture proxy, and linked them to the sea level pressure and 500 hPa geopotential height fields, to investigate their relation with the atmospheric patterns in summer and winter. We defined summer and winter $\delta^{18}O$ as the average among the values above the 75th and below the 25th quantile, respectively, following the procedure suggested in [1]. Using the same $\delta^{18}O$ based classification we also obtained summer and winter deuterium excess values.

ANALYSIS OF FIELDS

For both proxies we selected the years with the highest (above the 80th quantile) and the lowest (below the 20th quantile) winter and summer values. We plotted the corresponding composite of sea level pressure and 500 hPa geopotential height anomaly fields (absolute units), using the Twentieth Century Reanalysis Project dataset [3]. We found anomalies generally stronger in winter than in summer, for both $\delta^{18}O$ and deuterium excess. In the years when winter $\delta^{18}O$ exceeds the 80th quantile, a positive sea level pressure anomaly is present over Mediterranean and a negative one over North Atlantic, slightly south of the Icelandic low. A similar pattern is found at 500 hPa. (Fig. 1). Higher than usual pressure conditions are therefore associated with enriched $\delta^{18}O$. A negative anomaly over British Isles was found in winter $\delta^{18}O$ lower than the 20th quantile. In summer, a similar negative anomaly is found over the same region and Northern Europe when $\delta^{18}O$ is lower than the 20th quantile. Summers with $\delta^{18}O$ higher than the 80th quantile show a positive anomaly over Northeastern Europe. The interpretation of the situations associated to the deuterium excess offers the opportunity to investigate the possible moisture sources of precipitation. This parameter is, at first approximation, associated with the air humidity at the evaporation site and is preserved along the air mass trajectory, except when secondary evaporation processes dominate (for example in summer, when moisture recycling occurs). When the winter deuterium excess exceeds the 80th quantile, a dipole structure, with generally positive anomalies over the North Atlantic and negative values over Scandinavia, is present. A pattern showing strong negative anomalies over North Atlantic and positive anomalies over the Mediterranean is found when deu-

terium excess is lower than the 20th quantile. This structure could lead to enhanced transport of Atlantic air to the Alps. Summers with the deuterium excess exceeding the 80th quantile show a complex structure with negative anomaly over the polar region, the Balkans and in correspondence of the Azores high, and a positive anomaly over the British Isles. The sea level field shows similar pattern, without the anomaly over the Balkans. When summer deuterium excess is lower than the 20th quantile, a negative anomaly is present over the North Sea and British Isles, together with a strengthening of the Azores high. This could increase the zonal flow over Europe, and reduce the land evaporation contribution, that usually increases the deuterium excess.
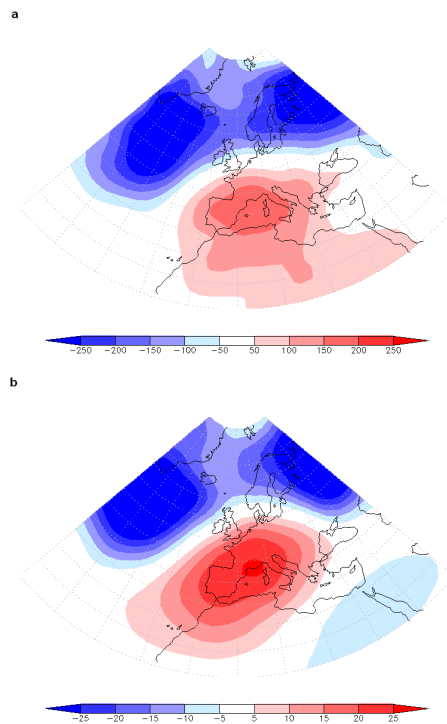
Fig. 1: Composite map of sea level pressure anomalies (a), and 500 hPa geopotential height anomalies (b), corresponding to the years having winter $\delta^{18}O > 80$th quantile. Anomaly fields, available on http://www.esrl.noaa.gov/psd/data/20thC_Rean/, evaluated for the reference period 1981-2010.

REFERENCES

[1] T. M. Jenk, PhD Thesis, Univ. of Bern (2006).
[2] I. Mariani, et al., Clim. Past Discuss., **8**, 5867-5891 (2012).
[3] G.P. Compo et al., Quart. J. Royal Met. Soc., **137**, 1 (2011).

TRACE ANALYSIS OF HYDROPHOBIC MICROPOLLUTANTS IN AQUEOUS SAMPLES USING TRAP CAPILLARIES

P.A. Pavlova (PSI, EMPA & Univ. Bern), P. Schmid, M. Zennegg (EMPA), C. Bogdal (ETHZ),
M. Schwikowski (PSI & Univ. Bern)

MOTIVATION

One of the main tasks of the project "Accelerated release of persistent organic pollutants (POPs) from Alpine glaciers" consists in analysing glacier ice for anthropogenic pollutants such as polychlorinated biphenyls (PCBs) [1]. Quantitative determination of such hydrophobic compounds in water poses several analytical challenges, including adsorption losses and high background contamination. Here, we present a new extraction method for organic pollutants in aqueous samples based on partitioning of the analytes from the water into the polydimethylsiloxane (PDMS) coating of an open tubular fused silica capillary developed in-house. It is aimed at easy handling, minimal sample volume, and reduced organic solvents consumption.

MATERIALS AND METHODS

Fused silica tubing of 0.32 mm internal diameter was coated with a film (thickness: 2 μm) of vinyl terminated PDMS. Coating of the capillary tubing and immobilization of the stationary phase using dicumyl peroxide as a cross-linker was based on methods described by Grob [2]. In order to avoid possible additional contamination and adsorptive loss of the analytes, the trap capillary is installed directly in the sampling container equipped with a special designed cap with an inlet for compressed air and a manometer. Before extraction, an internal standards mixture is added to the sample. Air pressure of approximately 100 kPa is applied to the bottle resulting in a flow rate through a 1 m capillary of around 1 mL/min. Following the extraction of the sample and the displacement of the water by air, the trapped analytes are eluted from the capillary with ethanol and the eluate is collected in a GC vial. Subsequently, after addition of a recovery standard, the extract is ready for analysis.

METHOD PERFORMANCE

Retention characteristics of the capillary trap were tested using a segmented capillary of 2 m total length consisting of four 0.5 m pieces connected with press-fit connectors. 250 mL water sample spiked with $^{13}C_{12}$-labeled iPCB mixture were passed through the capillary. The 4 segments were disconnected and eluted individually with ethanol. Figure 1 shows the cumulated recoveries of the $^{13}C_{12}$-labeled PCBs for the 4 segments. The partition of the analytes between the mobile and the stationary phase is defined as a first order kinetic process. The fraction of amount f_c, retained as a function of the length of the capillary is used to express the total fraction of amount entering the capillary f_{tot}. A curve fitted with the measured parameters revealed a capillary length ensuring recovery of 50% of the available PCBs below 1 m. The low

values of f_{tot} indicate losses of the respective analytes by adsorption to the walls of the sample container before entering the capillary.
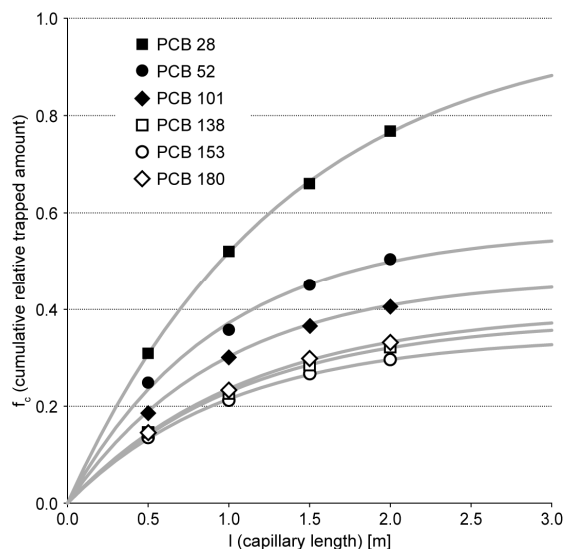
Fig. 1: Cumulated relative trapped amounts – f_c (points) and fraction of total amount – f_{tot} (grey lines) of $^{13}C_{12}$-labeled PCB congeners in the capillary segments relative to the set concentrations in the water sample [3].

CONCLUSIONS

Our method is shown to be comparatively impregnable to contamination, reproducible, and suitable for a wide range of applications. Therefore, the only restraint for detection of the analytes in environmental samples is determined by the measurement uncertainty and the instrumental detection limit.

ACKNOWLEDGEMENT

REFERENCES

[1] P. Pavlova et al., Ann. Rep. Lab. Radio- & Environ. Chem., Univ. Bern & PSI, p.38 (2011).
[2] K. Grob, Making and Manipulating Capillary Columns for Gas Chromatography, Dr. Alfred Hüthig Verlag, Heidelberg, Basel, New York, (1986).
[3] Pavlova et al. to be submitted to J. Chromatogr. A.

SETUP OF A PICARRO WATER STABLE ISOTOPES SPECTROMETER

I. Mariani (Univ. Bern & PSI), A. Eichler, S. Brütsch (PSI), M. Schwikowski (PSI & Univ. Bern)

CAVITY RING DOWN SPECTROSCOPY

In December 2011 a laser spectrometer for the measurement of liquid water isotopologues (L2130-I, Picarro) was installed in our laboratory at PSI (Fig. 1, left). The major advantage of this instrument compared to the conventional mass spectrometric methods is the simultaneous analysis of $\delta^{18}O$ and δD.
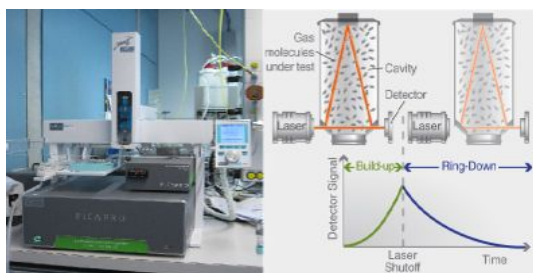
Fig. 1: (Left) L2130-i Picarro laser spectrometer, consisting of an autosampler, vaporizer of the liquid samples, cavity, wash stations to clean the syringe (milli-Q water and methylpyrrolidinone solution), two pumps for the sample removal, hardware and analyzer software. To keep a continuous flow, N_2 is flushed into the system during the measurement cycle. (Right) Scheme of the WS-CRDS technique.

The instrument is based on the Wavelength Scanned-Cavity Ring Down Spectroscopy technique (WS-CRDS, Fig. 1): A near-infrared laser (wavelengths corresponding to the water absorption lines), is used to illuminate a cavity with high reflectivity mirrors (99.999%) that increase the path length up to 20 km. After a build-up phase, the laser is abruptly shut off. Its intensity decreases exponentially, according to the Lambert-Beer law, because of the non-perfect reflectivity of the mirrors ("empty cavity" factor) and the absorbing species (sample). The analyzer measures this decreasing intensity and the total absorption coefficient (empty cavity and sample absorption) is calculated. With a known "empty cavity" factor, the contribution from the sample can be determined. The laser scans over different wavelengths to measure the absolute content of the isotopologues of water ($H_2^{16}O$, $H_2^{18}O$, HDO). An individual measurement, including injection, pre- and post-cleaning of the syringe, evaluation, and sample removal takes about nine minutes. For each sample this procedure is repeated six times to avoid memory effects, so that a complete analysis takes about 1 hour.

TESTS AND LABORATORY STANDARDS PREPARATION

Stability and memory tests were performed to characterize the instrument. Stability was evaluated performing a long-term measurement of two laboratory standards Haus3 ($\delta^{18}O$=-10.03‰, δD=-71.7‰), and Miki2 ($\delta^{18}O$=-20.2‰, $\delta D \approx$-95‰). A drift was observed depending on the isotopic value. $\delta^{18}O$ drift:

0.15‰/day for Haus3 and 0.2‰/day for Miki2. δD drift: 0.7‰/day for Haus3 and 1‰/day for Miki2. The memory effect was evaluated following the procedure suggested on www.picarro.com. Among six injections, we assumed as true value the average over the last three and compared each injection with it. The memory effect decreased from 2% for the first three injections to less than 0.2% for the last three. We therefore established to use the average over the last three injections as final result. The analytical uncertainty, defined as the standard deviation among the last three injections was 0.1‰ for $\delta^{18}O$ and 0.5‰ for δD, not significantly dependent on the isotopic value, and stable over time. The δD uncertainty is lower than with other methods (Fig.2).
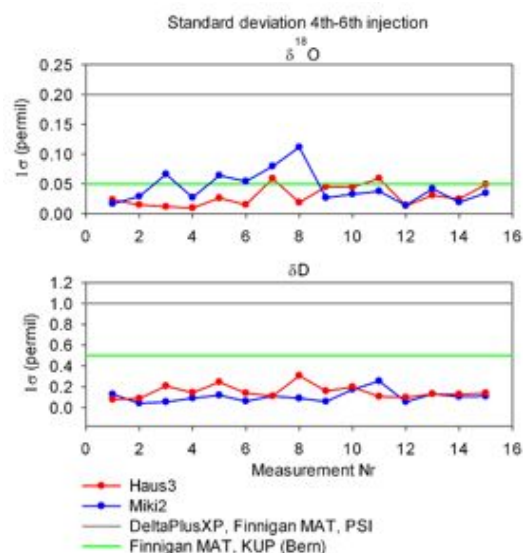
Fig. 2: Standard deviation of the 4th-6th injection as a function of time. $\delta^{18}O$ (top), δD (bottom). Haus 3 (red), Miki2 (blue). Gray and green lines are the estimated analytical uncertainty from other methods.

Finally, three internal laboratory standards Scuol ($\delta^{18}O$=-23.77‰, δD=-181.3 ‰), Rueras ($\delta^{18}O$=-17.09‰, δD=-124.1 ‰), and Labwater ($\delta^{18}O$=-9.95‰, δD=-70.6‰) were prepared and calibrated with four IAEA standards [1]. Each of them is stored in 2.5 L bottles for future use.

ACKNOWLEDGEMENTS

REFERENCE

[1]   M. Ahmad, et al., IAEA Final report (2012).

FIRST RESULTS FOR THE DISTRIBUTION OF ^{129}I IN MEGAPIE SAMPLES

B. Hammer, A. Türler (Univ. Bern & PSI), D. Schumann, J. Neuhausen (PSI), M. Wohlmuther (PSI/GFA),
C. Vockenhuber (ETHZ/Laboratory of Ion Beam Physics)

INTRODUCTION

When LBE is used as coolant or target material in future accelerator driven nuclear power plants, isotopes of practically all chemical elements will be produced by different nuclear reactions [1]. For a safe operation of such facilities, the knowledge of their radionuclide inventory is mandatory. Therefore, the radiochemical analyses of irradiated LBE is important to benchmark theoretical predictions as well as estimating safety hazards of future LBE nuclear facilities during and after operation, including also options for intermediate or final disposal.

In a liquid metal spallation target, among others, the long-lived halogen radionuclides ^{129}I ($t_{1/2}$= 1.57x10^7 y) and ^{36}Cl ($t_{1/2}$= 3.01x10^5 y) are produced. We chemically separated these nuclides from samples taken from the MEGAPIE target [2] and analysed them by accelerator mass spectrometry (AMS). First results about the distribution of ^{129}I in MEGAPIE are presented here.

EXPERIMENTAL

Iodine and chlorine were separated from the LBE by distillation. For this purpose, 12 mg of LBE, iodine carrier (about 12 mg) and chlorine carrier (10 mg) were dissolved in 5 ml 7 M HNO$_3$ in a three-neck-flask in a N$_2$ atmosphere at room temperature. After completely dissolving the LBE, the reaction mixture was heated up to 100 °C. Iodine and chlorine were distilled into an aqueous hydrazine solution. The hydrazine solution was acidified with 7 M HNO$_3$ and AgNO$_3$ was added, forming a white precipitate of AgI and AgCl. The precipitate was filtered and redissolved in NH$_3$ (25%). AgCl is soluble in NH$_3$, whereas AgI is insoluble. AgI was filtered and washed 3 times with 5 ml 7 M HNO$_3$ and dried for about 24 hours at 80 °C. The AgCl fraction was acidified with 7 M HNO$_3$ and AgCl was re-precipitated and washed with bi-distilled H$_2$O. The chlorine samples were dried for about 24 hours at 80 °C. The iodine and chlorine samples were diluted for the AMS measurement at ETHZ.

RESULTS

The ^{129}I samples were measured at the 500 kV AMS facility TANDY at Laboratory of ion Beam Physics at ETH Zurich. The preliminary results obtained for ^{129}I are shown in Tab. 1 and Fig. 1. The measured activity concentrations found for ^{129}I are 3 to 6 orders of magnitude lower than those predicted by calculations [3]. At the moment we have no explanation for this finding. From the studies in [4], we know that the method for the separation of iodine works well. An explanation of these observations could be that, due to its volatility, iodine has been evaporated from the LBE. However, according to [5] iodine starts to evaporate from LBE only at about 500 °C. Because the

operating temperature of MEGAPIE was < 340 °C, significant evaporation is unlikely. If iodine was indeed evaporated from the LBE, either the isotope ^{131}I should have been detected in the off-gas during operation, which was not the case, or the evaporated iodine was completely deposited within the cover gas system of MEGAPIE. In the latter case, it should be partly deposited on the absorber foils installed into the cover gas system. The analysis of these foils is ongoing. Another explanation could be that iodine is deposited in sections of the target that have not been sampled. The results of ^{36}Cl by AMS measurements will be available in the beginning of 2013.

Tab. 1: Results of ^{129}I samples. The uncertainty of these measurements was ± 10 %.

Sample	A_{conc} (Bq/g)	Sample	A_{conc} (Bq/g)
H02-U2_St1	4.61E-8	H06-U-b	7.07E-8
02-U2_St2	3.16E-8	H06-D2-b	1.68E-6
H02-D2	7.52E-8	H06-D2-S	3.09E-6
H03-U6	4.96E-7	H06-S	2.69E-8
H03-U12	1.11E-7	H07-Ub	2.15E-8
H03-D2	2.41E-6	H07-S-b	2.26E-8
H03-D4	8.48E-8	H07-D-b	3.46E-8
H04-B	1.57E-8	H07-U2	1.06E-6
H04-U	3.48E-8	H07-S	4.5E-7
H04-D	4.21E-8	H07-S10	2.79E-8
H05-U2-b	5.49E-8	H08-U1-b	1.48E-6
H05-D3-b	3.46E-8	H08-U2	2.47E-7
H05-B-b	2.18E-6	FLUKA	1.09E-2
H05-D22	1.52E-8	MCNPX	9.35E-3
H05-U	4.04E-8		
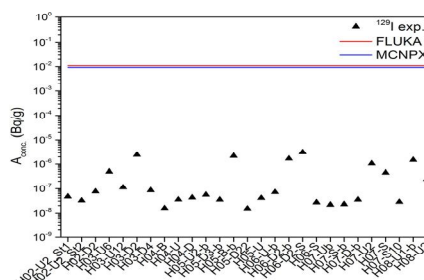
Fig. 1: First results for ^{129}I compared with FLUKA and MCNPX predictions.

REFERENCES

[1] A.Yu. Konobeyev et al., Nucl. Instrum. Meth. Phys. Res. A, **605** (2009).
[2] B. Hammer et al., Ann. Rep. Lab. of Radio- & Environ. Chem., Univ. Bern & PSI, p. 52 (2011).
[3] L. Zanini et al., PSI Report Nr. 08-04 (2008).
[4] T. Lorenz et al., Ann. Rep. Lab. of Radio- & Environ. Chem., Uni Bern & PSI p. 46 (2012).
[5] J. Neuhausen et al., Radiochim. Acta, **94** (2006).

NEUTRON CAPTURE CROSS SECTION OF UNSTABLE ^{63}Ni: IMPLICATIONS FOR STELLAR NUCLEOSYNTHESIS

C. Lederer (Goethe University of Frankfurt), D. Schumann, R. Dressler (PSI), N. Kivel (PSI/NES),
C. Massimi (INFN Bologna), and the n_TOF Collaboration (www.cern.ch/ntof)

INTRODUCTION

The elements heavier than Fe are dominantly synthesized by neutron capture reactions in stars. The slow neutron capture process (s-process), which is taking place in environments of relatively small neutron densities, is responsible for about half of the overall elemental abundances. The reaction path of the s-process proceeds close to the valley of stability on the nuclear chart, since radioactive decays are usually faster than neutron captures on unstable species. For long lived radioisotopes, however, subsequent neutron capture may compete with β-decay. This is the case, e.g. for ^{79}Se (half life 0.5 Myear) or ^{63}Ni (half life of 101 years). In particular, ^{63}Ni is produced in massive stars during two different burning stages: During the He-core burning phase, where neutron densities are too low for an additional neutron capture of ^{63}Ni, and later, during the C-shell burning phase, where neutron densities are magnitudes higher and therefore, ^{63}Ni is dominantly expended via neutron capture rather than β-decay. This means that during C-shell burning ^{63}Cu and subsequent ^{64}Zn are bypassed and ^{63}Cu can only be produced by β-decay of the remaining ^{63}Ni. To understand and model the abundance of Cu isotopes in our universe the neutron capture cross section on ^{63}Ni provides an important information since it determines the amount of ^{63}Ni which is left after the s-process [1]. This motivated the first measurement of the ^{63}Ni(n, γ) reaction at neutron energies above thermal (25 meV) at the n_TOF (neutron time-of-flight) facility at CERN.

MEASUREMENTS AND RESULTS

At n_TOF, a highly intense, pulsed neutron beam is produced via spallation reactions of 20 GeV/c protons on a massive Pb target. The pulsed proton beam allows determining the energy of a single neutron via its time-of-flight. The initially very energetic neutrons are slowed down by a water moderator around the spallation target. Afterwards, the neutron spectrum is ranging from thermal neutron energies up to several GeV. The neutrons travel a distance of 185 m to the target and measurement station, which guarantees a high resolution of the neutron energy. The prompt capture γ–rays were measured using a pair of liquid scintillation detectors, optimized for a low sensitivity to the background from scattered neutrons [2].

The ^{63}Ni sample was produced about 20 years ago by irradiating 1 g of highly enriched ^{62}Ni in a high flux reactor. This resulted in an amount of about 12% of ^{63}Ni. To avoid background reactions due to the neutron capture of the decay product ^{63}Cu, the sample was chemically purified by dissolving the Nickel foil in 7 M HNO$_3$ and precipitating CuS with H$_2$S. After separation of the liquid phase from the copper sulphide, NaOH was added to the Ni-containing

solution to produce Ni(OH)$_2$, which was transformed into the oxide by calcination at 800°C. Details of the sample preparation are described in [3].
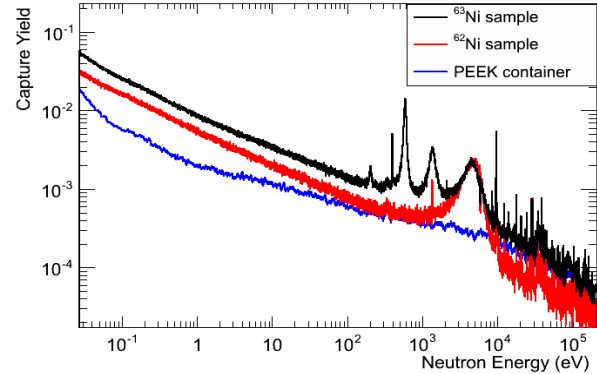
Fig. 1: Neutron capture yield of the ^{63}Ni sample (black) compared to the empty sample container (blue) and a ^{62}Ni sample (scaled to the ^{62}Ni content in the ^{63}Ni sample) [4].

The neutron capture cross section of ^{63}Ni was measured up to 200 keV neutron energy [4]. Figure 1 shows a comparison of the capture yield of the ^{63}Ni sample, the empty sample container made of PEEK (Polyetheretherketone), and a ^{62}Ni reference sample, because ^{62}Ni represents the largest impurity in the sample. In total 12 resonances of the ^{63}Ni(n, γ) reaction were observed for the first time and the capture kernels, which are a measure for the strength of the resonance, were determined. The cross section averaged over the stellar neutron spectrum (Maxwellian Averaged Cross Section) was determined from temperatures corresponding to kT=5 keV to kT=100 keV with uncertainties around 20%.

The presented results are about a factor of 2 larger than previous theoretical estimates quoted in the KADoNiS compilation [5]. Stellar model calculations show a large effect of the new cross section on the s-process abundances of the species ^{63}Cu, ^{64}Ni, and ^{64}Zn. This new information will allow stronger constraints on explosive nucleosynthesis in the supernova explosion.

REFERENCES

[1] M. Pignatari, et al., Astroph. J. **710**, 1557 (2010).
[2] C. Guerrero, et al. (the n_TOF Collaboration), *submitted to* Eur. Phys. J. (2012).
[3] D. Schumann, et al., *submitted to* Radiochim. Acta (2012).
[4] C. Lederer, et al. (the n_TOF Collaboration), Phys. Rev. Lett. **110**, 022501 (2013).
[5] I. Dillmann, et al., EFNUDAT workshop, JRC-IRMM, (2009). http://www.kadonis.org

THERMOCHROMATOGRAPHY STUDY OF TELLURIUM.
PART 1: ELEMENTAL TELLURIUM

E.A. Maugeri, J. Neuhausen, D. Piguet, A. Vögele, D. Schumann (PSI), R. Eichler (Univ. Bern & PSI)

INTRODUCTION

Lead-Bismuth Eutectic (LBE) is an alloy proposed as coolant and spallation target material for accelerator-driven systems. One of the main problems of using LBE in such systems is related to the production of Po, due to its radiotoxicity and the relatively high volatility of its compounds. The formation of different Po compounds at operating conditions depends on the cover gas, i.e. its redox potential and presence of moisture. The method of thermochromatography can be used to obtain different polonium compounds at different conditions and to study their relative volatility. Here, we present the results of thermochromatography experiments with Te in inert and reducing carrier gas atmospheres. Te was chosen as the closest light homologue of Po, to model and design the experiment for studying Po.

EXPERIMENTAL

A target of metallic Sn was irradiated with α-particles (36 MeV, 200 nA) for 10 hours at the PSI Philips Cyclotron to produce ^{121}Te. The obtained Te was separated from the Sn matrix by evaporation at 1223 K under He flow and deposition onto Au or Ta foils. The obtained samples were studied using a thermochromatography setup consisting of a fused silica tube in a negative gradient furnace with a temperature profile ranging from 1223 to 168 K equipped with a carrier gas inlet and a Ta-getter. The deposition distribution was measured with 1 cm resolution using standard γ-spectrometry with a lead collimator (window size 1 cm) in front of a HPGe-detector.

THERMOCHROMATOGRAPHY WITH REDUCING AND WITH INERT CARRIER GAS

The thermochromatogram of Te evaporated from a Ta-foil using pure hydrogen, purified by a hot Ta getter, as carrier gas, is presented in Fig. 1 (yellow bars). It shows a sharp peak centered at 702 K, indicating that only one species was transported and deposited in the column. Only elemental Te, SnTe, and TeH_2 can be formed at these chemical conditions, considering the absence of water and oxygen and the reduction potential of pure hydrogen. The formation of TeH_2 can be excluded since this compound has a boiling point of 269 K and is unstable above 273 K [1]. Using the Monte Carlo adsorption model [2] (solid red line in Fig. 1), an adsorption enthalpy of the Te species on quartz surfaces was calculated as -163 ± 10 kJ·mol^{-1}. The thermochromatogram of Te evaporated from gold using as carrier gas pure, dry and O_2 free He, is presented in Fig. 1 (grey dots). Also in this case a single sharp peak, centered at 722 K, was obtained. Using the Monte Carlo simulation method, an adsorption enthalpy of this Te species on quartz was

calculated as -171 ± 10 kJ·mol^{-1}. Considering the uncertainty of the method, ± 10 kJ·mol^{-1}, it was concluded that the same species were obtained in the two experiments. Using the adsorption enthalpy of -167 ± 10 kJ·mol^{-1} (averaged value) in the empirical correlation between the adsorption enthalpy and the sublimation enthalpy of the elements [3], a sublimation enthalpy of 229.3 ± 16 kJ·mol^{-1} was calculated for the species. Taking into account the uncertainly of our results, it is not possible to conclude whether this deposition corresponds to elemental Te or SnTe (formed in the separation of ^{121}Te from the irradiated Sn matrix), since their sublimation enthalpies are 211.7 and 222 kJ·mol^{-1} [4], respectively.
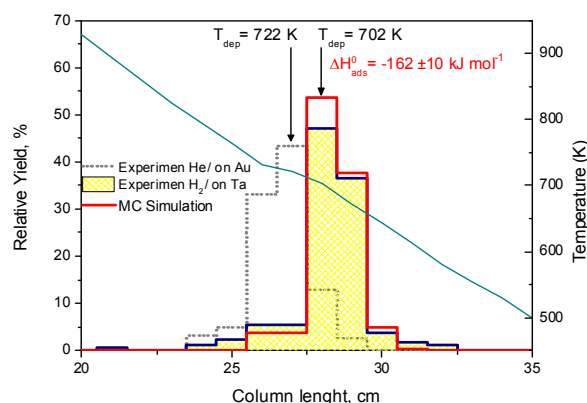
Fig. 1: Thermochromatogram of ^{121m}Te deposited on gold using as He (grey dots) and on tantalum using as carrier gas H_2 (yellow bars). The solid red line represents the Monte Carlo simulation of the Te deposited on tantalum.

CONCLUSION

One single species of Te was obtained in thermochromatography experiments starting from Ta and Au foils, using inert (He) and reducing (H_2) carrier gases. The adsorption and sublimation enthalpies of the observed species were calculated to be -167 ± 10 kJ·mol^{-1} and 219.3 ± 16 kJ·mol^{-1}, respectively. Based on these values it was not possible to determine wether the deposited species is elemental Te or SnTe. No volatile compound, such as TeH_2, was observed.

REFERENCES

[1] N.N. Greenwood, A. Earnshaw, "Chemistry of the Elements", Elsevier Science & Technology Books (1984).
[2] I. Zvara, Radiochim Acta, **38**, 95 (1985).
[3] A. Serov, et al. Radiochim. Acta, **99**, 95 (2011).
[4] K.C. Mills, "Thermodynamic data for inorganic sulphides, selenides and tellurides", Butterworths, London (1974).

THERMOCHROMATOGRAPHY STUDY OF TELLURIUM.
PART 2:TELLURIUM OXIDES

E.A. Maugeri, J. Neuhausen, D. Piguet, A. Vögele, D. Schumann (PSI), R. Eichler (Univ. Bern & PSI)

INTRODUCTION

This report presents the results obtained on the volatility of Te oxides by thermochromatography (TC). Sample preparation and device description are given in [1]. The different Te oxides were obtained by using carrier gases with varying redox potential.

RESULTS

Table 1 summarizes the experimental conditions, the deposition temperatures, and the deduced adsorption and sublimation enthalpies of the proposed chemical species of each studied sample.

Tab. 1: Summary of the results.

Sample number	Te01		Te02	Te03
Carrier gas	H_2/H_2O		O_2	O_2
T_{dep} (K)	1030	702	857	780
ΔH_{ad}(kJ·mol^{-1})	-237±10	-162±10	-204±10	-185±10
ΔH_s(kJ·mol^{-1})	339 ± 20	219 ±16	291 ±25	255±15
Chemical species	TeO	Te	TeO_2	TeO_3

Sample Te01 was studied by TC using H_2 with 0.3% of water as carrier gas. The obtained thermochromatogram (TCm), Fig. 1 (A), shows two main peaks, at 1030 and 702 K, and a broad band ranging from 550 to 330 K. The presence of water increases the oxidizing potential of the carrier gas, promoting the formation of Te-compounds with higher oxidation state, compared to those found in pure H_2. The peak at 702 K was attributed to elemental Te or SnTe [1]. The broad band can be due to transport reactions of elemental Te by a reaction with water, forming more volatile compounds, most likely hydroxides. The peak at 1030 K was assigned to TeO. The Monte Carlo simulation (MCS) [2] of the peak at 1030 K (red solid line in Fig. 1 (A)) yields an adsorption enthalpy of -236.8 ± 10 kJ·mol^{-1}. Using the correlation reported in [3], a value of sublimation enthalpy of 339 ± 20 kJ·mol^{-1} was calculated. Using the enthalpy of formation of solid TeO calculated in [4] as -156.2 kJ·mol^{-1} and the enthalpy of formation of gaseous TeO reported in [5] as 180 kJ·mol^{-1}, (other works report different values, ranging from 69 to 92 kJ·mol^{-1} [6]), a sublimation enthalpy of 336 kJ·mol^{-1} was estimated, in good agreement with the value derived empirically from the adsorption results in this work. Sample Te02 was studied using oxygen as carrier gas dried with P_2O_5. Fig. 1 (B) (yellow bar) shows the obtained TCm characterized by one peak centred at 857 K. The most probable species was considered to be TeO_2 since it is the most stable oxide of tellurium [7]. Using the MCS [2], an adsorption enthalpy of -204 ± 10 kJ·mol^{-1} was obtained (red solid line in Fig. 1 (B)). Using this value in the empirical

correlation [3] a sublimation enthalpy of 290 ± 25 kJ·mol^{-1} was calculated. This value is in good agreement with the sublimation enthalpy reported in [8] and [9] for TeO_2, 291 and 264 kJ·mol^{-1}, respectively.

In one experiment, Te03, using dry O_2 as carrier gas, a deposition at 780 K was obtained, green bar in Fig. 1 (B). Adsorption and sublimation enthalpies of -185± 10 and 255 ± 25 kJ·mol^{-1}, respectively, were calculated for this species. Considering the absence of large amounts of water, the high oxidation potential of the carrier gas and the higher volatility (compared to TeO_2) we tentatively assign this species to TeO_3.
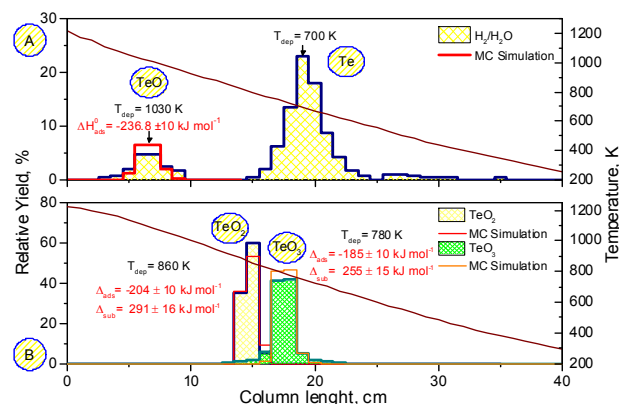
Fig. 1: (A) TCm of Te and TeO using as carrier gas H_2/H_2O; (B) TCm of TeO_2 and TeO_3 using as carrier gas dry O_2.

CONCLUSION

TeO, TeO_2 and TeO_3 were obtained using carrier gases with varied redox potential. This work proves that the volatility of Te oxides increases with the Te oxidation state, which can be expected for a main group element.

REFERENCES

[1] M. Maugeri et al., Ann. Rep. Lab. of Radio- & Environ. Chem., Univ. Bern & PSI p. 40 (2012).
[2] I. Zvara, Radiochim Acta, **38**, 95 (1985).
[3] A. Serov et al., Radiochim. Acta, **99**, 95 (2011).
[4] J. Neuhausen, R. Eichler, "Extension of Miedema's Macroscopic Atom Model to the Elements of Group 16 (O, S, Se, Te, Po)", Report No. 03-13, PSI (2003).
[5] J.P. Coughlin, Bulletin No. 542, U. S. Bureau of Mines, Washington, D. C., 1954.
[6] T.S.L. Narasimhan et al., Thermochim. Acta, **427**, 137 (2005).
[7] V.P. Itkin, C.B. Alcock, JPE, **17,** 533 (1996).
[8] D.W. Muenow et al., T. Faraday Soc., **65**, 3210 (1969).
[9] I. Barin, "Thermochemical data of pure substances", Weinheim, New York (1995).

THERMOCHROMATOGRAPHY STUDY OF TELLURIUM.
PART 3: EFFECTS OF H_2O ON TELLURIUM OXIDES

E.A. Maugeri, J. Neuhausen, D. Piguet, A. Vögele, D. Schumann (PSI), R. Eichler (Univ. Bern & PSI)

INTRODUCTION

This report presents the transport reactions of TeO_2 induced by variable contents of moisture in the carrier gases with different oxidizing potential studied by thermochromatography (TC). The device description is given in [1].

RESULTS

Sample TeO_x1, Table 1, was pre-oxidized in a furnace at around 700 K in oxygen, to oxidize the Te to TeO_2. The sample was then studied with TC using pure He as carrier gas. Fig. 1 (A), blue bars, shows the obtained thermochromatogram (hereafter TCm), which is characterized by the deposition of one single species at 930 K.

Tab. 1: Carrier gas composition in different experiments.

	TeO_x1^*	TeO_x2	TeO_x3	TeO_x4
Carrier gas	He	O_2	O_2	$He/H_2O_2^{**}$
% H_2O	-	10^{-4}	0.3	0.3

*The sample was pre-oxidized. **H_2O with 30% of H_2O_2.

Considering the inertness of the carrier gas, the deposited species can only be TeO_2. After TeO_2 was deposited, the same column was subjected to another TC experiment using He with 0.3% of H_2O as carrier gas to study the reaction between TeO_2 and H_2O. The obtained TCm, grey dot bars in Fig. 1 (A), shows that no transport reaction occurs at the deposition temperature of 930 K. Another pre-oxidized sample was directly studied using He with 0.3% of H_2O as carrier gas. The TCm (not shown) also does not show any transport reaction. This results confirm that TeO_2 does not react with water [2].
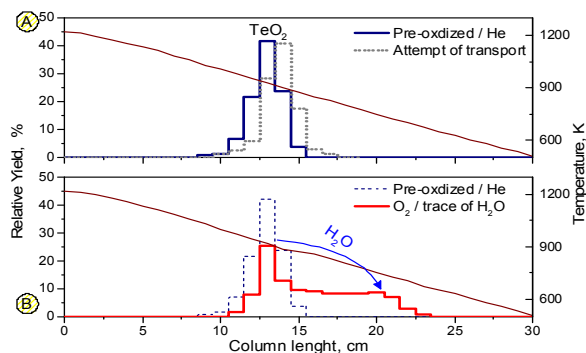
Fig. 1: (A) TCm of TeO_2 from a pre oxidized sample using He as carrier gas (blue bars); (B) TCm of a TeO_2 using as carrier gas O_2 with trace of H_2O (red bars).

Sample TeO_x2 was studied using O_2 with traces of H_2O (~ 10 ppm) as carrier gas. The obtained TCm, red bars in Fig. 1 (B), shows that a transport reaction took place, forming a more volatile species, likely an oxyhydroxide. In this case O_2 could react at the high temperatures in the gradient (1223 K) with H_2O forming hydroxide ions, hydroperoxide ions and H_2O_2, which are more reactive than H_2O. At this stage, we are unable to identify the formed species. Theoretical studies are currently performed to study the stability of the different Te-oxyhydroxides.

For the sample TeO_x3, O_2 with 0.3% of H_2O was used as carrier gas. The TCm obtained, green bars in Fig.2 (C), shows a more pronounced transport reaction, due to the higher concentration of water in the carrier gas.

The formation of more volatile compounds is more pronounced in the TCm of the experiment TeO_x4 (orange bars, Fig. 2 (D)) obtained using He with 30% of H_2O_2 as carrier gas. In this case H_2O_2 could be converted through catalysis on the gold foil (where the Te is deposited) into hydroxyl radicals, which are highly reactive, leading to a faster rate of oxyhydroxide formation. It is possible to note the dependence of the retention from the kinetics of the transport reaction.
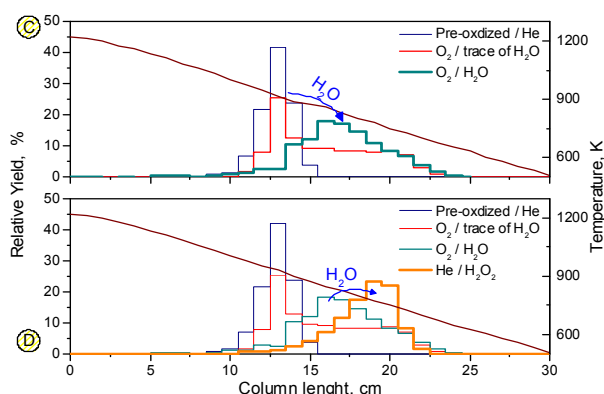
Fig. 2: (C) TCm of TeO_2 using O_2/H_2O as carrier gas (green bars); (D) TCm of a TeO_2 using as carrier gas He/H_2O_2 (orange bars).

CONCLUSION

TeO_2 does not react with water contained in inert gas in a temperature range of 1223 to 860 K. Depending on the amount of H_2O and the oxidative conditions a transport reaction is observed by formation of more volatile species, most likely oxyhydroxides.

REFERENCES

[1] M. Maugeri et al., Ann. Rep. Lab. of Radio- & Environ. Chem., Univ. Bern & PSI, p. 40 (2012).
[2] N.N. Greenwood, A. Earnshaw, "Chemistry of the Elements", Elsevier (1984).

NEW TRANSPIRATION SETUP FOR VAPOR PRESSURE DETERMINATION

M. Rizzi, R. Eichler, A. Türler (Univ. Bern & PSI), J. Neuhausen, D. Piguet, D. Schumann (PSI)

INTRODUCTION

The contamination of the environment during operation, maintenance or a severe accident is a major concern for the operation of future liquid metal spallation targets. Especially, radionuclides which can form volatile and/or semi-volatile species, pose a significant risk [1]. Determination of vapor pressures of such radionuclides over liquid metals and studying the influence of different experimental conditions on their evaporation behavior is therefore an important prerequisite for safety assessments. For this purpose we developed a new experimental setup employing the transpiration technique. To verify our method, the vapor pressure of pure liquid Bismuth containing traces of ^{207}Bi was determined experimentally by monitoring mass and activity loss.

THEORY

The transpiration method – in the literature also referred to as transportation method - is a simple and versatile dynamic method for vapor pressure determination [2]. Originally developed to determine vapor pressures of pure samples, however, the method can also be adapted to study dissolved compounds at trace quantities. An important issue is the verification of saturation conditions. The experimental proof of equilibrium conditions is achieved by measuring the vapor pressure as a function of carrier gas flow. In the saturation regime, the measured vapor pressure is independent of the flow rate of the carrier gas.
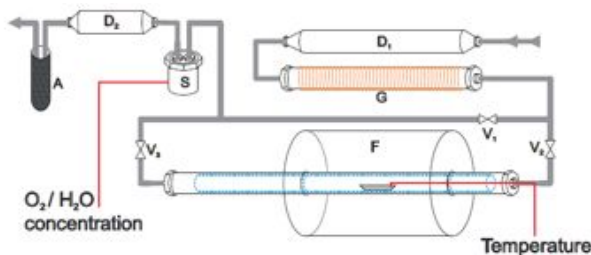
Fig. 1: experimental setup

EXPERIMENTAL

The experimental setup for the transpiration experiments is shown in Figure 1. Before entering the release tube (F), the carrier gas, in our case an Ar/5% H_2-mixture, was cleaned by passing it first through a drying cartridge (D1) and subsequently over a tantalum-filled getter furnace (G) heated to about 1000 °C. The gas then passed over the sample which was placed inside a quartz (fused silica) tube. The sample vapor was collected downstream inside the quartz tube. The whole tube was enclosed by an Inconel 600 stainless steel cladding tube to prevent ingress of air. To avoid back diffusion of oxygen and

humidity, a second drying cartridge (D2) was installed at the gas outlet. To catch eventually formed very volatile products an activated charcoal filter (A) was installed as well. Three valves (V1-V3) were switched in such a way that the release tube was bypassed during the heating-up of the sample. The sample temperature, the oxygen and the water concentration in the carrier gas were monitored during the experiment. The vapor pressure was calculated from the weight loss of the sample after each experiment as well as by activity measurements of the sample and of the collected vaporized sample material deposited downstream from the sample inside of the quartz tube.

RESULTS AND DISCUSSION
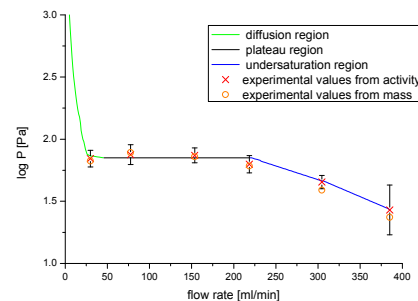
Fig. 2: Proof of saturation, comparison of experimental results with a scheme of the theoretical behavior (colored lines)

A comparison of our experimental results derived from mass and activity measurements, respectively, are shown in Figure 2. The vapor pressure of Bi was found to be independent from the carrier gas flow rate between 30 and 150 ml/min and was 79.4±2.80 Pa at 900°C, which is in good agreement with Bi saturation vapor pressure data given in the LBE Handbook [3] i.e. 85.1 Pa at 900°C. The excellent agreement of mass and activity measurements confirm the validity of vapor pressure data derived using radioactive tracer.

ACKNOWLEDGEMENTS

REFERENCES

[1] D. Gorse-Pomonti, V. Russier, J. Non-Cryst. Solids, **353,** 3600 (2007).
[2] H. van Limpt, R. Beerkens, A. Lankhorst, A. Habraken, Int. J. Heat Mass Tran., **48**, 4265 (2005).
[3] Handbook on Lead-bismuth Eutectic Alloy and Lead Properties, Nuclear Energy Agency (2007).

POLONIUM RELEASE FROM DIFFERENT LIQUID METALS

M. Rizzi, R. Eichler, A. Türler (Univ. Bern & PSI), J. Neuhausen, D. Schumann (PSI), A. Aerts (SCK-CEN)

INTRODUCTION

Liquid lead and liquid lead-based alloys are currently under discussion for application as spallation target material and coolant in neutron sources and Accelerator Driven Systems (ADS) [1]. The main disadvantage of targets based on bismuth-containing alloys is the formation of α-emitting polonium isotopes. To reduce the hazards resulting from polonium release, pure lead and lead gold eutectic (LGE) have been considered as alternative liquid spallation target materials and reactor coolants. Though the production of polonium in these materials is much lower compared to Lead Bismuth Eutectic (LBE), still considerable amounts are formed [2]. In the present work we studied the evaporation behavior of Po from Pb, LBE, and LGE using the transpiration method. The transpiration method is a dynamic vapor pressure determination method. It can be adopted to measure the vapor pressure of diluted species. To do so the mole fraction change of the evaporating species must be taken into account. Therefore, a new approach based on a 1st order kinetic model was developed.

EXPERIMENTAL

^{206}Po was produced by either proton irradiation of Bi or α-irradiation of Pb at the Injector I Phillips Cyclotron at PSI. Particle energies were 40 MeV for proton and 80 MeV for alpha irradiation. Beam intensities differed from 120 - 150 nA and irradiation times varied between 2 h and 15 h.

The experimental setup consisted of a quartz tube, where the quartz boat with the sample was placed. For the transpiration experiments, a carrier gas flow of 53 ml/min (measured at 276.15 K) of an Ar/7% H$_2$-mixture (purity $\geq$ 99.995 %) was used. Po-release experiments were performed in a temperature range of 500 - 1100°C. The activity of the sample was measured before and after each experiment by gamma spectroscopy using HPGe gamma detectors from Canberra. The vapor pressure was calculated using following equation, which takes the solute depletion into account:

$$\frac{n_{Po}^{lm}(t)}{n_{Po}^{lm}(0)} = \exp\left[-\frac{K_{Po}^{lm} \cdot \dot{V} \cdot t}{n_{lm} \cdot R \cdot T}\right]$$

where $n_{Po}(0)$ and $n_{Po}(t)$ are the molar amounts of Po present in the liquid metal before and after each experiment, $\dot{V}$ is the carrier gas flow rate, n_{lm} the molar amount of liquid metal, R the gas constant, T the experimental temperature, t the experimental time and K_{Po} the Henry constant.

RESULTS AND DISCUSSION

The evaporation of Po from LBE, LGE and pure lead was found to be similar. The derived Henry Constants and their corresponding functions of temperature (Figure 1 and Table 1) for lead and LBE are similar.
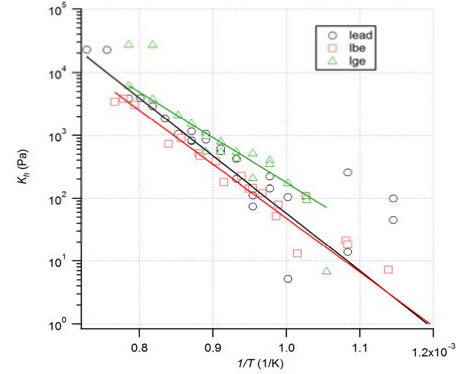
Fig. 1: Henry constants for Po in liquid Pb, LBE and LGE. Symbols: data, Solid lines: relations derived from fitting the experimental release curves.

The significantly higher apparent vapor pressure of Po over LGE may be explained by a repulsive interaction with Au. The enthalpies of solution of Po in liquid Au, Pb and Bi are predicted to be 69.3 kJ/mol, -10.2 kJ/mol and -7.3 kJ/mol, respectively [3]. The extrapolation of vapor pressures of Po from LGE to operational temperatures of liquid metal spallation targets i.e. 350°C results in a vapor pressure, which is more than 20 times higher than from LBE and 40 times higher than from Pb. The positive effect of lower Po production in non Bi-containing alloys is therefore partially compensated by the considerably higher vapor pressure.

Tab. 1: Experimentally derived vapor pressure functions and corresponding enthalpies of evaporation.

	H^{vap} of Po [kJ/mol]	log P^{app} of Po [Pa]
Pb	175.5 ± 5.6	10.93±0.24-(9171.87±295.00/T)
LBE	164.4 ± 2.9	10.22±0.13-(8592.1±154.14/T)
LGE	137.9 ± 4.5	9.45±0.20-(7205.1±233.76/T)

ACKNOWLEDGEMENTS

REFERENCES

[1] D. Gorse-Pomonti, V. Russier, J Non-Cryst. Solids, **353**, 3600 (2007).

[2] M. Medarde et al., J. Nucl. Mat. **411,** 72 (2011).

[3] J. Neuhausen, B. Eichler "Extension of Miedema's Macroscopic Atom Model to the Elements of Group 16 (O, S, Se, Te, Po)", Report No. 03-13, PSI (2003).

APPARENT POLONIUM VAPOR PRESSURE OVER LEAD-BISMUTH EUTECTIC

M. Rizzi, R. Eichler, A. Türler (Univ. Bern & PSI), J. Neuhausen, D. Schumann (PSI)

INTRODUCTION

Lead Bismuth Eutectic (LBE) is foreseen as spallation target and cooling material in the MYRRHA project, a prototype for future Accelerator Driven Systems (ADS) currently planned in Mol, Belgium. During its high energy proton beam driven operation a considerable amount of polonium is formed, which poses a significant health risk. Hence, release of Po during operation maintenance, and accidents is under debate. Here, we show experimental release data of Po at typical operational conditions in ADS.

EXPERIMENTAL

A series of release experiments with our new transpiration setup [1] was performed to determine the apparent vapor pressure of polonium over liquid LBE between 200°C and 500°C using the γ-emitting isotope ^{206}Po [2]. Therefore, ^{206}Po was purchased from Zyklotron AG in Karlsruhe, Germany. Two Po-containing LBE samples with masses of 4.85 g and 4.63 g, respectively, were prepared.
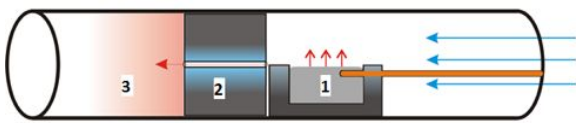
Fig. 1: Scheme of release tube (for details see text).
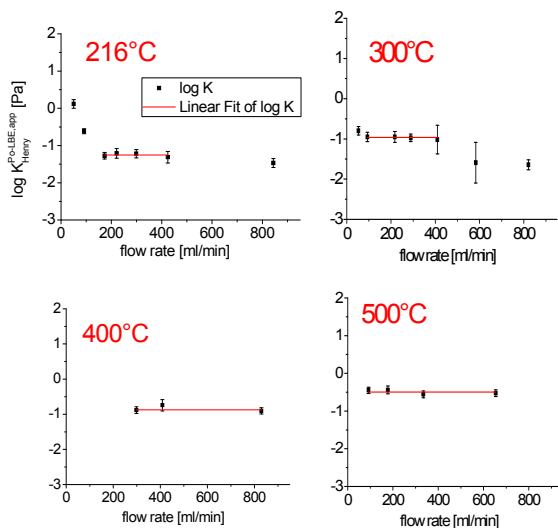
Fig. 2: Experimental proof of saturation at different temperatures.

In Figure 1 a schematic of the release tube is shown. The sample (1) is placed in a quartz boat with a thermocouple attached to it. The Po species evaporate and get transported through a transfer capillary (2) by the carrier gas into the colder region of the tube, where they condense (3).

RESULTS AND DISUSSION

Figure 2 shows that equilibrium was reached for Po-evaporation from LBE using He as carrier gas at 216, 300, 400, and 500°C between 200 and 400 ml/min. The apparent vapor pressure of Po as derived from these experiments (Fig. 3) was found to be significantly larger than expected from extrapolating vapor pressure data for Po over LBE at higher temperatures [3]. Together with the weak temperature dependence this suggests different volatilization mechanisms at lower temperatures even involving other Po species.
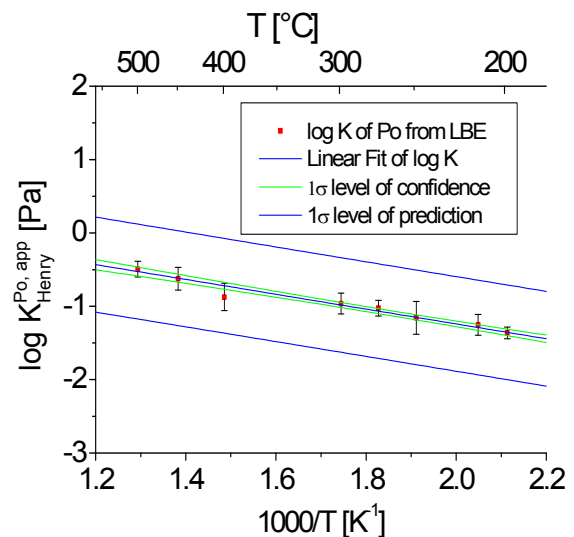
Fig. 3: Apparent vapor pressure function of polonium over LBE between 200°C and 500°C

ACKNOWLEDGEMENT

REFERENCES

[1] M. Rizzi et al., Ann. Rep. Lab. of Radio- & Environ. Chemistry, Univ. Bern & PSI, p. 43 (2012).

[2] M. Rizzi et al., Ann. Rep. Lab. of Radio- & Environ. Chemistry, Univ. Bern & PSI, p. 44 (2012).

[3] S. Ohno, S. Miyahara, Y. Kurata, J. Nucl. Sci. Technol. **42,** 593 (2005).

ANALYTICS OF ^{129}I PRODUCED BY PROTON IRRADIATION IN A LEAD TARGET AT SINQ

T. Lorenz, A. Türler (Univ. Bern & PSI), Y. Dai (PSI/NES), D. Schumann (PSI), C. Vockenhuber (ETHZ)

INTRODUCTION

At PSI one of the most powerful continuous proton accelerators with a proton energy of 590 MeV and a beam current of 1.8 mA is driving a spallation neutron source named SINQ. In this facility the proton beam is fully stopped in a solid lead target in order to produce neutrons for research in material science, basic physics and particle science. After two years of operation and a total deposited beam dose of more than 10 Ah the target system is highly radioactive. In order to take care of this kind of radioactive waste and also to evaluate the risks and harms of operation and decommissioning of such high power targets, the precise knowledge of the radionuclide inventory is mandatory. Safety-relevant volatile isotopes and long-lived nuclides are a basic topic in the total description of the radionuclide inventory. By spallation, fragmentation, and high-energy fission processes, isotopes in all mass regions below the matrix element are formed. In this work Accelerator Mass Spectrometry (AMS) was used to determine ^{129}I as an example for volatile isotopes ($t_{1/2}$=1.57·10^7 yr) after chemical separation from lead of SINQ-Target 4 which was irradiated in 2000/2001.

EXPERIMENTAL

Details of the SINQ target design from STIP-II are available in [1] and the sample preparation is described in [2]. The content and longitudinal distribution of ^{129}I along a lead rod from the central position near the beam entry was determined from samples with varying distance to the beam centre. Several lead pieces from each sample and 10 mg of inactive iodine carrier were dissolved in hot 7 M nitric acid under bubbling nitrogen.
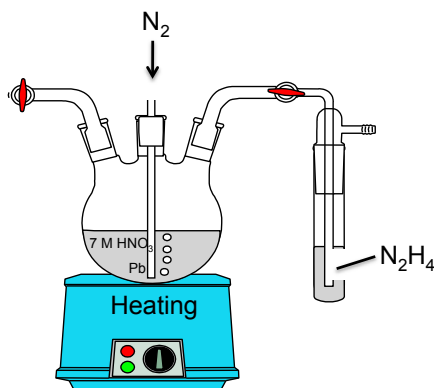
Fig. 1: Schematic view of the dissolution set-up of the lead pieces from SINQ Target 4, iodine is separated by distillation into a hydrazine solution.

Iodine was separated from the matrix by distillation into hydrazine solution (1):

$$2\ I_{2(g)} + N_2H_{4(aq)} \rightarrow 4\ HI_{(aq)}\ N_{2(g)}\uparrow \quad (1)$$
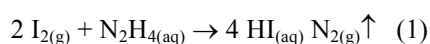
The iodide was precipitated with AgNO$_3$ in diluted nitric acid as AgI. After drying at 80°C for several days, the yield was determined gravimetrically (47 to 77%) and the samples were diluted to 1:2500 with AgI (Sigma 99.999%) by milling. AMS measurements were performed at the 0.6 MV TANDY AMS facility at ETH Zurich.

RESULTS AND CONCLUSION

The evaluation of the ^{129}I concentration is presented in Tab. 1. The gradient of distribution is in good correlation to the proton dose gradient, assuming that no iodine evaporated from the lead phase during operation despite the high operation temperatures up to 425 °C [1]. Previous studies revealed that iodine remains solved in lead-based alloys up to 500 °C [3]. But one has to consider also the chemical constitution of the produced iodine in lead. At the moment it is unclear whether an elementary or ionic state is produced.

Tab. 1: Sample overview with calculated proton and neutron doses and averaged activity concentration of ^{129}I per gram lead – (uncertainties indicated in parenthesis; date of measurement: 11/2012)

Sample	**D03**	**D09**	**D10**	**D12**	**D14**
d^1 *(mm)*	1.5	25	27	47	49.5
Proton dose[1] *(10^{25} p/m^2)*	5.2	3.0	2.7	1.0	0.8
Neutron dose [1] *(10^{25} p/m^2)*	9.2	7.6	7.4	5.7	5.5
^{129}I *(Bq/g Pb)* *(atoms/g Pb)*	0.4(1) 2.95·10^{14}	0.5(2) 3.41·10^{14}	0.24(8) 1.79·10^{14}	0.12(2) 0.91·10^{14}	0.11(1) 0.81·10^{14}

^{1}d is the distance of the sample to the beam centre

The dilution of the sample with solid AgI is inducing high uncertainties due to strong scattering caused by microscopic inhomogeneities of some particles in the samples. This could be improved by diluting the liquid phase before precipitation of AgI.

ACKNOWLEDGEMENTS

REFERENCES

[1] Y. Dai et al., J. Nucl. Mater., **343,** 33 (2005).
[2] T. Lorenz et al., Ann. Rep. Lab. of Radio- & Environ. Chem., Univ. Bern & PSI, p. 47 (2012).
[3] J. Neuhausen et al., Radiochim. Acta, **94**, 239 (2006).

ANALYTICS OF POLONIUM PRODUCED BY PROTON IRRADIATION IN A LEAD TARGET AT SINQ

T. Lorenz, A. Türler (Univ. Bern & PSI), D. Schumann (PSI), Y. Dai (PSI/NES)

INTRODUCTION

At PSI the spallation neutron spource SINQ is driven by a 590 MeV proton beam in the Megawatt range. The beam is fully stopped in a solid lead target producing neutrons by spallation. High energetic particle reactions lead to a highly radioactive target system. The spectrum of residual nuclides within a spallation target is very complex and differs completely from the nuclide spectrum known from nuclear reactors. The precise knowledge of the radionuclide inventory, especially of safety-relevant α-emitting isotopes and long-lived radionuclides, is one of the basic topics in the evaluation of risks and hazards concerning the operation, decommissioning, and disposal of high power targets. We have investigated SINQ Target 4 operated in 2000-2001 which received an integral proton charge of 10.03 Ah. Special attention was paid to radiotoxic polonium isotopes ^{208}Po (2.898 yr), ^{209}Po (102 yr) and ^{210}Po (138 d). A chemical separation procedure was performed in order to separate Po from the matrix and interfering isotopes and to prepare thin samples suiting for α-spectrometry.

EXPERIMENTAL

A detailed description of the target design and irradiation conditions can be found in [1]. In 2006, after 5 years of cooling time, one rod from Target 4, designated as "Rod 3", has been selected for examination of the target system, due to its central position near the beam entry. The content and longitudinal distribution of Po was determined from samples with varying distance to the beam centre. These samples were cut into small pieces of about 10 to 60 mg. Each lead piece was dissolved in hot 7 M nitric acid. After heating to dryness the flask was rinsed with hydrochloric acid and nitric acid. The thin-sample preparation was performed via spontaneous deposition [2] of Po on a silver disc with a diameter of 8 mm in 1 M hydrochloric acid at 70 °C within 3 h. This procedure was done four to five times for each lead piece using aliquots from the stock solution. α-counting was performed on a Canberra α-measurement device for each silver disc with sufficient measurement time for good statistics (3000 to 200.000 counts per peak area). A typical spectrum is shown in Figure 1.

RESULTS AND CONCLUSION

The evaluation of the Po concentration depending on the distance to the beam centre is presented in Table 1. A correlation between the gradient of proton dose and the gradient of $^{208/209/210}$Po concentration can be notified. The high values for ^{210}Po are remarkable.
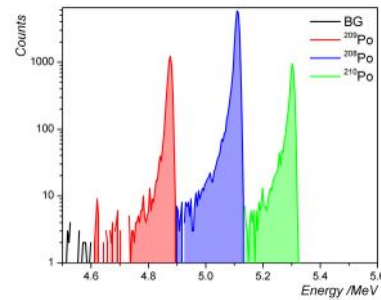
Fig. 1: Typical spectrum of deposited $^{208/209/210}$Po - peak areas for integration are colored.

A comparison to previous Po analysis of the same sample D14 in 2011 revealed, that the activity of ^{210}Po is not diminishing according to its half-life. It is assumed, that a considerable amount of ^{210}Pb (22.3 yr) was produced, which is in equilibrium with its grand daughter nuclide ^{210}Po. Theoretical investigations on the possible production paths of ^{210}Pb by secondary particle reactions were recently started.

Tab. 1: Sample overview with calculated proton and neutron doses (taken from [1]) and activity concentration of $^{208/209/210}$Po per gram lead – (Date of measurement: 07/2012)

Sample	D03	D09	D10	D12	D14
Distance to the beam centre (mm)	1.5	25	27	47	49.5
Proton dose (10^{25} p/m^2)	5.2	3.0	2.7	1.0	0.9
Neutron dose (10^{25} p/m^2)	9.2	7.5	7.3	5.4	5.3
^{208}Po (kBq/g Pb) (atoms/g Pb)	217 $2.9 \cdot 10^{13}$	111 $1.5 \cdot 10^{13}$	115 $1.5 \cdot 10^{13}$	52 $0.7 \cdot 10^{13}$	28 0.4
^{209}Po (kBq/g Pb) (atoms/g Pb)	59 $2.7 \cdot 10^{14}$	31 $1.4 \cdot 10^{14}$	31 $1.4 \cdot 10^{14}$	14 $0.7 \cdot 10^{14}$	8 $0.4 \cdot 10^{14}$
^{210}Po (kBq/g Pb) (atoms/g Pb)	45 $7.8 \cdot 10^{11}$	21 $3.6 \cdot 10^{11}$	19 $3.3 \cdot 10^{11}$	9 $1.6 \cdot 10^{11}$	6 $1.0 \cdot 10^{11}$

REFERENCES

[1] Y. Dai et al., J. Nucl. Mater., **343**, 33 (2005).
[2] P. Vesterbacka et al., Anal. Chim. Acta, **545,** 252 (2005).

ACTIVITY CONCENTRATIONS OF POLONIUM IN MEGAPIE SAMPLES

B. Hammer, A. Türler (Univ. Bern & PSI), D. Schumann, J. Neuhausen (PSI), M. Wohlmuther (PSI/GFA)

INTRODUCTION

Lead-bismuth eutectic (LBE) is considered to be used as target material in future high power spallation targets for neutron production. One of the most significant problems when using LBE as target or coolant material in future reactors or spallation targets is the production of significant amounts of the highly radiotoxic ^{210}Po. Volatilization of polonium can occur when the LBE primary loop is open, so it can cause problems in case of LBE coolant leak accidents and in case of maintenance of the LBE primary loop [1]. Due to its α-emission in connection with the relatively high specific activity, polonium is extremely radiotoxic. Therefore, the behavior of polonium in LBE should be studied in more detail. ^{210}Po is produced in LBE spallation targets mainly by neutron capture of ^{209}Bi (^{209}Bi(n,γ)^{210}Bi(β$^-$)^{210}Po). ^{209}Po and ^{208}Po are mainly produced in LBE by (p,xn) reactions. We report here on the analysis of $^{208-210}$Po in samples from the MEGAPIE target by α-spectrometry.

EXPERIMENTAL

Typically, a 12 mg sample of LBE was dissolved in 7 M HNO$_3$. Two samples were spiked with ^{206}Po (T$_{1/2}$ = 8.8 d), a γ-emitting polonium isotope, to monitor polonium during the separation procedure and to determine the overall chemical yield. The remaining samples were analyzed without adding ^{206}Po. The first step of the separation procedure was the distillation of chlorine and iodine in a N$_2$ atmosphere, as described in [2, 3]. The medium of the residue was changed from HNO$_3$ to HCl by dissolving the residue 3 times in conc. HCl and evaporation to dryness. This step is important, because otherwise the spontaneous deposition of polonium will not take place. Afterwards, the residue was dissolved in 5 ml 0.8 M HCl. One aliquot (1 ml) of this solution was taken and a silver disc was added. The spontaneous deposition of Po onto a silver disc was performed for about 2 hours at 72 °C by stirring the solution.

RESULTS

The yield of the spontaneous deposition of polonium is about 50%. The other 50% of polonium are sticking to the glass wall of the used vessel. The spontaneous deposition of Po was performed for 22 different LBE samples from the MEGAPIE target. Each deposition was repeated at least twice, and the mean value was taken as analysis result. For all silver discs, both sides of the disc were measured by α-spectroscopy for 1800 s (Fig. 1). The activity concentrations in MEGAPIE at shutdown (EOB) predicted from nuclear calculations assuming homogeneous distribution in LBE are 3.28E6 Bq/g, 1.63E4 Bq/g and 1.61E8 Bq/g for ^{208}Po, ^{209}Po, and ^{210}Po, respectively [4]. The results of chemical analysis (average of 22 samples) give

2.86E6 Bq/g, 1.83E4 Bq/g, and 8.86E7 Bq/g for ^{208}Po, ^{209}Po, and ^{210}Po, respectively. Thus, the predictions were in reasonable agreement with the experimental values (Fig. 2). No strong inhomogeneity of the polonium distribution was found in the samples.
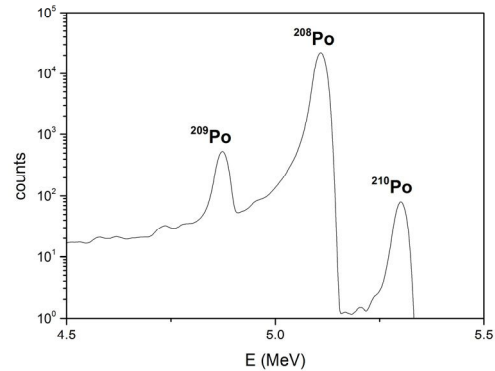
Fig. 1: Measured α-spectrum, measuring time was 1800 s.
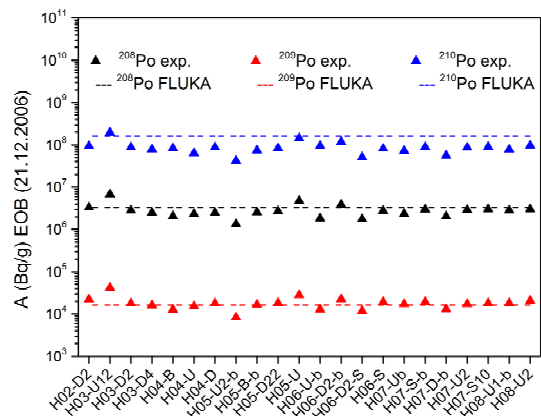
Fig. 2: Measured activity concentrations of $^{208-210}$Po in Bq/g at EOB (21.12.2006) for different MEGAPIE samples compared to FLUKA predictions.

REFERENCES

[1] T. Obara et al., Prog. Nucl. Energ., **47**, 1147 (2005).

[2] D. Schumann et al. Nucl. Instr. Meth. Phys. Res. A, **562**, 1057 (2006).

[3] B. Hammer et al., Ann. Rep. Lab. of Radio- & Environ. Chem., Univ. Bern & PSI, p. 36 (2010).

[4] L. Zanini et al., PSI Report Nr. 08-04 (2008).

DETERMINATION OF SOLUBLE RADIONUCLIDES IN LBE SAMPLES FROM MEGAPIE

B. Hammer, A. Türler (Univ. Bern & PSI), D. Schumann, J. Neuhausen (PSI), M. Wohlmuther (PSI/GFA), V. Boutellier, H.P. Linder, N. Shcherbina (PSI/Hotlab)

INTRODUCTION

MEGAPIE (MEGAwatt Pilot Experiment) is a joint initiative by six European research institutions, Japan, Korea, and the USA to demonstrate the feasibility of a liquid lead-bismuth (LBE) target for spallation facilities at a beam power level of 1 MW. The LBE target was operated in the Swiss Spallation Neutron Source (SINQ) at PSI in 2006 for 123 days close to the megawatt range [1]. An extended Post-Irradiation-Examination (PIE) program was launched in order to study the properties and the behavior of the applied materials as well as the content and distribution of the induced radioactivity. We will report here on the determination of radionuclides soluble in liquid LBE measured by γ-spectrometry.

SAMPLE POSITION AND γ-ANALYSIS

In total, 74 samples were taken from different locations in the MEGAPIE target [2]. 30 samples were taken from the LBE/steel and LBE/cover gas interface and the rest represent the bulk LBE. All samples were measured by γ-spectroscopy, without prior chemical separation.

RESULTS

We could identify ^{207}Bi, ^{101}Rh, ^{102}Rh, ^{108m}Ag, ^{110m}Ag, ^{194}Hg/Au, ^{195}Au, ^{60}Co and ^{202}Pb/Tl in all samples by γ-spectroscopy. ^{207}Bi is homogeneously distributed in the whole target, as expected. The activity concentration of ^{207}Bi is about 3600 kBq/g.

Tab. 1: Summarized activity concentrations of radionuclides, which were identified in the bulk LBE. The mean value was taken of all bulk LBE samples from MEGAPIE and their corresponding deviation. The activity concentration was calculated to end of beam (EOB, 21.12.2006).

	bulk LBE (Bq/g)
^{207}Bi	3.64e6 ± 0.80e6
^{202}Pb/Tl	2.77e3 ± 4.30e3
^{195}Au	3.24e4 ± 3.74e4
^{194}Hg/Au	6.27e4 ± 5.43e4
^{110m}Ag	3.10e4 ± 4.51e4
^{108m}Ag	1.84e3 ± 2.41e3
^{102}Rh	1.65e5 ± 2.37e5
^{101}Rh	8.70e3 ± 7.20e3
^{60}Co	7.78e2 ± 1.61e3

Soluble noble metals such as Au, Ag, and Rh are found throughout the target. The distribution of these radionuclides is not fully homogeneous, but they have similar behavior (Fig. 1). The activity concentrations for the noble metals are summarized in Tab. 1. The rare earth elements, represented by e.g. ^{173}Lu, were not found in the bulk LBE, though their solubility limit is not expected to be exceeded based on predictions on their production [1]. Probably, these electropositive elements form oxides that have low solubility in LBE and thus separate from the liquid metal.

In Fig. 2 a typically measured γ-spectrum of the bulk LBE is shown.
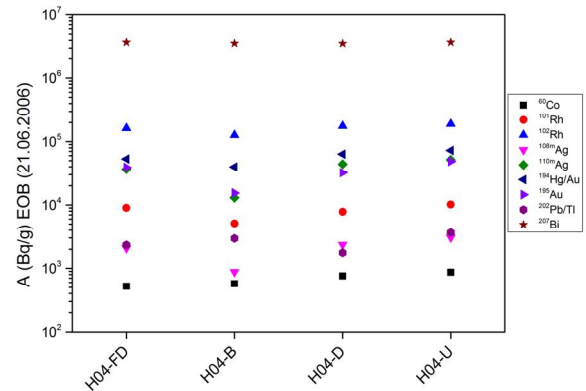
Fig. 1: Distribution of radionuclides, which were found in the bulk LBE, taken from segment H04.
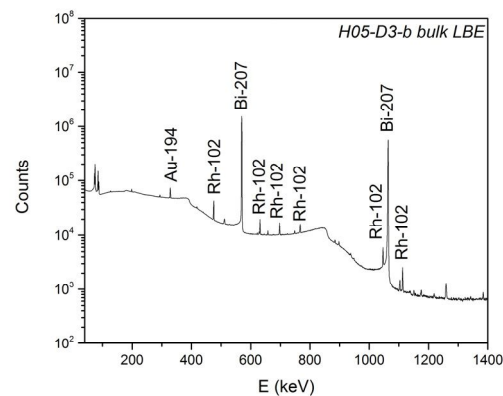
Fig. 2: Typically measured γ-spectrum of a bulk LBE sample (H05-D3-b).

REFERENCES

[1] L. Zanini et al., PSI Report Nr. 08-04 (2008).
[2] B. Hammer et al., Ann. Rep. Lab. of Radio- & Environ. Chem., Univ. Bern & PSI, p. 52 (2011).

DISTRIBUTION OF RADIONUCLIDES WITH LOW SOLUBILITY IN THE MEGAPIE TARGET

B. Hammer, A. Türler (Univ. Bern & PSI), D. Schumann, J. Neuhausen (PSI), M. Wohlmuther (PSI/GFA), V. Boutellier, H.P. Linder, N. Shcherbina (PSI/Hotlab)

INTRODUCTION

For the safety assessment of a high-power, liquid-metal based neutron spallation facility, the distribution of the produced radionuclides within the target is of essential importance concerning dose rate estimations, material damage considerations, and disposal strategies. Enrichment of radioactivity can be expected especially on exposed interfaces (steel/LBE or cover gas/LBE). The PIE analysis of the MEGAPIE target will provide – among others – the necessary information on these issues.

EXPERIMENTAL

30 samples from the MEGAPIE target were taken comprising the above mentioned interfaces. Some of the samples are core drills (size: cylindrical, Ø 2mm x 5 mm, Ø 1.5mm x 5 mm; 50 to 100 mg each) taken from the interface of LBE with the steel of the target vessel. During drilling, some samples were broken into two parts, resulting in pieces with only steel and ones with only LBE. One example is shown in Figure 1. Details of the MEGAPIE sample taking can be found in [1].

Fig. 1: Photo of the H05-D6-b sample, broken into 2 parts

Other samples consist of material, which was sticking to the walls in the upper part of the target vessel (70 to 900 mg each). These surfaces were in contact with LBE during the operation of the target, but did not contain LBE anymore after shutdown because of thermal contraction of the liquid metal. These 30 samples were analyzed by γ-spectroscopy without prior chemical separation. ^{173}Lu represents in all these samples the rare earth elements, which are sensitive to oxidation.

RESULTS

We present here the results of typical samples from the steel/LBE interface (H05-D6-b, Figure 2) and H07-U3 for the cover gas/LBE interface (Figure 3), respectively. Analysis results for samples H05-D6 are also compiled in Table 1. Apart from the soluble nuclides also found in bulk LBE, in both interfaces we detected nuclides of electropositive elements, e.g. ^{172}Hf/Lu, ^{173}Lu, and ^{133}Ba that were not found in LBE. These elements obviously separate from the liquid metal and deposit on the walls of the target and the free liquid metal surface. On the contrary, the

soluble noble metals Ag and Au do not show such a pronounced tendency to stick to the steel wall. However, they are enriched in the near surface region within the LBE compared to their bulk concentrations. Rh is found to accumulate both on the steel surface and in the near surface region of the LBE.
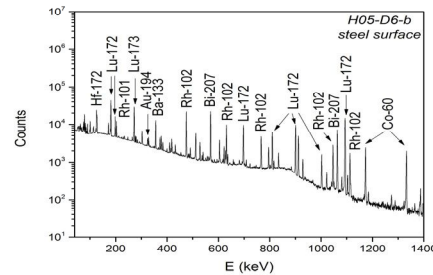
Fig. 2: γ-spectrum of a steel sample (H05-D6-b)
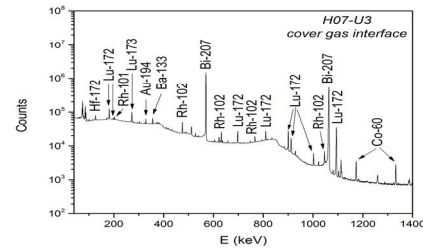
Fig. 3: γ-spectrum of the LBE/cover gas interface

	H05-D6-b LBE (Bq/g)	H05-D6-b Steel surface (Bq/g)	H05-D3-b bulk LBE (Bq/g)
^{207}Bi	3.79e6	7.07e4	3.58e6
^{195}Au	2.33e6	5.50e4	6.95e3
^{194}Hg/Au	3.76e5	7.69e3	4.76e4
^{173}Lu	3.99e5	3.24e5	0
^{172}Hf/Lu	2.74e5	2.28e5	0
^{133}Ba	3.86e4	3.23e4	0
^{110m}Ag	7.76e5	3.81e3	1.26e4
^{108m}Ag	3.65e4	5.89e2	9.24e2
^{102}Rh	1.31e6	2.00e5	1.29e5
^{101}Rh	1.46e5	1.94e4	6.31e3
^{60}Co	2.61e4	3.13e4	3.24e2

Tab. 1: Comparison of near surface LBE and steel surface of H05-D6-b with a bulk LBE sample (H05-D3-b). Activities corrected to EOB (21.12.06).

REFERENCE

[1] B. Hammer et al., Ann. Rep. Lab. of Radio- & Environ. Chem., Univ. Bern & PSI, p. 52 (2011).

PRODUCTION OF ^{44}Sc BY IRRADIATION OF ^{44}Ca-TARGETS AT THE CYCLOTRON FOR RADIOPHARMACEUTICAL APPLICATIONS

M. Bunka, A. Türler (Univ. Bern & PSI), C. Müller, J. Reber, R. Schibli (ETH & PSI)

INTRODUCTION

The positron emitter ^{44}Sc ($t_{1/2}$ = 3.97 h, $E_{\beta+}$ 1475.4 keV, 94.34%) has attractive properties for positron emission tomography (PET) and could be an alternative to the currently used short-lived ^{68}Ga ($t_{1/2}$ = 1.1 h).Furthermore, with a chemistry similar to that of the lanthanides and rare earth elements (i.e. ^{90}Y, ^{177}Lu), ^{44}Sc can be used in already established labelling reactions for radiopharmaceutical purposes. The aim of this study was to produce ^{44}Sc via the ^{44}Ca(p,n)^{44}Sc nuclear reaction at a cyclotron [1-4]. The separation of ^{44}Sc from irradiated targets was developed and *in vitro* and *in vivo* studies including PET imaging with ^{44}Sc-labeled compounds were performed.

EXPERIMENTAL

Irradiation. For the production of ^{44}Sc via the ^{44}Ca(p,n)^{44}Sc nuclear reaction solid calcium targets were irradiated at the cyclotron. ^{44}Ca-targets were prepared by mixing 5-10 mg of enriched ^{44}CaCO$_3$ with 150 mg graphite powder, pressed and encapsulated in aluminium. The targets were irradiated with protons of up to 15 MeV and a beam current of 50 μA for about 30 min.

Chemical separation. For the separation of ^{44}Sc from the irradiated ^{44}CaCO$_3$ solid target, 3 M HCl was used to dissolve the ^{44}CaCO$_3$ and to adsorb the ^{44}Sc(III) on the extraction chromatography resin N,N,N'N'-tetra-n-octyldiglycolamide (DGA) (Fig. 1). Since ^{44}Ca(II) is not retained on the DGA under these conditions it was flushed through the column. For the elution of ^{44}Sc(III) a solution of 0.05–0.1 M HCl was employed.
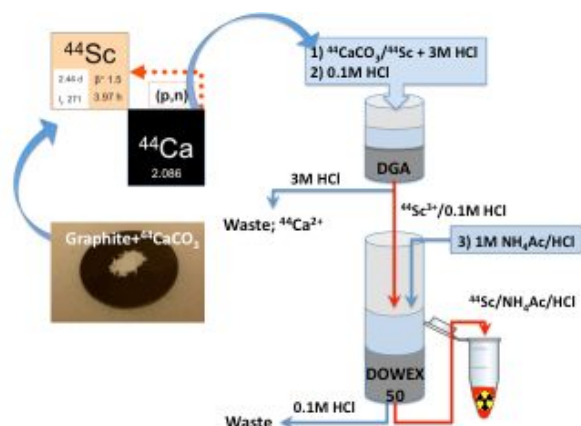
Fig. 1: ^{44}CaCO$_3$/graphite target and scheme of the separation procedure of the irradiated target.

To reduce the volume and acidity of the ^{44}Sc-eluate (2-3 mL, pH = 0.5) a second column consisting of the cation exchange resin DOWEX 50 was used. ^{44}Sc in 0.05-0.10 HCl solution was adsorbed on DOWEX 50

and subsequently eluted with a solution of 1 M CH$_3$COONH$_4$/HCl (0.5 mL, pH = 4.5-5). The ^{44}Sc-acetate solution was used for labelling of a DOTA-folate conjugate and DOTATATE for subsequent *in vitro* and *in vivo* experiments.

RESULTS AND DISCUSSION

Using the above described irradiation conditions up to 250-300 MBq per target have been produced. The irradiated ^{44}CaCO$_3$ provided a high radionuclidic purity of ^{44}Sc and less than 1% of the co-produced longer-lived ^{44m}Sc ($t_{1/2}$ = 2.4 d). The developed separation system showed excellent results. Over 85 % of the initial ^{44}Sc-activity could be eluted in a volume of only 0.5 mL of CH$_3$COONH$_4$/HCl solution and was successfully used for radiolabeling reactions with DOTA-folate and DOTATATE. *In vitro* and *in vivo* studies were performed with these ^{44}Sc-radioconjugates. PET imaging studies in mice, which were performed at the ETH Zürich, showed excellent results with regard to tumour visualization using ^{44}Sc-DOTA-folate or ^{44}Sc-DOTATATE, respectively (Fig. 2).
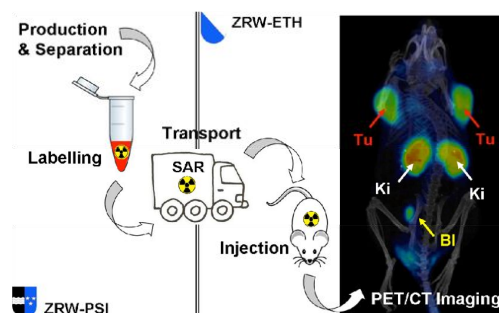
Fig. 2: The way from the production to the PET image with ^{44}Sc (Tu – tumour, Ki – kidneys, Bl – bladder).

REFERENCES

[1] A. Bilewicz et al., 3rd-INCC, Italy, 18-23 September (2011).

[2] K. Zhernosekov et al., Radiother. Oncol. **102,** 141 (2012).

[3] G. W. Severin et al., Appl. Radiat. Isotopes, **70,** 1526 (2012) .

[4] E. Koumarianou et al., Appl. Radiat. Isotopes, **70,** 2669 (2012).

PRODUCTION OF THE THERAPEUTIC ALPHA-EMITTER ^{149}Tb
VIA PROTON INDUCED SPALLATION OF TANTALUM

H. Dorrer, A. Türler (Univ. Bern & PSI), K. Zhernosekov (ITG, Garching), C. Müller (PSI/ZRW),
U. Köster (ILL), K. Johnston (CERN), R. Schibli (ETHZ & PSI/ZRW)

INTRODUCTION

The alpha-emitting radionuclide ^{149}Tb, a very promising candidate for targeted radionuclide therapy, is available via proton induced spallation reactions of tantalum followed by online mass separation at ISOLDE [1, 2]. Recently, we reported the test-production of up to 6 MBq ^{149}Tb in a one step separation process. The radionuclide was obtained in a solution of α–HIB (α–hydroxyisobutyrate), which was used for purification. Gradient elution of the chromatographic column was required to minimize the product solution volume [3].

In this study we further optimized the separation procedure by introducing a concentration step at the end of the purification of ^{149}Tb, which should be obtained with high chemical and radionuclidic purity in a physiological solution allowing direct radiolabeling and *in vivo* application without further purification steps.

EXPERIMENTAL

The radionuclide ^{149}Tb was produced by spallation of tantalum and online mass separation at ISOLDE. The ion beam was deposited onto zinc-covered gold foils.

The zinc layer with the deposited ions was dissolved in 1 ml solution of a mixture of 0.1 M HNO_3/0.1 M NH_4NO_3 at ~50 °C. Chemical separation of ^{149}Tb from isobaric and pseudo-isobaric impurities and stable zinc was performed by cation exchange chromatography with the complexing agent α-HIB. A miniaturized chromatographic column of 35 x 5 mm dimension, filled with a strong cation exchange resin in NH_4^+-form, was used in order to optimize the required duration of separation. The solution was loaded onto the column. The purification of ^{149}Tb from impurities was accomplished by isocratic elution of the chromatographic column with 0.13 M α-HIB solution.

Fractions containing purified ^{149}Tb in form of its α-HIB-complex were acidified with HCl and loaded onto a second chromatographic column of 4 x 4 mm dimension, filled with a strong cation exchange resin in H^+-form. The elution took place with ~250 µl 0.4 M L-lactate solution, which was diluted afterwards with ~ 425 µl MilliQ water to adjust the osmolarity to a physiological value.

For radiolabeling of the tumour specific tracer DOTA-folate 18 µl of DOTA-folate solution (1 nmol/µl) were added to the produced ^{149}Tb in 0.15 M L-lactate solution, pH = 4.69. The mixture was incubated at 95°C for 10 minutes. The radiolabeling yield was monitored by means of HPLC.

RESULTS

Activities of up to 55 MBq of ^{149}Tb were produced at ISOLDE. The radionuclide was successfully purified from impurities of ^{149}Gd, ^{133m}Ce, ^{133}Ce, ^{133}La and stable zinc (Fig. 1).
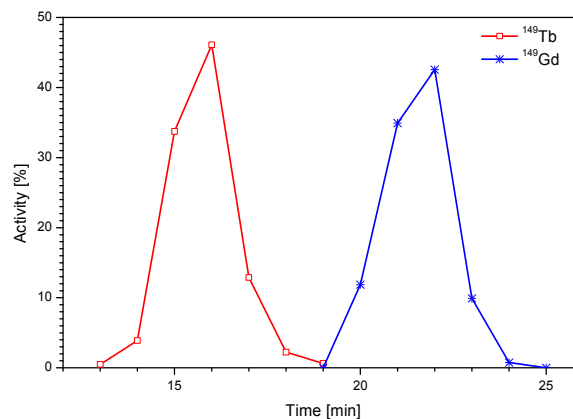
Fig. 1: Elution profile of the separation. The impurities ^{133m}Ce, ^{133}Ce, ^{133}La and stable zinc remain on the column during elution.

Finally, up to 25 MBq of purified ^{149}Tb in ~ 600µl L-lactate solution were available for radiopharmaceutical studies at PSI. The vitamin derivate DOTA-folate was successfully radiolabeled with reaction yields > 96 %, confirming the high chemical purity of the preparation. The L-lactate based physiological formulation allowed direct radiolabeling as well as *in vivo* application without further purification steps.

ACKNOWLEDGEMENT

REFERENCES

[1] G.-J. Beyer et al., Eur. J. Nucl. Med., **31,** 547-554 (2004).
[2] C. Müller et al., J. Nucl. Med., **53,** 1951-1959 (2012).
[3] H. Dorrer et al., Ann. Rep. Lab. of Radio- & Environ. Chem., Univ. Bern & PSI, p. 60 (2011).

FIRST OPERATION OF THE BERN ^{14}C AMS MICADAS

S. Szidat, G. Salazar, E. Vogel, M. Battaglia (Univ. Bern), L. Wacker, H.-A. Synal (ETHZ),
A. Türler (Univ. Bern & PSI)

INTRODUCTION

Analysis of the long-lived radionuclide radiocarbon (^{14}C) has wide applications in environmental research, archaeological dating, life science, and other fields. In order to strengthen the application of ^{14}C as dating tool for the Oeschger Centre for Climate Change Research, the University of Bern decided to set up an accelerator mass spectrometer (AMS) at the Department of Chemistry and Biochemistry [1]. In a first step, a new laboratory for preparation of radiocarbon samples was installed including an automated graphitzation equipment (AGE) [2]. In a second step, an AMS system (Mini Carbon Dating System, MICADAS [3]) was built at the ETH Zurich during 2012, which will be transferred to Bern beginning of 2013. This work describes the setup and testing phase of the MICADAS.

RESULTS AND DISCUSSION

After careful planning of the complete system, procuring of individual parts and preparation of several sub-units of the instrumentation, the MICADAS was assembled in summer 2012. A first test beam could be realized in October. Since then, the performance of the new instrument has been evaluated in detail. Fig. 1 shows the new MICADAS during this phase. This setup includes an inlet system for gaseous samples to the hybrid ion source [4], which will be used for small samples (<100 µgC) and for hyphenation of sample-preparation instrumentation and ^{14}C analysis.

Fig. 1: The new MICADAS during the testing phase with the gas inlet system at the front.

The IAEA reference materials C4 (wood, 0.32 pMC), C5 (wood, 23.05 pMC), C6 (sucrose, 150.61 pMC) and C7 (oxalic acid, 49.53 pMC) were analysed after combustion and graphitization using the AGE system (Fig. 2). The reference values were reproduced within measurement uncertainties, although the intensive final optimization of the MICADAS remained to be done at that time.
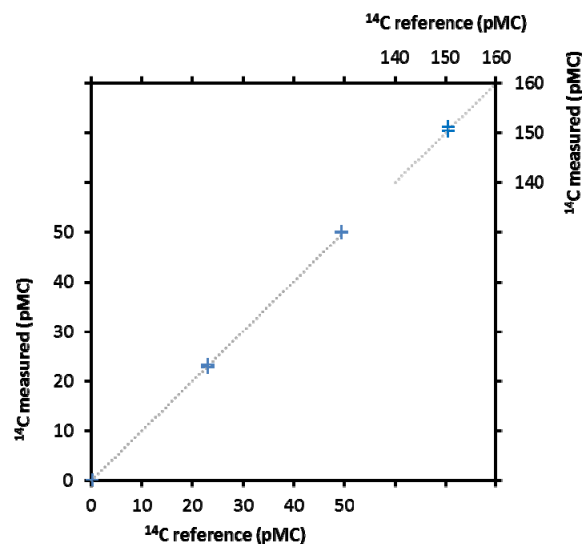
Fig. 2: Double ^{14}C analysis of the reference materials IAEA C4, C5, C6 and C7. Measurement uncertainties range from 0.2 to 0.5 pMC.

ACKNOWLEDGEMENTS

REFERENCES

[1] S. Szidat et al., Ann. Rep. Lab. of Radio & Environ. Chem., Univ. Bern & PSI, p. 63 (2010).
[2] S. Szidat et al., Ann. Rep. Lab. of Radio & Environ. Chem., Univ. Bern & PSI p. 63 (2011).
[3] H.-A. Synal et al., Nucl. Instrum. Meth. Phys. Res. B, **259**, 7 (2007).
[4] L. Wacker et al., Nucl. Instrum. Meth. Phys. Res. B, **294**, 315 (2013).

EVALUATION OF CO$_2$ TRAPPING MATERIALS FOR ONLINE ACCELERATOR MASS SPECTROMETRY RADIOCARBON DATING

G. Salazar, S. Szidat (Univ. of Bern), C. McIntyre, M. Seiler, F. Theodor, L. Wacker (ETHZ)

INTRODUCTION

It is important to study the apportionment of environmental aerosols in order to find out their emission source. Accelerator Mass Spectrometry (AMS) is an analytical technique for carbon-containing aerosols by measuring the $^{14}C/^{12}C$ ratio. Therefore, apportionment of the aerosol source can be inferred from its radiocarbon value (fossil or contemporary) and from their nature (elemental or organic carbon) [1]. Conventional sample preparation methods for AMS are highly time and effort consuming. The sampled carbon must be efficiently converted into CO$_2$; which is captured and transformed into graphite. A solution for this situation is to skip the graphitization step by trapping the CO$_2$ and then inject it into the AMS. A trapping method, using zeolite, has been already investigated and applied for routine analysis [2]. In this work, we investigated in detail the trapping properties of other materials for exploratory purposes.

EXPERIMENTAL

Different materials were characterized by measuring their CO$_2$ breakthrough during trap loading and their thermal CO$_2$ release efficiency. For the breakthrough experiment (Fig. 1), a CO$_2$/He mixture (5% CO$_2$) was pressurized into the 1.8 mL loop by switching the valve "1" to connect the points B-A-D-C-I. Then the valve was switched to connect H-A-D-E-G-F, allowing the He flow to carry the CO$_2$ into the trap. The constant He flow (30 mL/min) eluted the CO$_2$, which was detected by a Residual Gas Analyzer (RGA). The trap was kept inside of a homemade cooling/heating copper block. The block ducts were cooled with a flow of ethanol and it was heated by a resistance cartridge.
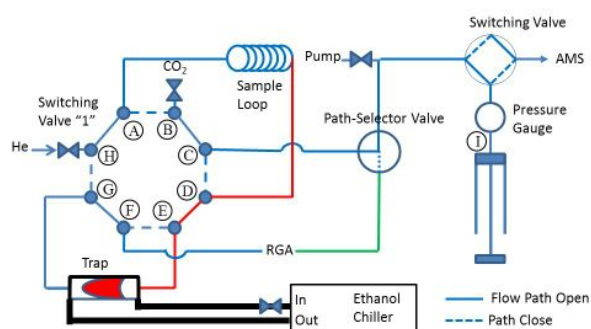
Fig. 1: Instrumental setup. Red color indicates CO$_2$ during loading and elution. Green line or RGA were disconnected during breakthrough or release experiments respectively.

For the thermal release experiment, the trap was loaded with CO$_2$ during 1 min. and the valve was switched to connect H-G-E-F-I (He valve closed, RGA excluded). While the trap was heated, the CO$_2$ was expanded and its pressure was measured at point "I".

RESULTS AND DISCUSSION

The time-related signal of the RGA rose when the CO$_2$ started to elute from the trap. The breakthrough (Fig. 2) was determined by the ratio of the integrated RGA signal until a selected time divided by the total area. As expected, the breakthrough was much less at 1 min than at 3 min of integration time. At high temperature, the breakthrough is lowest for zeolite and highest for silica. When the temperature is low enough (25°C, -30°C and -40°C for zeolite, carbosphere and silica, respectively), the breakthrough is zero. This difference is due to the trapping strength of each material, i.e. size exclusion for zeolite, C¨O or C¨C and Si¨O or Si¨C adsorption for carbosphere and silica, respectively.
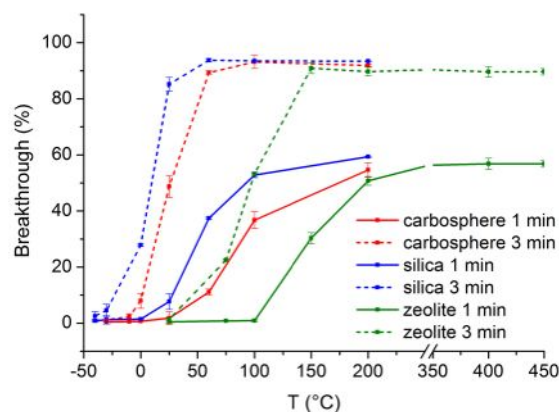
Fig. 2: Breakthrough of CO$_2$ (45 µgC) from the traps.

The dependence of the release pressure to the temperature revealed that optimum release temperatures were 400°C, 250°C, and 200°C for zeolite, carbosphere, and silica respectively. These temperatures indicate the point when 100% release was reached first coming from low temperature.

We can conclude that carbosphere and silica present similar trapping capacity as zeolite at their respective working temperatures.

REFERENCES

[1] Y.L. Zhang et al., Atmos. Chem. Phys., **12**, 10841 (2012).

[2] L. Wacker et al., Nucl. Instrum. Meth. Phys. Res. B, **294**, 315 (2013).

ISOLATION OF ELEMENTAL CARBON OF ATMOSPHERIC AEROSOL SAMPLES FOR ^{14}C MEASUREMENTS BY AN OPTIMIZED THERMO-OPTICAL PROTOCOL

V.G. Ciobanu, Y.L. Zhang (Univ. Bern & PSI), P. Zotter, N. Perron, A.S.H. Prevot (PSI/LAC),
M.C. Minguillon (CSIC Barcelona), L. Wacker (ETHZ), S. Szidat (Univ. Bern)

INTRODUCTION

Carbonaceous aerosols represent a major fraction of the fine aerosol mass and their total carbon content can be divided into two main fractions: organic carbon (OC) and elemental carbon (EC) [1]. Since both fractions have significant, but different impacts on climate and human health, it is important to establish their origins and source intensities separately. EC originates from incomplete fossil-fuel combustion and biomass burning while OC can be emitted directly as primary organic aerosol or can be formed in the atmosphere as secondary organic aerosol. Analysis of the radioactive isotope ^{14}C is a useful tool to quantitatively apportion the fossil and non-fossil sources of the OC and EC fractions. In order to determine the ^{14}C/^{12}C content in the EC and OC fractions, however, a clear and physical separation of the two fractions is required.

The THEODORE system [2] was earlier employed to separate the OC fraction of the atmospheric aerosol samples for offline ^{14}C analysis. Because the evolution of the OC and EC fractions with similar thermal behaviour could not be monitored with this system, a new thermo-optical protocol was developed [3].

THE SWISS_4S PROTOCOL

For EC separation, the water-soluble organic carbon and inorganic catalytic compounds are removed by water extraction prior the thermal treatment in order to minimize the OC charring. In this case, a thermo-optical OC/EC analyser (Sunset Inc.) is used for combustion which allows monitoring the filter transmission by a 660 nm tuned diode laser and the quantification of the resulting CO_2 by a non-dispersive infrared (NDIR) detector.

The Swiss_4S protocol is a 4 steps thermo-optical method with different temperatures and durations for each step that allows the complete OC removal prior the EC recovery, with negligible charring and premature EC evolution. O_2 is used as carrier gas except for S3 when samples are heated in helium.

Figure 1 shows a typical thermogram of a water-extracted aerosol filter. In the first step, S1, most of the OC is removed at $375°$C. In S2 higher molecular organic compounds and the non-refractory EC are removed at $475°$C. The S3 step in He is used to remove the remaining OC and the charred OC (typically lower than 10%) fractions. In the last step, the remaining EC (the refractory fraction) is removed at $760°$C. The yield of EC in S4 for the investigated aerosol samples ranged between 74 and 85% as shown in Table 1.
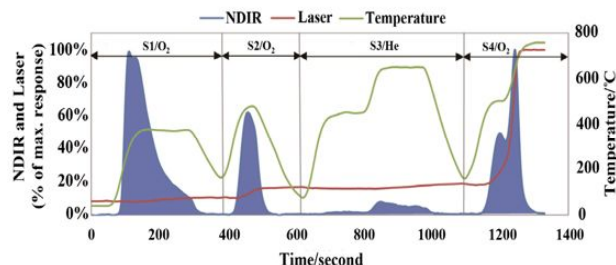
Fig. 1: A typical thermogram of a water-extracted aerosol sample (Solothurn) by the Swiss_4S protocol.

The ^{14}C measurements are performed offline with the accelerator mass spectrometer MICADAS equipped with a gas ion source [4]. The ^{14}C results of EC are given as fraction of modern (f_M) and are shown in the Table 1. The aerosol samples analyzed in this study were collected in Sweden (Gothenburg) and at different sites in Switzerland (Solothurn, Zurich, Magadino, Bern and Sissach). Larger fossil-fuel contributions to the EC fraction were found for the urban samples from Gothenburg and Bern, while the least fossil EC fraction was measured for rural Magadino.

Tab. 1: EC yield and fraction of modern (f_M) of the refractory EC (rEC, isolated during S4 of the Swiss_4S protocol), non-refractory EC (non-rEC, EC fractions in S2 and S3 of the Swiss_4S protocol) and total EC (tEC, i.e. rEC+non-rEC).

Sample	f_M(rEC)	f_M(non-EC)	f_M(tEC)	EC yield rEC/tEC
GOT2	0.17±0.01	0.23±0.07	0.18±0.04	0.80±0.06
GOT3	0.18±0.01	0.27±0.08	0.19±0.04	0.76±0.06
SOL	0.33±0.01	0.42±0.06	0.35±0.06	0.74±0.05
ZUR	0.38±0.01	0.58±0.06	0.35±0.06	0.77±0.05
MAG	0.38±0.01	0.56±0.07	0.42±0.04	0.80±0.05
BER	0.22±0.01	0.35±0.06	0.24±0.04	0.85±0.04
SIS	0.30±0.01	0.36±0.06	0.31±0.06	0.82±0.05

REFERENCES

[1] S. Szidat et al., J. Geophys. Res., **111**, D07206 (2006).

[2] S. Szidat et al., Nucl. Instrum. Meth. Phys. Res. B, **223-224**, 829 (2004).

[3] Y.L. Zhang et al., Atmos. Chem. Phys., **12**, 10841 (2012).

[4] M. Ruff et al., Radiocarbon, **49**, 307 (2007).

FOSSIL AND NON-FOSSIL SOURCES OF ORGANIC AND ELEMENTAL CARBON IN FINE AND COARSE PARTICLES BY RADIOCARBON MEASUREMENT

Y.L. Zhang (Univ. Bern & PSI), S. Szidat (Univ. Bern),
P. Zotter, N. Perron, A.S.H. Prévôt (PSI/LAC), L. Wacker (ETHZ)

INTRODUCTION

Carbonaceous particles, which significantly contribute to the atmospheric particulate matter (PM), are of worldwide concern due to their effects on climate, human health, and visibility [1]. These particles vary in size and can be classified into fine (*i.e.*, with an aerodynamic diameter smaller than 1 or 2.5 µm) and coarse fractions (*i.e.*, larger than fine fraction, but smaller than 10 µm). Fine and coarse particles have different sources, chemical compositions and life times in the atmosphere. Moreover, health impacts of fine particles in air are more adverse than for coarse particles [2]. Therefore, it is essential to accurately conduct the source apportionment based on their sizes for determination of their separate reduction regulations.

Radiocarbon (^{14}C) measurements of elemental carbon (EC) and organic carbon (OC) separately allow an unambiguous quantification of their non-fossil and fossil sources and represent an improvement in source apportionment of PM [3].

METHODOLOGY

PM samples were collected on prebaked quartz-fiber filters at Roveredo (ROV), Zurich (ZUR), Moleno (MOL), and Bern (BER) in Switzerland during various field campaigns using high-volume samplers with PM10 and PM1 or PM2.5 inlets. OC and EC was isolated with a commercial thermo-optical OC/EC analyzer (Model4L, Sunset Laboratory Inc, USA) using the recently developed protocol Swiss_4S for their subsequent ^{14}C measurement [3]. ^{14}C analysis of resulting CO_2 was performed by the accelerator mass spectrometer MICADAS at ETH Zurich with a gas ion source [4]. A correction of biases in ^{14}C results of EC due to premature EC removal during the thermal treatment was applied in this study according to the approach described in [3].

RESULTS

Overall, EC was dominated by fossil sources except for Roveredo, where intensive residential wood burning emission and strong inversion conditions frequently occurred during the sampling periods. Fossil (*i.e.*, from diesel emissions) and non-fossil (*i.e.*, from wood burning) EC in the fine size fractions on average contributed 80±5% and 73±14% to those in PM10 for all sites, respectively, indicating both biomass-burning and fossil EC is enriched in fine particles. In addition, on average 20±5% fossil EC was found in the coarse fractions, which is very likely associated to the vehicle non-exhaust emissions (*e.g.*, tire/brake/surface road wear). For OC, non-fossil contributions were always larger than corresponding EC regardless of season, site and size fraction. A major fraction of both fossil and non-fossil OC was found in the fine fraction. However, this enrichment in fine particles was often less pronounced for non-fossil OC compared to fossil OC, implying that fossil OC (mainly vehicle emissions) is smaller than non-fossil OC (mainly biomass burning and/or biogenic emissions). The non-fossil OC in coarse particles is probably attributed to an important contributor from primary biogenic materials such as microorganisms, plant debris, and pollen.
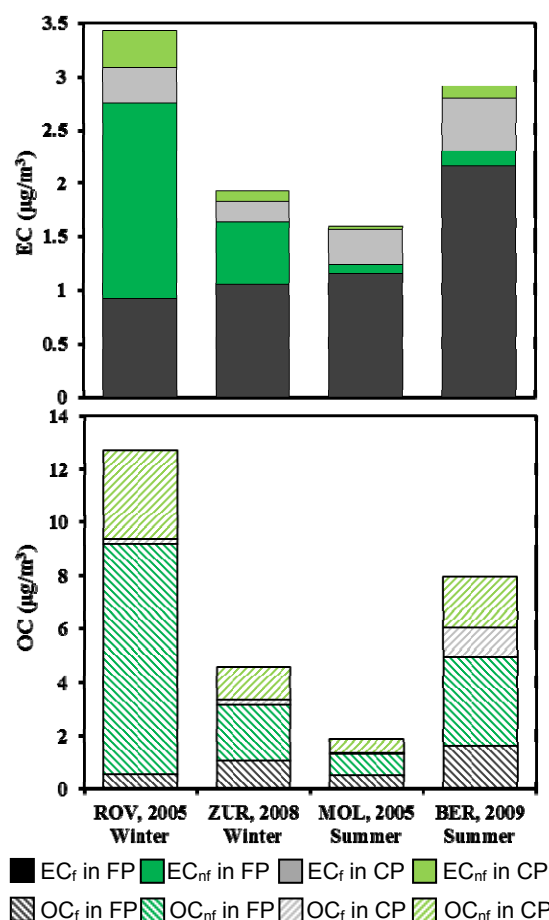
**Fig. 1:** Average concentrations of fossil (f) and non-fossil (nf) EC and OC in fine and coarse particles (FP and CP) for the four campaigns.

REFERENCES

[1] U Pöschl, Angew. Chem. Int. Edit., **44**, 7520 (2005).
[2] A. Nel, Science, **308**, 804 (2005).
[3] Y.L. Zhang et al., Atmos. Chem. Phys., **12**, 10841 (2012).
[4] L. Wacker et al., Nucl. Instrum. Meth. Phys. Res. B, **294**, 315 (2013).

FOSSIL AND BIOGENIC CO$_2$ FROM WASTE INCINERATION BASED ON A YEARLONG RADIOCARBON STUDY

J. Mohn, K. Zeyer, L. Emmenegger (EMPA Dübendorf), S. Szidat (Univ. Bern)

INTRODUCTION

Solid waste or solid recovered fuels (SRF) contain resources that can be recovered as material or energy. Although re-use and recycling should be favored as they lead to reduced energy use and less environmental impact, combustion of mixed or non-recyclable material streams in efficient waste-to-energy (WTE) plants is part of an integrated waste management system. As fossil CO$_2$ emissions are regarded as non-renewable, there is a growing interest in the determination of the share of biogenic and fossil carbon in SRF. The ^{14}C measurement of flue gas from WTE plants is a powerful method for the determination of the fossil fraction of the incinerated SRF [1]. We describe the first long-term implementation of the radiocarbon (^{14}C) method to study the share of biogenic and fossil (% Fos C) carbon in combustion CO$_2$ [2].

MATERIALS AND METHODS

At 5 Swiss WTE plants, 24 three-week measurement campaigns were performed over one year. ^{14}C was analyzed in temporally averaged bag samples by the accelerator mass spectrometer (AMS) MICADAS. The samples were introduced into the system as CO$_2$ using the direct gas inlet and a gas-capable ion source [3].

RESULTS AND DISCUSSION

Tab. 1: Share of fossil carbon in combustion CO$_2$ (%Fos C) with 95% confidence intervals [2].

WTE plant	Sampling interval	%Fos C
WTE A	13th Sep–4th Oct 2010	47.8 ± 4.2
	15th Nov–6th Dec 2010	46.0 ± 4.1
	10th Jan–31st Jan 2011	44.4 ± 4.2
	22nd Mar–12th Apr 2011	48.9 ± 4.1
	10th May–31st May 2011	50.1 ± 4.5
	19th Jul–8th Aug 2011[a]	49.0 ± 4.5
Mean value WTE A		47.7 ± 3.6[b]
WTE B	13th Sep–11th Oct 2011	44.0 ± 4.7
	15th Nov–6th Dec 2010	43.5 ± 4.3
	10th Jan–31st Jan 2011	43.1 ± 4.3
	15th Mar–5th Apr 2011	44.1 ± 4.4
	6th Jun–4th Jul 2011 [c]	42.3 ± 5.0
	11th Jul–2nd Aug 2011	43.2 ± 4.9
Mean value WTE B		43.4 ± 3.9[b]
WTE C	4th Oct–11th Oct 2010[d]	51.4 ± 3.7
	15th Nov–6th Dec 2010	49.6 ± 3.8
	10th Jan–31st Jan 2011	51.8 ± 3.6
	15th Mar–5th Apr 2011	50.0 ± 3.9
	10th May–31st May 2011	51.7 ± 3.9
	12th Jul–2nd Aug 2011	49.3 ± 4.3
Mean value WTE C		50.6 ± 3.4[b]
WTE D	19th Oct–2nd Nov 2010[a]	54.5 ± 3.7
	8th Feb–1st Mar 2011	54.8 ± 3.6
	15th Jun–6th Jul 2011	54.0 ± 4.3
Mean value WTE D		54.5 ± 3.1[b]
WTE E	18th Oct–8th Nov 2010	44.9 ± 4.4
	8th Feb–15th Feb 2011[d]	46.8 ± 4.0
	27th Jun–18th Jul 2011	45.9 ± 4.5
Mean value WTE E		45.9 ± 3.7[b]

a, c, d Duration of sampling: 2, 4, 1 weeks, respectively.
b The uncertainty of the ^{14}C reference value for pure biogenic emissions ($f_{M,bio}$ = 1.113 ± 0.038) is given as a measure for the uncertainty of the plant mean value, as it exceeds the standard error of the mean for the individual WTEs.

Significant differences between the plants were observed in the share of fossil CO$_2$. Based on our dataset, an average of 48 ± 4% Fos C was determined for waste incineration in Switzerland. This is distinctly higher than the 40% Fos C, currently employed in the Swiss greenhouse gas inventory.

No clear annual trend was observed for four of the monitored incinerators, with fluctuations within the uncertainty of the analytical results (Tab. 1). One incinerator, however, shows considerable variations in the share of fossil and biogenic CO$_2$, which are likely due to the storage of waste with high biogenic carbon that is incinerated during winter to increase the plant's heat production. Significant and persistent differences in %Fos C throughout the year between the plants are consistent with the waste composition of the respective WTE incinerators (Fig. 1).
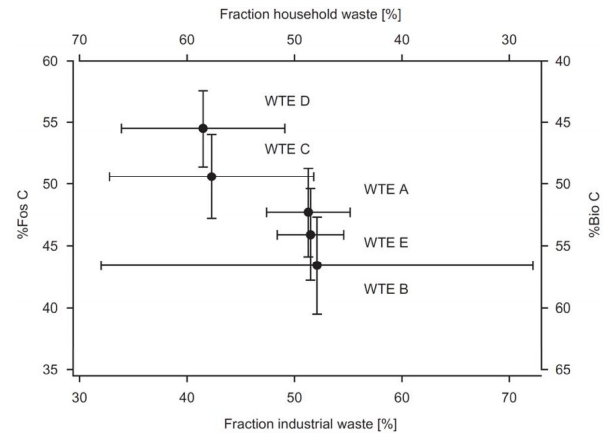
**Fig. 1:** Schematic drawing of the field setup for exhaust gas sampling. Particle-free and dehumidified exhaust gas is sampled at approx. 3 sccm in an aluminum-lined gas bag.

ACKNOWLEDGEMENTS

REFERENCES

[1] J. Mohn et al., Bioresour. Technol., **99**, 6471-6479 (2008).

[2] J. Mohn et al., Waste Manage., **32**, 1516-1520, doi:10.1016/j.wasman.2012.04.002 (2012).

[3] M. Ruff et al., Radiocarbon, **49**, 307-314 (2007).

IMPROVEMENT OF THE LOW-LEVEL γ-SPECTROMETER AT UNIVERSITY BERN

S. Szidat (Univ. Bern), R. Dressler (PSI)

MOTIVATION

Naturally occurring and man-made radionuclides in the environment can be used for dating of paleoscientific archives such as sediments, ice cores and speleothems. For the dating of limnic sediments, γ-spectrometry is a powerful tool, which allows non-destructive analysis of radionuclides such as ^{210}Pb, ^{137}Cs, ^{7}Be, and ^{241}Am [1]. For the determination of activities in the upper to medium mBq range within gram amounts of sample material, however, low-level γ-spectrometer setups are required with high detection efficiency and effective background suppression.

ORIGINAL INSTRUMENTATION

The original setup was performed in 2009. A specially designed Broad Energy Germanium (BEGe) detector from Canberra GmbH (Rüsselsheim, Germany) was used. This system is composed of a high-purity germanium crystal of 50 cm^2 area and 30 mm thickness with a 0.6 mm thick carbon epoxy window. This setup offers γ-measurements from <10 keV to >2000 keV with high absolute full-energy peak efficiencies for close on-top geometries of >20% and ~5% for ^{210}Pb (46.5 keV) and ^{137}Cs (662 keV), respectively. The detector was characterized by the supplier using a series of grid measurements taken into account the individual dimensions and positions of the crystal inside the detector end-cup. Based on these γ-measurements a dedicated Monte-Carlo code was made to calculate certified full-peak efficiencies with less than 5% uncertainty for on axis geometries using the so-called ISOCS/LabSOCS [2] algorithm.

For the realization of a low background count rate, the following measures were adopted [3]:

- Application of low-background materials for detector head, detector holder and internal hardware
- The remote detector chamber construction separates the pre-amplifier from the Ge-crystal and offsets the cryostat from the dip-stick axis to minimize unwanted radiation from below
- Installation in lowest/third underground floor (~10 meters of water-equivalent overburden)
- Passive shielding (outside to inside): 10 cm low-background lead, 3 mm ancient lead with negligible ^{210}Pb content, 2 mm cadmium
- Flushing of shield interior with N_2 from liquid nitrogen supply for expulsion of radon and daughter nuclides from laboratory air

ACTIVE ANTICOSMIC SHIELD

In 2012, an active anti-cosmic shield was installed to further reduce the background count rate of the system. Two plastic scintillator panels of totally 1 m^2 area where mounted directly above the passive shielding, i.e. ~20 cm above the top of the detector crystal subtending a zenith angle down to approximately 45° from the vertical axis. The analog signals from the two photo-multiplier tubes of the scintillator panels were added, shaped, and discriminated providing a logic veto signal to gate the analog-to-digital converter. The width of the gate signal is set to 11 µs with an additional signal delay of 15 µs between scintillator and discriminator. This optimized settings increased the dead time only slightly to 0.4%.

The integrated background for the energy range of 30 keV – 1800 keV was reduced from 0.58 s^{-1} without the active anti-cosmic shield to 0.20 s^{-1}. If normalized to 100 cm^3 Ge volume, the integrated background count rate of the improved system amounts 0.13 s^{-1}, which is comparable to similar setups directly at or slightly below ground level [4]. The obtained detection limits for ^{210}Pb and ^{137}Cs are 0.5 mBq and 4 mBq, respectively. With this setup, dating of sediments with γ-spectrometry is feasible with high reliability (Fig. 1).
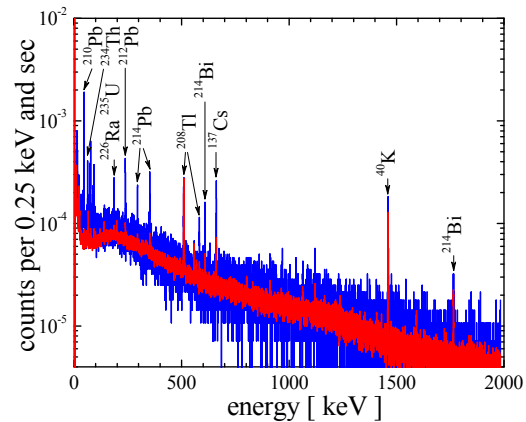
Fig. 1: γ-spectrum of a sediment sample (blue line; total mass 4.5 g, 72 h measurement period) and background spectrum (red line, 1000 h measurement period) recorded with active anti-cosmic shield.

REFERENCES

[1] P. G. Appelby, The Holocene, **18**, 83 (2008).
[2] Bronson, F.L., and Wang, L., Proc. Int. Conf. WM '96, February 25-29, 1996, Tucson, AZ.
[3] P. P. Povinec et al., Radioact. Environ., **11**, 163 (2008).
[4] T. M. Semkow et al., Appl. Radiat. Isotopes, **57**, 213 (2002).

LIST OF PUBLICATIONS

HEAVY ELEMENTS

J. Even, A. Yakushev, C. E. Düllmann, J. Dvorak, R. Eichler, O. Gothe, D. Hild, E. Jäger, J. Khuyagbaatar, J. V. Kratz, J. Krier, L. Niewisch, H. Nitsche, I. Pysmenetska, M. Schädel, B. Schausten, A. Türler, N. Wiehl, D. Wittwer
Rapid synthesis of radioactive transition-metal carbonyl complexes at ambient conditions
Inorg. Chem. **51** (12): 6431-6433, doi: 10.1021/ic300305m (2012).

J. Khuyagbaatar, D. Ackermann, L. L. Andersson, J. Ballof, W. Brüchle, C. E. Düllmann, J. Dvorak, K. Eberhardt, J. Even, A. Gorshkov, R. Graeger, F. P. Heßberger, D. Hild, R. Hoischen, E. Jäger, B. Kindler, J. V. Kratz, S. Lahiri, B. Lommel, M. Maiti, E. Merchan, D. Rudolph, M. Schädel, H. Schaffner, B. Schausten, E. Schimpf, A. Semchenkov, A. Serov, A. Türler, A. Yakushev
Study of the average charge states of ^{188}Pb and $^{252,254}No$ ions at the gas-filled separator TASCA
Nucl. Instrum. Methods Phys. Res., Sect. A **689**: 40-46, doi: 10.1016/j.nima.2012.06.007 (2012).

W. Maneschg, L. Baudis, R. Dressler, K. Eberhardt, R. Eichler, H. Keller, R. Lackner, B. Praast, R. Santorelli, J. Schreiner, M. Tarka, B. Wiegel, A. Zimbal
Production and characterization of a custom-made ^{228}Th source with reduced neutron source strength for the Borexino experiment
Nucl. Instrum. Methods Phys. Res., Sect. A **680**: 161-167, doi: 10.1016/j.nima.2012.04.019 (2012).

I. Usoltsev, R. Eichler, R. Dressler, D. Piguet, D. Wittwer, A. Türler, R. Brütsch, E. A. Olsen, J. P. Omtvedt, A. Semchenkov
Preparation of Pd-based intermetallic targets for high intensity irradiations
Nucl. Instrum. Methods Phys. Res., Sect. A **691**: 5-9, doi: 10.1016/j.nima.2012.06.060 (2012).

J. Lachner, I. Dillmann, T. Faestermann, H. Korschinek, M. Poutivtsev, G. Rugel, Ch. Lierse von Gostomski, A. Türler, U. Gerstmann
Attempt to detect primordial ^{244}Pu on Earth
Phys. Rev. C **85** (1): 015801, doi: 10.1103/PhysRevC.85.015801 (2012).

A. Türler
Nuclear structure and reaction studies near doubly magic ^{270}Hs
Radiochim. Acta **100** (2): 75-83, doi: 10.1524/ract.2011.1874 (2012).

M. Lezius, K. Predehl, W. Stöwer, A. Türler, M. Greiter, Ch. Hoeschen, P. Thirolf, W. Assmann, D. Habs, A. Prokofiev, C. Ekström, T.W. Hänsch, R. Holzwarth
Radiation Induced Absorption in Rare Earth Doped Optical Fibers
IEEE T. Nucl. Sci. **59** (2): 425-433, doi: 10.1109/TNS.2011.2178862 (2012).

SURFACE CHEMISTRY

T. Bartels-Rausch, V. Bergeron, J. H. E. Cartwright, R. Escribano, J. L. Finney, H. Grothe, P. J. Gutiérrez, J. Haapala, W. F. Kuhs, J. B. C. Pettersson, S. D. Price, C. I. Sainz-Díaz, D. J. Stokes, G. Strazzulla, E. S. Thomson, H. Trinks, N. Uras-Aytemiz
Ice structures, patterns, and processes: A view across the icefields
Rev. Mod. Phys. **84** (2): 885-944, doi: 10.1103/RevModPhys.84.885 (2012).

T. Bartels-Rausch, M. Schneebeli
Comment on 'possible contribution of triboelectricity to snow–air interactions'
Environ. Chem. **9** (2): 119-120, doi: 10.1071/EN11147 (2012).

M. A. Brown, F. Vila, M. Sterrer, S. Thurmer, B. Winter, M. Ammann, J. J. Rehr, J. A. van Bokhoven
Electronic structures of formic acid (HCOOH) and formate (HCOO$^-$) in aqueous solutions
J. Phys. Chem. Lett. **3** (13): 1754-1759, doi: 10.1021/Jz300510r (2012).

D. J. Donaldson, M. Ammann, T. Bartels-Rausch, U. Pöschl
Standard states and thermochemical kinetics in heterogeneous atmospheric chemistry
J. Phys. Chem. A **116** (24): 6312-6, doi: 10.1021/jp212015g (2012).

C. George, B. D'Anna, H. Herrmann, C. Weller, V. Vaida, D. J. Donaldson, T. Bartels-Rausch, M. Ammann
Emerging areas in atmospheric photochemistry, in *Topics in current chemistry: Atmospheric chemistry*
Ariya, P. A., (Editor), Springer: Berlin Heidelberg. in press, doi: 10.1007/128_2012_393 (2012).

A. Liati, P. Dimopoulos Eggenschwiler, D. Schreiber, V. Zelenay, M. Ammann
Variations in diesel soot reactivity along the exhaust after-treatment system, based on the morphology and nanostructure of primary soot particles
Combust. Flame in press, doi: 10.1016/j.combustflame.2012.10.024 (2012).

V. F. McNeill, A. M. Grannas, J. P. D. Abbatt, M. Ammann, P. Ariya, T. Bartels-Rausch, F. Domine, D. J. Donaldson, M. I. Guzman, D. Heger, T. F. Kahan, P. Klán, S. Masclin, C. Toubin, D. Voisin
Organics in environmental ices: Sources, chemistry, and impacts
Atmos. Chem. Phys. **12** (20): 9653-9678, doi: 10.5194/acp-12-9653-2012 (2012).

F. Riche, T. Bartels-Rausch, S. Schreiber, M. Ammann, M. Schneebeli
Temporal evolution of surface and grain boundary area in artificial ice beads and implications for snow chemistry
J. Glaciol. **58** (210): 815-817, doi: 10.3189/2012JoG12J058 (2012).

M. Shiraiwa, K. Selzle, H. Yang, Y. Sosedova, M. Ammann, U. Pöschl
Multiphase chemical kinetics of the nitration of aerosolized protein by ozone and nitrogen dioxide
Environ. Sci. Technol. **46** (12): 6672-80, doi: 10.1021/es300871b (2012).

T. Ulrich, M. Ammann, S. Leutwyler, T. Bartels-Rausch
The adsorption of peroxynitric acid on ice between 230 K and 253 K
Atmos. Chem. Phys. **12** (4): 1833-1845, doi: 10.5194/acp-12-1833-2012 (2012).

ANALYTICAL CHEMISTRY

S. Brönnimann, I. Mariani, M. Schwikowski, R. Auchmann, A. Eichler
Simulating the temperature and precipitation signal in an Alpine ice core
Clim. Past Discuss. **8** (6): 6111-6134, doi: 10.5194/cpd-8-6111-2012 (2012).

F. Cao, T.X. Liu, C.Y. Wu, F.B. Li, X.M. Li, H.Y. Yu, M.J. Chen
Enhanced biotransformation of DDTs by an iron- and humic-reducing bacteria Aeromonas hydrophila HS01 upon addition of goethite and AQDS
J. Agric. Food Chem. **60** (45): 11238-44, doi: 10.1021/jf303610w (2012).

A. Eichler, L. Tobler, S. Eyrikh, G. Gramlich, N. Malygina, T. Papina, M. Schwikowski
Three centuries of Eastern European and Altai lead emissions recorded in a Belukha ice core
Environ. Sci. Technol. **46** (8): 4323-4330, doi: 10.1021/es2039954 (2012).

I. Mariani, A. Eichler, S. Brönnimann, R. Auchmann, T. M. Jenk, M. C. Leuenberger, M. Schwikowski
Temperature and precipitation signal in two Alpine ice cores over the period 1961- 2001
Clim. Past Discuss. **8** (6): 5867-5891, doi: 10.5194/cpd-8-5867-2012 (2012).

M. Schwikowski, M. Schläppi, P. Santibañez, A. Rivera, G. Casassa
Net accumulation rates derived from ice core stable isotope records of pío XI glacier, southern Patagonia icefield
The Cryosphere Discuss. **6** (6): 5291-5316, doi: 10.5194/tcd-6-5291-2012 (2012).

I. G. M. Wientjes, R. S. W. Van De Wal, M. Schwikowski, A. Zapf, S. Fahrni, L. Wacker
Carbonaceous particles reveal that late Holocene dust causes the dark region in the western ablation zone of the Greenland ice sheet
J. Glaciol. **58** (210): 787-794, doi: 10.3189/2012JoG11J165 (2012).

RADWASTE ANALYTICS

A. Wallner, M. Bichler, K. Buczak, D. Fink, O. Forstner, R. Golser, M. A. C. Hotchkis, A. Klix, A. Krasa, W. Kutschera, C. Lederer, A. Plompen, A. Priller, D. Schumann, V. Semkova, P. Steier
High-sensitivity isobar-free AMS measurements and reference materials for ^{55}Fe, ^{68}Ge and ^{202g}Pb
Nucl. Instrum. Methods Phys. Res., Sect. B **294**: 374-381, doi: 10.1016/j.nimb.2012.03.029 (2013).

Y. Dai, W. Gao, T. Zhang, E. Platacis, S. Heinitz, K. Thomsen
A comparative study on the compatibility of liquid lead–gold eutectic and liquid lead–bismuth eutectic with T91 and SS 316LN steels
J. Nucl. Mater. **431** (1–3): 113-119, doi: 10.1016/j.jnucmat.2012.04.015 (2012).

R. Dressler, M. Ayranov, D. Bemmerer, M. Bunka, Y. Dai, C. Lederer, J. Fallis, A. S. Murphy, M. Pignatari, D. Schumann, T. Stora, T. Stowasser, F. K. Thielemann, P. J. Woods
^{44}Ti, ^{26}Al and ^{53}Mn samples for nuclear astrophysics: The needs, the possibilities and the sources
J. Phys. G: Nucl. Part. Phys. **39** (10): 105201, doi: 10.1088/0954-3899/39/10/105201 (2012).

N. Kivel, D. Schumann, I. Günther-Leopold
Quantification of ^{60}Fe atoms by MC-ICP-MS fort he redetermination of the half-life
Anal. Bioanal. Chem. in press, doi: 10.1007/s00216-012-6587-1 (2012).

J. Neuhausen, D. Schumann, R. Dressler, B. Eichler, S. Horn, T. Stora, M. Eller
Radiochemical aspects of liquid mercury spallation targets
J. Nucl. Mater. **431**: 224-234, doi: 10.1016/j.jnucmat.2011.11.019 (2012).

E. Noah, V. Boutellier, R. Brütsch, R. Catherall, D. Gavillet, J. Krbanjevic, H. P. Linder, M. Martin, J. Neuhausen, D. Schumann, T. Stora, L. Zanini
Post-irradiation analysis of the tantalum container of an ISOLDE LBE target
J. Nucl. Mater. **431**: 60-65, doi: 10.1016/j.jnucmat.2011.11.034 (2012).

D. Schumann, D. Kiselev, S. Teichmann, H.-A. Synal, P. Kubik
Radiochemical analysis of concrete samples from accelerator waste
Radiochim. Acta **100** (11): 851-856, doi: 10.1524/ract.2012.1976 (2012).

RADIONUCLIDE DEVELOPMENT – CHEMISTRY

J.C. Müller, K. Zhernosekov, U. Köster, K. Johnston, H. Dorrer, A. Hohn, N. T. van der Walt, A. Türler, R. Schibli
A unique matched quadruplet of terbium radioisotopes for PET and SPECT and for α- and β−-radionuclide therapy: An in vivo proof-of-concept study with a new receptor-targeted folate derivative
J. Nucl. Med. **53** (12): 1951-1959, doi: 10.2967/jnumed.112.107540 (2012).

ENVIRONMENTAL RADIONUCLIDES UNIVERSITÄT BERN

S. M. Fahrni, L. Wacker, H. A. Synal, S. Szidat
Improving a gas ion source for ^{14}C AMS
Nucl. Instrum. Methods Phys. Res., Sect. B **294**: 320-327, doi: 10.1016/j.nimb.2012.03.037 (2013).

L. Wacker, S. M. Fahrni, I. Hajdas, M. Molnar, H. A. Synal, S. Szidat, Y. L. Zhang
A versatile gas interface for routine radiocarbon analysis with a gas ion source
Nucl. Instrum. Methods Phys. Res., Sect. B **294**: 15-319, doi: 10.1016/j.nimb.2012.02.009 (2013).

R. Bahreini, A. M. Middlebrook, J. A. de Gouw, C. Warneke, M. Trainer, C. A. Brock, H. Stark, S. S. Brown, W. P. Dube, J. B. Gilman, K. Hall, J. S. Holloway, W. C. Kuster, A. E. Perring, A. S. H. Prevot, J. P. Schwarz, J. R. Spackman, S. Szidat, N. L. Wagner, R. J. Weber, P. Zotter, D. D. Parrish
Gasoline emissions dominate over diesel in formation of secondary organic aerosol mass
Geophys. Res. Lett. **39** (6): L06805, doi: 10.1029/2011gl050718 (2012).

J. Mohn, S. Szidat, K. Zeyer, L. Emmenegger
Fossil and biogenic CO_2 from waste incineration based on a yearlong radiocarbon study
Waste Manage. (Oxford) **32** (8): 1516-1520, doi: 10.1016/j.wasman.2012.04.002 (2012).

Y. L. Zhang, N. Perron, V. G. Ciobanu, P. Zotter, M. C. Minguillón, L. Wacker, A. S. H. Prévôt, U. Baltensperger, S. Szidat
On the isolation of OC and EC and the optimal strategy of radiocarbon-based source apportionment of carbonaceous aerosols
Atmos. Chem. Phys. **12** (22): 10841-10856, doi: 10.5194/acp-12-10841-2012 (2012).

S. Farooq, S.A. Eqani, R.N. Malik, A. Katsoyiannis, G. Zhang, Y.L. Zhang, J. Li, X. Liu, K.C. Jones, Z.K. Shinwari
Occurrence, finger printing and ecological risk assessment of polycyclic aromatic hydrocarbons (PAHs) in the Chenab River, Pakistan
J. Environ. Monit., 13, 3207-3215 (2011).

J. Li, Q.L. Li, R. Gioia, Y.L. Zhang, G. Zhang, X.D. Li, B. Spiro, R.S. Bhatia, K.C. Jones
PBDEs in the atmosphere over the Asian marginal seas, and the Indian and Atlantic oceans.
Atmos Environ, 2011, 45(37): 6622-6628. DOI: 10.1016/j.atmosenv.2011.09.010.

S.F.L. Mertens, M. Gara, A.S. Sologubenko, J. Mayer, S. Szidat, K.W. Krämer, T. Jacob, D.J. Schiffrin, T. Wandlowski
Au@Hg nanoalloy formation through direct amalgamation: Structural, spectroscopic, and computational evidence for slow nanoscale diffusion
Adv. Funct. Mater. **21** (17): 3259-3267 (2011).

M.C. Minguillón, N. Perron, X. Querol, S. Szidat, S.M. Fahrni, A. Alastuey, J.L. Jimenez, C. Mohr, A.M. Ortega, D.A. Day, V.A. Lanz, L. Wacker, C. Reche, M. Cusack, F. Amato, G. Kiss, A. Hoffer, S. Decesari, F. Moretti, R. Hillamo, K. Teinilä, R. Seco, J. Peñuelas, A. Metzger, S. Schallhart, M. Müller, A. Hansel, J.F. Burkhart, U. Baltensperger, A.S.H. Prévôt
Fossil versus contemporary sources of fine elemental and organic carbonaceous particulate matter during the Daure campaign in northeast spain
Atmos. Chem. Phys. **11** (23): 12067-12084 (2011).

Y.L. Zhang, X.Q. Lee, F. Cao
Chemical characteristics and sources of organic acids in precipitation at a semi-urban site in Southwest China
Atmos. Environ. **45**, 413-419, doi:10.1016/j.atmosenv.2010.09.067 (2011).

Y.L. Zhang, X.Q. Lee, F. Cao, D.K. Huang
Seasonal variation and sources of low molecular weight organic acids in precipitation in the rural area of Anshun
Chinese Science Bulletin **56**, 1005-1010, doi:10.1007/s11434-011-4411-5 (2011).

PATENT

HEAVY ELEMENTS

C. Düllmann, J. Dvorak, M. Schädel, A. Türler, J. Even, J.V. Kratz, L.Niewisch, N. Wiehl, A. Yakushev
Providing metal elements in gaseous phase into carrier gas useful e.g. for scintigraphy, comprises combining carrier gas containing carbon monoxide and metal elements in reaction volume and synthesizing metal element-carbonyl-complexes
DE102011000908-A1 ; WO2012113877-A1 ; WO2012113877-A8 , 30.8.2012.

CONTRIBUTIONS TO CONFERENCES, WORKSHOPS AND SEMINARS

HEAVY ELEMENTS

R. Dressler. P. Rasmussen
pureCOLD fast electronics for β-α and α-α pile-up suppression
MARC IX: Ninth International Conference on Methods and Applications of Radioanalytical Chemistry
Kailua-Kona, USA, 25–30 March, 2012.

R. Dressler, P. Rasnussen
Fast β-α-pile-up suppression electronics for super heavy element identification
8th Nuclear Chemistry and Radiochemistry Conference (NRC-8), Como, Italy, 16-21 September, 2012.

R. Dressler, R. Eichler
Predicting the retention time of nuclear reaction products in the PSI recoil chamber using COMSOL®
Multiphysics Conference 2012, Milan, Italy, 10-12 October, 2012.

R. Eichler, F. Sh. Abdullin, N. V. Aksenov, Yu. V. Albin, G. A. Bozhikov, V. I. Chepigin, R. Dressler, S. N. Dmitriev, H. W. Gäggeler, V. A. Gorshkov, R. A. Henderson, M. G. Itkis, J. M. Kenneally, V. Ya. Lebedev, O. N. Malyshev, K. J. Moody, Yu. Ts. Oganessian, O. V. Petrushkin, A. N. Polyakov, D. Piguet, A. G. Popeko, P. Rasmussen, R. N. Sagaidak, A. Serov, I. V. Shirokovsky, D. A. Shaughnessy, A. M. Sukhov, P. Steinegger, M. A. Stoyer, N. J. Stoyer, A. I. Svirikhin, E.E. Tereshatov, Yu. S. Tsyganov, I. Usoltsev, V. K. Utyonkov, A. Voegele, G. K. Vostokin, M. Wegrzecki, P. A. Wilk, D. Wittwer, A. V. Yeremin
First foot prints of chemistry on the shore of the Island of Superheavy Elements
Nucleus-Nucleus Collision Conference 2012 (NN2012) San Antonio, TX, USA, 27 May – 01 June, 2012.

R. Eichler
The Observation of a volatile compound formation with bismuth and polonium during experiments with superheavy elements
8th Nuclear Chemistry and Radiochemistry Conference (NRC-8), Como, Italy, 16-21 September, 2012.

J. Even, A. Yakusehv, D. Wittwer, Ch. Düllmann, J. Dvorak, R. Eichler, O. Gothe, D. Hild, E. Jäger, J. Khuyagbaatar, J.V. Kratz, J. Krier, L. Niewisch, H. Nitsche, I. Pysmenetska, M. Schädel, B. Schausten, A. Türler, N. Wiehl
On the way to the synthesis of the first transactinide carbonyl complex
8th Nuclear Chemistry and Radiochemistry Conference (NRC-8), Como, Italy, 16-21 September, 2012.

H.W. Gäggeler, P. Schwerdtfeger
Heavy element properties
Nerd Club Wellington, Hotel Bristol, Wellington New Zealand, 13 February, 2012.

H.W. Gäggeler
Chemistry experiments with heaviest elements
Victoria University, Wellington, New Zealand, 17 February, 2012.

H.W. Gäggeler
Status and perspective of chemical studies of heaviest elements,
EXON 2012, Vladivostok, Russia, 30 September – 08 October 2012.

P. Steinegger, R. Dressler, R. Eichler, N. Hänni, A. Türler
Diamond detectors for transactinide chemistry
8th Nuclear Chemistry and Radiochemistry Conference (NRC-8), Como, Italy, 16-21 September, 2012.

A. Türler
Nuclear- and radiochemistry at PSI and Bern University
Universität Zürich, Switzerland, 09 March, 2012.

A. Türler
Radioaktivität: Fluch oder Segen?
Gesamtschule Lindenthal, Switzerland, 31 May, 2012.

A. Türler
Experimental chemical investigation of superheavy elements
VIII Tours Symposium on Nuclear Physics and Astrophysics, Lenzkirch-Saig, Germany, 02-07 September, 2012.

A. Türler
Experimental chemical investigation of superheavy elements
Tenth International Conference on Relativistic Effects In Heavy-Elements (REHE 2012), Corrientes, Argentina, 02-16 September, 2012.

A. Türler
Recent advances in superheavy element research
8th Nuclear Chemistry and Radiochemistry Conference (NRC-8), Como, Italy, 19 September, 2012.

A. Türler
Forschungsaktivitäten des Labors für Radio- und Umweltchemie
Seminar Fortbildung für Strahlenschutzsachverständige bzw. Strahlenschutzbeauftragte, Novarits, Basel, Switzerland, 15 October, 2012.

I. Usoltsev
Preparation and performance of Pd-based intermetallic ion beam targets
INTDS conference, Mainz, Germany, 19-24 August, 2012.

I. Usoltsev
Production of Pd-based intermetallic targets for high intensity irradiations
First-Year Graduate Symposium of the Department for Chemistry and Biochemistry University Bern, Switzerland, 12 September, 2012.

I. Usoltsev, R. Eichler, A. Türler
Pd-based intermetallic targets for high intensity irradiations
8th Nuclear Chemistry and Radiochemistry Conference (NRC-8), Como, Italy, 16-21 September, 2012.

I. Usoltsev
Application of Pd-based intermetallic targets and preparation of the Sg(CO)6 experiment at RIKEN (Japan)
Seminar of the Laboratory of Radiochemistry and Environmental Chemistry, Paul Scherrer Institut and University of Berne, Bern, Switzerland, 28 September, 2012.

D. Wittwer
Thermal release investigation of radioactive tracers from metal matrices II
Seminar of the Laboratory of Radiochemistry and Envrionmental Chemistry, Berne, Switzerland, 24 February, 2012.

D. Wittwer, R. Dressler,, R. Eichler, H. Gäggeler, J.P. Omtvedt, D. Piguet, A. Türler
On the fast release of tracer elements from metallic hosts – a step towards vacuum chromatography
8th Nuclear Chemistry and Radiochemistry Conference (NRC-8), Como, Italy, 16-21 September, 2012.

SURFACE CHEMISTRY

M. Ammann, S. Steimer, M. T. Lee, G. Grzinic, M. Shiraiwa, U. Pöschl, A. J. Huisman, U. K. Krieger, T. Peter, T. Berkemeier, T. Koop
Constraining kinetic parameters of gas particle interactions in the transition from liquid to solid
22nd International Symposium on Gas Kinetics, Boulder, USA, 18-22 June, 2012.

M. Ammann
Chemistry on aerosol particles and ice
4th EuCheMS Chemistry Congress, Prague, Czech Republic, 26-30 August, 2012.

M. Ammann
Adsorption of acetone on ice
Seminar of the Laboratory of Radiochemistry and Environmental Chemistry, Paul Scherrer Institute and University of Berne, Villigen, Switzerland, 30 November, 2012.

T. Bartels-Rausch, S. Wren, F. Riche, S. Schreiber, B. Pinzer, M. Kerbrat, T. Huthwelker, M. Schneebeli, M. Ammann
Adsorption of trace gases and their diffusion through surface snow
International Polar Year (IPY), Montreal, Canada, 22-27 April, 2012.

T. Bartels-Rausch, S. Schreiber, S. Wren, F. Riche, M. Schneebeli, M. Ammann
The microstructure and effective diffusion
12th IGAC Open Science Conference "Atmospheric Chemistry in the Anthropocene", Peking, China, 17-21 September, 2012.

E. Coz, S. Platt, I. El Haddad, J. G. Slovik, A. S. H. Prévôt, S. Steimer, G. Grzinic, M. Lampimäki, B. Artinano, M. Ammann
Aging fingerprints on the carbon functional groups in 2-stroke scooter exhaust particles with STXM/NEXAFS
European Aerosol Conference, Granada, Spain, 02-07 September, 2012.

G. Gržinić, M. Birrer, M. Ammann
N_2O_5 kinetics in the atmosphere: A lab study of uptake to aerosol particles at ambient conditions using the ^{13}N radioactive tracer
European Research Course on Atmospheres, Grenoble, France, 09 January - 10 February, 2012.

G. Gržinić, T. Bartels-Rausch, M. Birrer, M. Ammann
Towards an experiment to investigate N_2O_5 uptake to aerosol particles at ambient conditions using the radioactive tracer ^{13}N
European Geoscience Union General Assembly, Vienna, Austria, 22-27 April, 2012.

G. Gržinić
Kinetics of N_2O_5 interaction with aerosols
First-Year Graduate Symposium of the Department for Chemistry and Biochemistry University Bern, Switzerland,
12 September, 2012.

G. Gržinić
Using ^{13}N-labeled N_2O_5 in atmospheric chemistry research: An update
Seminar of the Laboratory of Radiochemistry and Environmental Chemistry, Paul Scherrer Institute and University of Berne,
Bern, Switzerland, 26 October, 2012.

S. Kato, A. Borgschulte, M. Bielmann, M. Ammann, A. Züttel
Interface reactions and stability of a hydride composite
International Symposium on Metal-Hydrogen Systems, Kyoto, Japan, 21-26 October, 2012.

M. Lampimäki
Electron spectroscopic studies on metal oxide surfaces: Influence of ozone and nitrogen oxides
Seminar of the Laboratory of Radiochemistry and Environmental Chemistry, Paul Scherrer Institute and University of Berne,
Villigen, Switzerland, 09 March, 2012.

M. Lampimäki, V. Zelenay, A. Křepelová, Z. Liu, R. Chang, H. Bluhm, M. Ammann
Ozone decomposition and nitrate formation on Fe- and Ti-oxide surfaces studied by ambient pressure XPS and NEXAFS
European Conference on Surface Science (ECOSS-29), Edinburgh, UK, 03-07 September, 2012.

M. Lampimäki, V. Zelenay, A. Křepelová, S. Schreiber, Z. Liu, R. Chang, H. Bluhm, M. Ammann
Electron spectroscopic studies on metal oxide surfaces: Effect of ozone, nitrogen oxides and UV-light
LIFE + PhotoPAQ, Photocatalysis: Science and Application for Urban Air Quality, Porticcio, France, 14-17 May 2012.

S. Steimer, E. Coz, G. Grzinic, A. Huisman, U. Krieger, M. Lampimäki, C. Marcolli, T. Peter, M. Ammann
Relating physical state and reactivity: Uptake of ozone on tannic and shikimic acid
European Reasearch School on Atmospheres, Grenoble, France, 09 January - 10 February, 2012.

S. Steimer
In situ oxidation of shikimic acid particles under humid conditions
SLS Symposium 'Dynamics', Villigen, Switzerland, 6 March, 2012.

S. Steimer, A. Huisman, U. Krieger, M. Lampimäki, C. Marcolli, T. Peter, M. Ammann
Relating physical state and reactivity: Humidity dependent ozone uptake on tannic and shikimic acid
European Geoscience Union General Assembly, Vienna, Austria, 22-27 April, 2012.

S. Steimer
Relating physical state and reactivity: Ozone uptake on tannic and shikimic acid
Seminar of the Laboratory of Radiochemistry and Environmental Chemistry, Paul Scherrer Institute and University of Berne, Bern, Switzerland, 04 May, 2012.

S. Steimer, M. Lampimäki, G. Grzinic, E. Coz, B. Watts, J. Raabe, M. Ammann
Processing of atmospheric particles caught in the act via STXM/NEXAFS
American Geophysical Union Fall Meeting, San Francisco, USA, 03-07 December, 2012.

T. Ulrich, T. Bartels-Rausch, M. Ammann, S. Leutwyler
A new reactor to investigate uptake of trace gases into grain boundaries of ice
Seminar of the Laboratory of Radiochemistry and Envrionmental Chemistry, Berne, Switzerland, 24 February, 2012.

T. Ulrich, S. Leutwyler, M. Ammann, M. Birrer, T. Bartels-Rausch
A new planar flow reactor for the investigation of uptake of trace gases into grain boundaries
European Geoscience Union General Assembly, Vienna, Austria, 07-12 April, 2012.

T. Ulrich, M. Ammann, S. Leutwyler, T. Bartels-Rausch
Loss processes of peroxynitric acid: Quantifying the adsorption to ice and snow
International Polar Year (IPY), Montreal, Canada, 22-27 April 2012.

ANALYTICAL CHEMISTRY

F. Cao
Source apportionment of carbonaceous particles in ice/firn cores by radiocarbon analysis
Seminar of the Laboratory of Radiochemistry and Environmental Chemistry, Paul Scherrer Institut and University of Berne, Bern, Switzerland, 25 May, 2012.

F. Cao, Y.L. Zhang, A. Zapf, S. Szidat, L. Wacker, M. Schwikowski
Microgram level radiocarbon (^{14}C) determination of carbonaceous particles in firn samples: towards pre-treatment and OC/EC separation
21st International Radiocarbon Conference, Paris, France, 09-13 July, 2012.

S. Crespo, L. Gomez, J. Aranibar, M. Schwikowski, J. Corvalan, F. Décima
Major ions and stable isotopes as indicators of snow, glacier, groundwater, and stream flow contributions to the Mendoza River basin, Central Andes of Argentina
II Reunión Argentina de Geoquímica de la Superficie, Bahía Blanca, Argentina, 23-27 April, 2012.

A. Eichler, W. Tinner, S. Brütsch, S. Olivier, T. Papina, M. Schwikowski
A 750 year ice-core record of Siberian forest fires
International Partnerships in Ice Core Sciences First Open Science Conference, Presqu'île de Giens, France, 01-05 October, 2012.

H.W. Gäggeler
Application of nuclear techniques for environmental sciences
Nanjing University, China, 28 September, 2012.

G. Gramlich
Trace-element records of an Illimani ice-core in context with two millenia of Bolivian history
Seminar of the Laboratory of Radiochemistry and Environmental Chemistry, Paul Scherrer Institut and University of Berne, Bern, Switzerland, 28 September, 2012.

M.H. Hermanson, P. Leonards, E. Isaksson, M. Schwikowski
Burdens and inputs of perflourinated compounds to the Lomonosovfonna Ice Core, Svalbard (2009)
6th SETAC World Congress/SETAC Europe 22nd Annual Meeting, Berlin, Germany, 20-24 May, 2012.

P.-A. Herren
Ice core based climate reconstruction of the Mongolian Altai
Seminar of the Laboratory of Radiochemistry and Environmental Chemistry, Paul Scherrer Institut and University of Berne, Villigen, Switzerland, 09 March, 2012.

P.-A. Herren, A. Eichler, H. Machguth, T. Papina, L. Tobler, A. Zapf, M. Schwikowski
Ice core based climate reconstruction of the Mongolian Altai
International Partnerships in Ice Core Sciences First Open Science Conference, Presqu'île de Giens, France, 1-5 October, 2012.

P.-A. Herren, A. Eichler, H. Machguth, T. Papina, L. Tobler, A. Zapf, M. Schwikowski
Complex age-depth relation in a mid-latitude glacier
10th Swiss Geoscience Meeting, Bern, Switzerland, 16-17 November, 2012.

T.M. Jenk, M. Rubino, D.M. Etheridge, M. Bigler, T. Blunier
Sources of excess CO_2 in Greenland ice cores
AGU Fall Meeting, San Francisco, USA, 03-07 December, 2012.

T. Kirchgeorg, A. Dreyer, J. Gabrieli, M. Sigl, M. Schwikowski, C.F. Boutron, A. Gambaro, C. Barbante, R. Ebinghaus
Emerging persistent organic pollutants in an Alpine ice core
European Research Course on Atmospheres – ERCA, Grenoble, France, 09 January - 10 February, 2012.

I. Mariani
Atmospheric imprint in two Alpine ice cores
Seminar of the Laboratory of Radiochemistry and Environmental Chemistry, Paul Scherrer Institut and University of Berne, Villigen, Switzerland, 09 March, 2012.

I. Mariani, R. Auchmann, S.Brönnimann, A. Eichler, M. Schwikowski
Precipitation and temperature signal in two Alpine ice cores
NCCR Summer School, Monte Verità, Switzerland, 09-14 September, 2012.

I. Mariani, A. Eichler, M. Schwikowski
Do Alpine ice cores record temperature and precipitation?
International Partnerships in Ice Core Sciences First Open Science Conference, Presqu'île de Giens, France, 01-05 October, 2012.

T. Papina, A. Eichler, P.-A. Herren, S. Eyrikh, N. Malygina, E. Mitrofanova, M. Schwikowski,
Biological species recorded in Belukha (Siberian Altai) and Tsambagarav (Mongolian Altai) ice cores
International Partnerships in Ice Core Sciences First Open Science Conference, Presqu'île de Giens, France, 01-05 October, 2012.

P. Pavlova, P. Schmid, C. Bogdal, M. Schwikowski
Accelerated release of POPs from Alpine glaciers
16th Alpine Glaciology Meeting, ETH Zürich, Switzerland, 02-03 February, 2012.

P. Pavlova, P. Schmid, C. Bogdal, M. Schwikowski
Tracing POPs in a temperate glacier
International Partnerships in Ice Core Sciences First Open Science Conference, Presqu'île de Giens, France, 01-05 October, 2012.

P. Pavlova, P. Schmid, C. Bogdal, M. Schwikowski
Tracing POPs in a temperate glacier
Seminar of the Laboratory of Radiochemistry and Environmental Chemistry, Paul Scherrer Institut and University of Berne, Villigen, Switzerland, 26 October, 2012.

P. Pavlova, P. Schmid, C. Bogdal, M. Schwikowski
Tracing POPs in a temperate glacier
Internal seminar of the Laboratory of Analytical Chemistry, EMPA, Dübdendorf, Switzerland, 06 November, 2012.

M. Rubino, D.M. Etheridge, C.M. Trudinger, C. Allison, M.O. Battle, M.L. Bender, R. Langenfelds, P. Steele, M. Curran, T. Blunier, T.M. Jenk, R. Francey
A revised atmospheric $\delta^{13}C$-CO_2 record covering the last 1000 years from Law Dome, Antarctica
AGU Fall Meeting, San Francisco, USA, 03-07 December, 2012.

J. Schindler, S. Szidat, M. Schwikowski
Radiocarbon microanalysis using dissolved organic carbon (DOC) for dating of glacier ice
Summer School on Radiocarbon in Ecology and Earth System Science, Max-Planck Institute for Biogeochemistry, Jena, Germany, 16-21 July, 2012.

M. Schwikowski, T. Papina
Temperature and drought reconstruction using Belukha ice core
2nd Pages Asia 2k workshop, Chiang Mai, Thailand, 09-11 January, 2012.

M. Schwikowski, I. Wendl, E. Isaksson
Recent pollution levels from Lomonosovfonna ice core
Svalbard, Svalbard Science Forum workshop No. 3 "Changes in snow/ice and pollutants and their effects on terrestrial ecosystems", Oslo, Norway, 13-16 February, 2012.

M. Schwikowski, M. Sigl, A. Eichler, I. Mariani
Mineral dust in ice cores as proxy for NAO and PDO variability
ESF Conference on Modes of Variability in the Climate System: Past-Present-Future, Obergurgl, Austria, 27 May - 01 June, 2012.

M. Schwikowski, A. Zapf, M. Sigl, S. Szidat
Reduced biogenic and fire emissions from the Amazon basin during the Little Ice Age
Paleofire Workshop, Ca' Foscari University of Venice, Italy, 21-23 June, 2012.

M. Schwikowski
Effects of impurities on glacier albedo and accelerated melt
ESF Exploratory Workshop on Geomicrobiology in glacial systems, Sogndal, Norway, 07-10 August, 2012.

M. Schwikowski, M Sigl, A. Eichler, I. Mariani, C. Boutron, J. Gabrieli, C. Barbante
Mineral dust in ice cores as proxy of drought conditions and atmospheric circulation
International Partnerships in Ice Core Sciences First Open Science Conference, Presqu'île de Giens, France, 01-05 October, 2012.

L. Tobler, A. Eichler, G. Gramlich, S. Eyrikh, N. Malygina, T. Papina, M. Schwikowski
Three centuries of Eastern European and Altai lead (Pb) emissions and its source apportionment from Belukha ice core
International Partnerships in Ice Core Sciences First Open Science Conference, Presqu'île de Giens, France, 01-05 October, 2012.

I. Wendl
Black Carbon in the Lomonosovfonna ice core
Seminar of the Laboratory of Radiochemistry and Environmental Chemistry, Paul Scherrer Institut and University of Berne, Bern, Switzerland, 28 September, 2012.

I. Wendl, A. Eichler, S. Brütsch, I. Budde, M. Laborde, M. Gysel, E. Isaksson, T. Martma, M. Schwikowski
The first Black Carbon record from a Svalbard ice core
International Partnerships in Ice Core Sciences First Open Science Conference, Presqu'île de Giens, France, 01-05 October, 2012.

A. Zapf
Radiocarbon dating of glacier ice
Seminar of the Laboratory of Radiochemistry and Environmental Chemistry, Paul Scherrer Institut and University of Berne, Bern, Switzerland, 04 May, 2012.

A. Zapf, A. Nesje, S. Szidat, L. Wacker, M. Schwikowski
^{14}C measurements of ice samples from "Juvfonne ice tunnel", Norway – a validation of a radiocarbon dating technique for glacier ice
21st International Radiocarbon Conference, Paris, France, 09-13 July, 2012.

A. Zapf, S. Szidat, L. Wacker, M. Schwikowski
Radiocarbon dating of ice cores
4th EuCheMS Chemistry Congress, Prague, Czech Republic, 26-30 August, 2012.

A. Zapf, S. Szidat, L. Wacker, M. Schwikowski
Radiocarbon dating of ice cores
International Partnerships in Ice Core Sciences First Open Science Conference, Presqu'île de Giens, France,
01-05 October, 2012.

RADWASTE ANALYTICS

B. Hammer, V. Boutellier, H.-P. Linder, N. Shcherbina, J. Neuhausen, D. Schumann, A. Türler, M. Wohlmuther
First results on radionuclide production and distribution in the MEGAPIE target
IWSMT-11, Gent, Belgium, 05-09 November, 2012.

B. Hammer, D. Schumann, J. Neuhausen,
Characterization of LBE samples from MEGAPIE
MEGAPIE PCG-PSC Meeting, Paul Scherrer Institute, Villigen, Switzerland, 22-23 February, 2012.

B. Hammer, D. Schumann, J. Neuhausen
Determination of long-lived radionuclides in an LBE target from ISOLDE
International Youth Nuclear Conference, Charlotte, USA, 05-11 August, 2012.

B. Hammer, D. Schumann,
Working with radiological samples
International Youth Nuclear Conference, Charlotte, USA, 05-11 August, 2012.

B. Hammer
Determination of long-lived radionuclides in an Lead-Bismuth Eutectic target
First-Year Graduate Symposium of the Department for Chemistry and Biochemistry University Bern, Switzerland,
12 September, 2012.

B. Hammer
Characterization of Lead-Bismuth Eutectic samples from MEGAPIE
Seminar of the Laboratory of Radiochemistry and Environmental Chemistry, Paul Scherrer Institute and University of Berne,
Villigen, Switzerland, 30 November, 2012.

T. Lorenz
Analytics and separation of long-lived radionuclides produced by proton irradiation in lead targets
Seminar of the Laboratory of Radiochemistry and Environmental Chemistry, Paul Scherrer Institute and University of Bern,
Villigen, Switzerland, 25 Mai, 2012.

T. Lorenz
Analytics and separation of long-lived radionuclides produced by proton irradiation in lead targets
First-Year Graduate Symposium of the Department for Chemistry and Biochemistry University Bern, Switzerland,
12 September, 2012.

T. Lorenz, D. Schumann, Y. Dai,
Analysis and separation of long-lived radionuclides produced by proton irradiation in lead targets
NuMat2012, Osaka, Japan, 22-25 October, 2012.

E. A. Maugeri, J. Neuhausen, R. Eichler, D. Piguet, D. Schumann
Thermochromatography study of volatile tellurium species in various gas atmospheres
EuCheMS International Conference on Nuclear and Radiochemistry (NRC-8), Como, Italy, 16-21 September, 2012.

E. A. Maugeri, J. Neuhausen, R. Eichler, D. Piguet, D. Schumann, T.M. Mendonça, T. Stora
Preliminary results on polonium gas phase transport and adsorption on quartz
11th International Workshop on Spallation Materials Technology, Ghent, Belgium, 05-09 November, 2012.

J. Neuhausen
Volatilization of radionuclides in HLM systems,
International Workshop on Innovative Nuclear Reactors Cooled by Heavy Liquid Metals: Status and Perspectives,
Pisa, Italy, 17-20 April, 2012.

J. Neuhausen, M. Rizzi, E. Maugeri
SEARCH WP6 Task6.1: Release, gas phase transport and capture studies of volatiles
SEARCH 1st semi-annual review meeting, Gothenburg, Sweden, 22-23 May, 2012.

J. Neuhausen
Radiochemical aspects of liquid metal spallation targets
Seminar, Center for Molecular Modeling, University of Gent Gent, Belgium, 09 November, 2012.

J. Neuhausen, M. Rizzi, E. Maugeri, R. Eichler
SEARCH WP6 Task6.1: Release, gas phase transport and capture studies of volatiles
SEARCH 2nd semi-annual review meeting, Sint-Genesius Rode, Rhode St-Genèse, Belgium, 20-21 November, 2012.

M. Rizzi
Saturation measurements for the determination of Henry constants of radionuclides over liquid metal solutions
Seminar of the Laboratory of Radiochemistry and Environmental Chemistry, Paul Scherrer Institut and University of Berne,
Bern, Switzerland, 04 May, 2012.

M. Rizzi, J. Neuhausen, R. Eichler, D. Schumann, A. Türler
Polonium evaporation studies from liquid lead-based alloys
8th Nuclear Chemistry and Radiochemistry Conference (NRC-8), Como, Italy, 16-21 September, 2012.

M. Rizzi, J. Neuhausen, R. Eichler, D. Piguet, D. Schumann, T. Stora, T. M. Mendonca, A. Türler
Polonium release from bismuth andlLead bismuth eutectic
IWSMT-11, Gent, Belgium, 05-09 November, 2012.

D. Schumann, M. Ayranov, T. Stowasser, M. Bunka, R. Dressler
Chemical separation of radionuclides from accelerator waste for nuclear astrophysics experiments
SESTEC-2012, Mumbai, India, 27 February – 01 March, 2012.

D. Schumann
Radioactive targets for nuclear astrophysics experiments
MARC IX, Kailua-Kona, USA, 25-30 March, 2012.

D. Schumann, T. Stowasser, R. Dressler, M. Ayranov
Exploitation of accelerator waste for the production of exotic radionuclides
8th Nuclear Chemistry and Radiochemistry Conference (NRC-8), Como, Italy, 16-21 September, 2012.

W. Wagner, M. Wohlmuther, U. Stuhr, V. Davidov, J. Repper, U. Filges, B. Blau, B. Lauss, L. Goeltl, M. Hildebrand,
K. Thomsen, B. Hammer, J. Neuhausen, D. Schumann
SINQ and UCN – two high-power spallation sources operating at PSI
ICANS XX, Bariloche, Argentina, 04-09March, 2012.

RADIONUCLIDE DEVELOPMENT

M. Bunka
Development of Sc-44 production for radiopharmaceutical applications
Seminar of the Laboratory of Radiochemistry and Environmental Chemistry, Paul Scherrer Institute and University of Bern,
Villigen, Switzerland, 25 May, 2012.

M. Bunka, K. Zhernosekov, C. Müller, A. Türler, R. Schibli
Development of ^{44}Sc production for radiopharmaceutical applications
8th Nuclear Chemistry and Radiochemistry Conference (NRC-8), Como, Italy, 16-21 September, 2012.

H. Dorrer, M. Béhé, K. Johnston, U. Köster, C. Müller, R. Schibli, A. Türler, K. Zhernosekov
Production of four terbium-radioisotopes for radiopharmaceutical applications
8th Nuclear Chemistry and Radiochemistry Conference (NRC-8), Como, Italy, 16-21 September, 2012.

H. Dorrer
Production of four terbium-radioisotopes for radiopharmaceutical applications
Seminar of the Laboratory of Radiochemistry and Environmental Chemistry, Paul Scherrer Institute and University of Bern, Villigen, Switzerland, 21 December, 2012.

ENVIRONMENTAL RADIONUCLIDES UNIVERSITÄT BERN

R. Bahreini, A.M. Middlebrook, J.A. de Gouw, C. Warneke, M. Trainer, C.A. Brock, H. Stark, S.S. Brown, W.P. Dube, J.B. Gilman, K. Hall, J.S. Holloway, W.C. Kuster, A.E. Perring, A.S.H. Prevot, J.P. Schwarz, J.R. Spackman, S. Szidat, N.L. Wagner, R.J. Weber, P. Zotter, D.D. Parrish
OrganicaAerosol formation and Processing in the Los Angeles Basin: Role of gasoline vs. diesel emissions
AAAR 31st Annual Conference, Minneapolis (MN), USA, 08-12 October, 2012.

U. Dusek, M. Monaco, S. Szidat, H. A. J. Meijer, J. van der Plicht, T. Röckmann
A yearly cycle of radiocarbon in organic and elemental carbon at a rural site in the Netherlands
21st Radiocarbon Conference, Paris, France, 09-13 July, 2012.

I. El Haddad, K. Dällenbach, P. Zotter, J. Slowik, V.G. Ciobanu, S. Szidat, U. Baltensperger, A. Prévôt
Off-line Organic aerosol analyses of filter samples usingaAerosol mass spectrometry
AAAR 31st Annual Conference, Minneapolis (MN), USA, 08-12 October, 2012.

J. Mohn, S. Szidat, K. Zeyer, L. Emmenegger
Fossil and biogenic CO_2 from waste incineration based on a yearlong radiocarbon study
21st Radiocarbon Conference, Paris, France, 09-13 July, 2012.

G. Salazar, T. Ognibene
Study of CO_2 absorption and negative ion formation during direct ionization of CO_2 with a Cs^+ beam
21st Radiocarbon Conference, Paris, France, 09-13 July, 2012.

G. Salazar
Different CO_2 traps for the MICADAS gas inlet system
Seminar Laboratory of Ion Beam Physics, ETH Hönggerberg, Zurich, Switzerland, 17 October, 2012.

D. Simpson, C. Alves, R. Bergström, K.E. Yttri, S. Szidat, S. Decesari, J. Genberg, S. Gilardoni, G. Kiss, E. Swietlicki, E. Vignati
Tracer-based source-apportionment from the EUCAARI project and comparison with the EMEP model
European Aerosol Conference, Granada, Spain, 02-07 September, 2012.

S. Szidat, Y.L. Zhang, P. Zotter, A.S.H. Prévôt, L. Wacker
Technical requirements for ^{14}C analysis of airborne particulate matter
DPG Frühjahrstagung, Stuttgart, Germany, 12-16 March, 2012.

S. Szidat
Source apportionment of carbonaceous aerosols using radiocarbon
Seminar State Key Lab Environmental Geochemistry, Institute of Geochemistry, Chinese Academy of Sciences, Guiyang, China, 21 March, 2012.

S. Szidat
^{14}C analysis of small samples: Technical realization and application to aerosol research
Seminar Climate and Environmental Physics, University of Bern, Bern, Switzerland, 21 May, 2012.

S. Szidat, G. Salazar, Y.L. Zhang, E. Vogel, M. Battaglia, L. Wacker, H.-A. Synal, A. Türler
A new radiocarbon AMS laboratory at the University of Bern
21st Radiocarbon Conference, Paris, France, 09-13 July, 2012.

S. Szidat, G. Bench, V. Bernardoni, G. Calzolai, M. Chiari, C. Czimczik, L. Derendorp, U. Dusek, K. Elder, M. Fedi, J. Genberg, Ö. Gustafsson, E. Kirillova, S. Nava, A.P. McNichol, N. Perron, G.M. Santos, K. Stenström, E. Swietlicki, M. Ushida, L. Wacker, Y.L. Zhang, A.S.H. Prévôt
Intercomparison of ^{14}C analysis of carbonaceous aerosols
21st Radiocarbon Conference, Paris, France, 09-13 July, 2012.

S. Szidat, Y.L. Zhang, V.G. Ciobanu, P. Zotter, N. Perron, M.C. Minguillón, L. Wacker, U. Baltensperger, A.S.H. Prévôt
Considering the different thermal behaviour of wood-burning and diesel emissions for ^{14}C-based source apportionment of elemental carbon
European Aerosol Conference, Granada, Spain, 02-07 September, 2012.

S. Szidat
The potential of radiocarbon analysis in environmental research
Departementsversammlung, Department of Chemistry and Biochemistry, University of Bern, Bern, Switzerland, 12 September, 2012.

S. Szidat
^{14}C analysis using a gas ion source: Technical realization and application to aerosol research
Seminar Centre for Dating and Diagnostics, University of Salento, Lecce, Italy, 13 September, 2012.

S. Szidat
^{14}C and biogeochemistry: Measurement techniques and applications
Seminar Centre of Ecology, Evolution and Biogeochemistry, EAWAG, Kastanienbaum, Switzerland, 22 October, 2012.

Y.L. Zhang
Source apportionment of organic carbon and elemental carbon in carbonaceous aerosols by ^{14}C analysis
Seminar Laboratory of Ion Beam Physics, ETH Zurich, Switzerland, 25 April, 2012.

Y.L. Zhang
On the isolation of OC and EC and the optimal strategy of radiocarbon-based source apportionment of carbonaceous aerosols
Seminar Laboratory of Atmospheric Chemistry, PSI, Switzerland, 18 June, 2012.

Y.L. Zhang, A.S.H. Prévôt, L. Wacker, S. Szidat
Radiocarbon determination of carbonaceous particles (organic carbon and elemental carbon) in precipitation
21st Radiocarbon Conference, Paris, France, 09-13 July, 2012.

Y.L. Zhang, P. Zotter, A.S.H. Prévôt, L. Wacker, S. Szidat
Radiocarbon determination of different carbon fractions in PM10 and PM1
21st Radiocarbon Conference, Paris, France, 09-13 July, 2012.

Y.L. Zhang, P. Zotter, V.G. Ciobanu, A.S.H. Prévôt, S. Szidat
Black carbon and organic carbon particulate matter in Switzerland: Wood burning or diesel emissions?
Annual meeting Oeschger Centre for Climate Change Research (OCCR) Working Group 3, Bern, Switzerland, 25 October, 2012.

Y.L. Zhang
^{14}C-based source apportionment of organic carbon and elemental carbon in aerosols and precipitation samples
Seminar of the Laboratory of Radiochemistry and Environmental Chemistry, Paul Scherrer Institute and University of Bern, Villigen, Switzerland, 21 December, 2012.

P. Zotter, A.S.H. Prévôt, I. El-Haddad, Y.L. Zhang, S. Szidat, L. Wacker, X. Zhang, Y.-H. Lin, P. Hayes, J.D. Surratt, J.L. Jimenez, R. Weber, U. Baltensperger
Diurnal cycle of fossil and non-fossil total carbon using ^{14}C analyses during CalNex
21st Radiocarbon Conference, Paris, France, 09-13 July, 2012.

P. Zotter, A.S.H. Prévôt, I. El-Haddad, Y.L. Zhang, S. Szidat, L. Wacker, X. Zhang, R. Bahreini, P. Hayes, J.L. Jimenez, R. Weber, U. Baltensperger
Diurnal cycle of fossil and non-fossil carbon using ^{14}C analyses during CalNex
European Aerosol Conference, Granada, Spain, 02-07 September, 2012.

PUBLIC RELATIONS AND OUTREACH ACTIVITIES

Analytical Chemistry

Women in Business
Frau Schwikowskis Gespür für Eis
February 2012

Blick
Bergführer von Lawine getötet
16 February 2012

Umwelttechnik Schweiz
Frau Schwikowskis Gespür für Eis
January/February 2012

ETHZ Biologiestudierende 4. und 6. Semester
Labor-Besuch "Analyse von Eisbohrkernen"
5 March 2012

Gymnasium Thun-Schadau, Schüler des Wahlpflichtfaches Klimawandel/Energiegewinnung
Labor-Besuch "Analyse von Eisbohrkernen"
21 March 2012

Media release Federal Department of Foreign Affairs, Presence Switzerland
Switzerland exports a piece of glacier to South Korea
22 March 2012

ATS Agence Télégraphique Suisse
La Suisse exporte un morceau de glacier en Corée du Sud
22 March 2012

ATS Agenzia Telegrafica Svizzera
Un pezzo di ghiacciaio svizzero in Corea del Sud
22 March 2012

Romandie News
La Suisse exporte un morceau du Mont Rose en Corée du Sud
22 March 2012

Romandie News
Un bout de glacier suisse en Corée du Sud
22 March 2012

RTS Radio Télévision Suisse
La Suisse exportera un morceau de glacier en Corée du Sud
22 March 2012

L'Agefi
Glacier suisse exporté en Corée du Sud
23 March 2012

Neue Luzerner Zeitung
Sarner exportieren Eis an die Expo in Korea
23 March 2012

Neue Nidwaldner Zeitung
Sarner exportieren Eis an die Expo in Korea
23 March 2012

Swissinfo
La Suisse exporte un morceau du Mont Rose en Corée du Sud
23 March 2012

LeMatinDimanche
La Corée accueillera un bout du Mont-Rose
1 April 2012

Tages-Anzeiger
Small Talk «Die Eisproben haben wir in ein Spital gebracht»
21 April 2012

Der Bund
Small Talk «Die Eisproben haben wir in ein Spital gebracht»
21 April 2012

Aqua & Gas
Ein Stück Schweizer Gletscher in Korea
4 May 2012

DRS 4 News
Weltausstellung in Südkorea
11 May 2012

Die Botschaft
Bleigehalt der Luft in Russland seit 1680 rekonstruiert
23 May 2012

SDA Schweizerische Depeschenagentur
Eiskern offenbart historischen Bleigehalt der Luft in Russland
23 May 2012

Aargauer Zeitung, Regio-Ausgabe
Bleigehalt der Luft seit 1680 rekonstruiert
24 May 2012

20 Minuten Zürich
Blei in der Luft rekonstruiert
25 May 2012

Basler Zeitung
Bleibenzin hat die Umwelt verschmutzt
16 September 2012

CHEMIEEXTRA
Bleigehalt der Luft in Russland seit 1860
September 2012

Geosciences ACTUEL
Sechs Tage bohren für tausendjähriges Eis
4/2012

Environmental Radionuclides Universität Bern

Eos, Transactions / American Geophysical Union (Vol. 93, No. 7)
R.H. Smittenberg, S.M. Bernasconi, S. Szidat: Pushing the size limits of radiocarbon analysis
14 February 2012

Jahrbuch des Archäologischen Dienstes des Kantons Bern 2012
A. Weigand, S. Klopf: Vier Methoden zur Messung von Chloriden bei der Natriumsulfitentsalzung im Vergleich
23 August 2012

American Geophysical Union
Gasoline worse than diesel when it comes to some types of air pollution
http://www.eurekalert.org/pub_releases/2012-03/agu-agw030212.php
02 March 2012

Institute of Geochemistry, Chinese Academy of Sciences
Dr. Soenke Szidat of the University of Bern visits IGCAS
http://english.gyig.cas.cn/ns/es/201203/t20120330_83337.html
30 March 2012

Science (Vol. 337, no. 6093, pp. 400-401)
Climate change: Using radiocarbon to go beyond good faith in measuring CO_2 emissions
http://www.sciencemag.org/content/337/6093/400.full
26 July 2012

Berner Zeitung BZ
Wo Bern in der Champions League spielt: Klimaforschung
http://www.bernerzeitung.ch/region/kanton-bern/Wo-Bern--in-der-Champions-League-spielt/story/15206031
13/14 October 2012

LECTURES AND COURSES

Prof. Dr. A. Türler
Universität Bern, FS2012
Bachelor
- Instrumentalanalytik II (with Dr. K. Krämer and Prof. M. Schwikowski) (3 ECTS)
- Allgemeine Chemie (Einführung Radioaktivität) (with Prof. R. Hähner and Prof. J. Hulliger) (4 ECTS)

Universität Bern, HS2012
Bachelor
- Physikalische Chemie IV (with Prof. T. Wandlowski) (3,75 ECTS)
- Praktikum Phys. Chemie II (with others) (4 ECTS)
- Biochemische Methoden I (with others) (3 ECTS)

Master
- Nuclear and Radiochemistry (with Dr. R. Eichler) (3 ECTS)
- Lab course: Nuclear and Radiochemistry at Bern, Basel, ETHZ and PSI (with others) (4 ECTS)
- Seminar Radio- und Umweltchemie in collaboration with Paul Scherrer Institut
  (organized by PD Dr. S. Szidat FS2012 / HS2012)

Prof. Dr. M. Schwikowski
Universität Bern, FS2012
Bachelor
- Instrumentalanalytik II (with Prof. A. Türler and Dr. K. Krämer) (3 ECTS)

Master
- Summer Course am Paul Scherrer Institut. 2months International Summer Student Programme
  (with Prof. A. Türler) (4 ECTS)

Dr. M. Ammann
ETH Zürich, FS2012
Bachelor
- Systempraktikum Atmosphäre und Klima, (7 ECTS)

Master
- Atmospheric Interface Chemistry (3ECTS)

Dr. T. Bartels-Rausch
Universität Bern, HS2012
Master
- Lab course: Nuclear and Radiochemistry at the PSI (with Prof. A. Türler and PD Dr. S. Szidat) (4 ECTS)
- PhD thesis committee Josué Bock, Contribution à l'élaboration d'un modèle d'évolution physico-chimique
  de la neige, University of Grenoble, 03. Mai 2012

Dr. R. Eichler
Universität Bern, HS2012
Master
- Nuclear and Radiochemistry (with Prof. A. Türler) (3 ECTS)

Universität Bern, HS2012
Bachelor
- Praktikum Phys. Chemie II (with Prof. A. Türler) (4 ECTS)

Master
- Lab course: Nuclear and Radiochemistry (with Prof. A. Türler and PD Dr. S. Szidat) (4 ECTS)

PD Dr. Sönke Szidat
FS2012 / HS2012
Seminar Radio- und Umweltchemie in collaboration with Paul Scherrer Institut

Universität Bern, FS2012
Bachelor
- Ergänzungen zur analytischen Chemie für Pharmaziestudierende (2 ECTS)

Universität Bern, HS2012
Bachelor
- Chemie für Studierende der Veterinärmedizin (with Prof. C. Leumann) (4.5 ECTS)
- Praktikum Physikalische Chemie II (with others) (4 ECTS)

Master
- Lab course: Nuclear and Radiochemistry (with Prof. A. Türler and Dr. R. Eichler) (4 ECTS)

MEMBERS OF SCIENTIFIC COMMITTEES
EXTERNAL ACTIVITIES

Dr. Markus Ammann
- Atmospheric Chemistry and Physics, member of editorial board
- IUPAC Task Group on Atmospheric Chemical Kinetic Data Evaluation, member
- PSI internal research commission (FoKo), member

Dr. Thorsten Bartels-Rausch
- Air-Ice Chemical Interactions (AICI), Member of Steering Committee

Dr. Robert Eichler
- PSI internal research commission (FoKo), member
- Associate Editor of the International Journal of Modern Physics E (IJMPE)
  World Scientific Publishing

Dr. Dorothea Schumann
- Nuklearforum Schweiz, member
- Schweizerische Gesellschaft der Kernfachleute, member
- PSI internal Neutron Source Development Group, member

Prof. Dr. Margit Schwikowski
- ERC Starting Grant evaluation panel, member
- Schweizerische Gesellschaft für Schnee, Eis und Permafrost (SEP), vice president
- Council of the International Glaciological Society, elective member
- Oeschger Centre for Climate Change Research (OCCR), member
- Member of PhD thesis committee Christo Buizert, The influence of firn air transport processes and
  radiocarbon production on gas records from polar firn and ice, University of Copenhagen, 23 March 2012

PD Dr. Sönke Szidat
- Oeschger Centre for Climate Change Research (OCCR), member
- Bernese Chemical Society (Berner Chemische Gesellschaft, BCG), treasurer

Prof. Dr. Andreas Türler
- Eidgenössische Kommission für Strahlenschutz und Überwachung der Radioaktivität (KSR), Vizepräsident
- Gesellschaft Deutscher Chemiker (GDCh), Fachgruppe Nuklearchemie, Vorstands-Beirat
- Radiochimica Acta, member of the advisory board
- Oeschger Centre for Climate Change Research (OCCR), Mitglied des Wissenschaftlichen Ausschusses
- Nuklearforum Schweiz, Mitglied des Vorstandes

DOCTORAL THESIS

David Wittwer

Thermal release of volatile elements from solid catcher materials for future vacuum adsorption chromatography of superheavy elements

Prof. Dr. H. W. Gäggeler / PSI & Uni Bern
Dr. R. Eichler/ PSI
September 2012

Fang Cao

Biochemical mechanisms and kinetics of reductive transformation of DDTs driven by Fe(III)-reducing bacteria together with iron species and humic substances

Prof. Fangbai Li / Guangdong institute of eco-environment and soil science, China
Prof. Dr. M. Schwikowski / PSI & Uni Bern
December 2012

MASTER THESIS

Matthias Vonwiller

Isolation and ^{14}C analysis of atmospheric humic-like substances (HULIS)

PD Dr. S. Szidat / Uni Bern
November 2012

BACHELOR THESIS

Sharmila Selvanayakam

*Source apportionment of carbonaceous aerosols from Austria and Slovenia for winter 2011
with radiocarbon (^{14}C) analysis*

PD Dr. S. Szidat / Uni Bern
May 2012

Ivo Budde

Black Carbon concentration in the Lomonosovfonna ice core

Prof. Dr. M. Schwikowski / PSI
June 2012

Marianne Hädener

Development and evaluation of a ^{44}Ti/^{44}Sc radionuclide generator for the production of the potential PET nuclide ^{44}Sc

Prof. Dr. A. Türler / Uni Bern & PSI
June 2012

AWARDS

I. Usoltsev

Production of Pd-based intermetallic targets for high intensity irradiations
Best Presentation Award

First-Year Graduate Symposium of the Department for Chemistry and Biochemistry, University Bern, 12 September 2012

Prof. Dr. M. Schwikowski

Unsere 100 Meinungsmacherinnen

Aargauer Zeitung, 14 September 2012

M. Rizzi

Polonium evaporation studies from liquid lead-based alloys
Poster Award

Conference (NRC-8), Como, Italy, 20 September 2012

P. Steinegger

Diamond detectors for transactinide chemistry
Poster Award

Conference (NRC-8), Como, Italy, 20 September 2012

I. Usoltsev

Pd-based intermetallic targets for high intensity irradiations
Poster Award

Conference (NRC-8), Como, Italy, 20 September 2012

SUMMER STUDENTS

Sebastian Takyua Den
A new transpiration setup for measuring saturation vapor pressure of Bi
University of Berne
March - May 2012

Emilie Steimle
Kinetics and products of heterogeneous reaction of ozone with halogens in the presence of light
University of Orleans, France
April - July 2012

Egbewande Folake
Analysis of γ-spectra from lead-bismuth eutectic samples from MEGAPIE
University of Bern
July - September 2012

Pascal Sutter
3-wöchiges Berufspraktikum zur chemischen Analyse von Gletschereis
Kantonsschule Wettingen
February/March 2012

Michaela Schertler
Schnuppertag zur chemischen Analyse von Gletschereis
Bezirksschule Obersiggenthal
15 November 2012

VISITING GUESTS AT PSI 2012

22-25 February
31 May - 4 June
Esther Coz, CIEMAT Avda. Complutense, 40, 28040 Madrid, Spain
Collaborative scanning transmission x-ray microscopy experiments at SLS

23 February
Mikael Jensen, Risø National Laboratory for Sustainable Energy, Denmark
Mining radioisotopes from spallation targets – is it worth the trouble?

27 February - 2 March
Mads Faurschou Knudsen, Fadil Inceoglu, Aarhus University, Denmark
Reconstruction of solar variability during the Holocene based on the first high-resolution ^{10}Be record from a non-polar ice core

20-21 March
Leon P. Saris, University of Utrecht, Netherlands
Preparation of Fiescherhorn ice core samples for determination of organic substances with PTR-TOF-MS

21-22 March
Anton Wallner, ANSTO, Canberra, Australia
The re-measurement of the ^{60}Fe-half-life

1-4 April
Susan Kaspari, Central Washington University, Ellensburg, USA
Black Carbon determination in ice with the SP2

30 April - 4 May
Xinqing Lee and Hui Zhou, Institute of Geochemistry, Chinese Academy of Sciences, Guiyang, China
Decomposition rate of charcoal in the soil: An approach of ^{14}C dating combined with geochemical analysis
The role of the climate change in historical developments: how climate works to a peculiar Chinese civilization

25 May
Jörg Steinbach, Inst. Radiopharmacy, Helmholtz-Zentrum Dresden-Rossendorf, Germany
Developments to radioimmunotherapy in the context of radiopharmaceutical and oncological developments

29-30 May
Daniel Bemmerer, HZDR, Dresden-Rossendorf, Germany
Preparation of a ^{44}Ti-target

6-13 August
Michael Kerbrat, LGGE-Laboratoire de Glaciologie et Géophysique de l'Environnement, France
The interference of HNO_4 in HONO measurements with the LOPAP

6-17 August
Borja Gonzales, SCK-CEN Mol, Belgium
Evaporation of Po from liquid matal

12-24 August
James Andrew Menking, Central Washington University, Ellensburg, USA
Method development for determining Black Carbon in snow and ice with the SP2

17-20 August
Patrik Karlsson,Uppsala, Sweden
Site acceptance tests of the NAPP Photoelectron-Spectrometer Scienta Scientific Company

15 October - 25 November
Erik Thomson, University of Gothenburg, Sweden
Uptake of trace gases into grain boundaries of ice

26 October
Zsolt Revay, FRM II, TU München, Germany
Prompt gamma activation analysis with high-flux cold neutron beams

11 October
Tatyana Papina, IWEP, Barnaul
Weather type analysis for interpreting ice core parameters

19 November
Moshe Gai, Yail University, New Haven, USA
^{7}Be and the problem of primordial ^{7}Li

30 November
Thomas Koop, Universität Bielefeld, Germany
Amorphous semi-solid and solid states in organic aerosol particles

20-22 December
Aleksander Bilewicz, Institute of Nuclear Chemistry and Technology, Warsaw, Poland
Radionuclides and radiopharmaceuticals at Institute of Nuclear Chemistry and Technology (Warsaw)

OBITUARY

Dein Leben fand ein unerwartet schnelles Ende.
Doch die Spuren deines Lebens,
in Gedanken, Bildern und Augenblicken,
werden uns immer an dich erinnern.
Du wirst immer in unserer Mitte bleiben.

Immer noch unfassbar für uns müssen wir mit tiefer Traurigkeit von Alexander Zapf Abschied nehmen. Viel zu früh ist er am 19.1.2013 bei einer seiner geliebten Skitouren aus unserer Mitte gerissen worden. Alex war für uns in den letzten Jahren ein Freund, Mitarbeiter und Gefährte, der unsere Liebe und Begeisterung für Forschung, Gletscher und Berge geteilt hat. Für ihn waren die Berge Erfüllung, Ausgleich, Herausforderung und Ort für einzigartige Erlebnisse, von denen er mit leuchtenden Augen erzählte.

Wir werden seinen Humor, seine Hilfsbereitschaft, seine Begeisterungsfähigkeit und die bereichernden Gespräche mit ihm sehr vermissen.

Unser tiefes Mitgefühl gilt in dieser schweren Zeit seiner Familie.

PAUL SCHERRER INSTITUT

LABOR FÜR RADIO- UND UMWELTCHEMIE
DES PAUL SCHERRER INSTITUTS UND DER UNIVERSITÄT BERN

31.12.2012

UNIVERSITÄT BERN

Prof. Dr. Andreas Türler

PSI

Uni Bern

Angela Blattmann (Secretary / 80 %)
Prof. Dr. Margit Schwikowski (Deputy)

Franziska Bornhauser (Secretary / 20 %)
Brigitte Oggier (Secretary / 20 %)

SURFACE CHEMISTRY
Dr. Markus Ammann
Dr. Thorsten Bartels-Rausch
Dr. Markus Lampimäki
Dr. Shunsuke Kato
Mario Birrer
Thomas Ulrich [1]
Goran Grzinic [1]
Sarah Steiner [1]
Sepp Schreiber [1]
Ming-Tao Lee [1]

ANALYTICAL CHEMISTRY
Prof. Dr. Margit Schwikowski
Leonhard Tobler
Dr. Theo Jenk (80 %)
Dr. Anja Eichler (50 %)
Dr. Gabriela Gramlich (50 %)
Roman Bentz
Sabina Brütsch
Silvia Köchli
Pierre-Alain Herren
Isabella Mariani [1]
Isabel Wendl [1]
Alexander Zapf [1]
Fang Cao [1]
Pavlina Pavlova [1]
Zlatina Paneva [2]

HEAVY ELEMENTS
Dr. Robert Eichler
Dr. Rugard Dressler
Dr. David Wittwer
Dave Piguet
Alexander Vögele
Stefan Söllradl [1]
Patrick Steinegger [1]
Ilya Usoltsev [1]
Nadine Chiera [1]

RADWASTE ANALYTICS
Dr. Dorothea Schumann (90 %)
Dr. Jörg Neuhausen
Dr. Emilio Maugeri
Sabrina Lüthi
Tanja Stowasser (60 %)
Matthias Rizzi [1]
Bernadette Hammer [1]
Tobias Lorenz [1]

RADIONUCLIDE DEVELOPMENT
Prof. Dr. Andreas Türler a.i.
Holger Dorrer [1]
Maruta Bunka [1]

ENVIRONMENTAL RADIONUCLIDES
PD Dr. Sönke Szidat
Dr. Gary Salazar
Edith Vogel
Michael Battaglia
Yanlin Zhang [1]
Konstantinos Agrios [1]

RADIOPHARMACEUTICAL R&D
Dr. Josue Moreno
N. N.

[1] Graduate student
[2] Master

AUTHOR INDEX

AFFILIATION INDEX

CERN	European Organization for Nuclear Research, CERN CH-1211, Genève 23, Switzerland
CIEMAT	Avda. Complutense, 40, 28040 Madrid, Spain
DRI Reno	Division of Hydrologic Sciences, Desert Research Institute, Reno, Nevada, USA
CSIC	Institute of Environmental Assessment and Water Research, CSIC, Barcelona, Spain
EC	European Commission, SDME 2/2, B-1049 Brussels - Belgium
EMPA	Forschungsinstitution im ETH-Bereich, Überlandstrasse 129, CH-8600 Dübendorf, Switzerland
ENE	General Energy Research Department (ENE), Paul Scherrer Institut, CH-5232 Villigen PSI, Switzerland
ESF	European Science Foundation, 1, quai Lezay Marnésia, BP 90015, F-67080 Strasbourg Cedex, France
ETHZ	Eidgen. Technische Hochschule Zürich, CH-8092 Zürich, Switzerland
EU	European Union
FLNR Dubna	Flerov Laboratory of Nuclear Reactions, Joliot Curie 6, 141980 Dubna, Russia
FRM II	Forschungs-Neutronenquelle Heinz Maier-Leibnitz (FRM II), Lichtenbergstr. 1, 85748 Garching, Germany
GFA	Large Research Facilities (GFA), Paul Scherrer Institut, CH-5232 Villigen PSI, Switzerland
GIG CAS	Guangzhou Institute of Geochemistry, Chinese Academy of Sciences, 511 Kehua Street, Wushan, Tianhe District, Guangzhou, GD 510640, China
Goethe University	Goethe-Universität Frankfurt, Senckenberganlage 31, 60325 Frankfurt am Main, Germany
Hotlab	The Hot Laboratory Division (AHL) of the Nuclear Energy and Safety Department (NES) of the Paul Scherrer Institut (PSI), Switzerland
ILL	Institut Laue-Langevin, 6, Rue Jules Horowitz, BP 156 - 38042 Grenoble Cedex 9, France
IMP	Institute of Modern Physics, Chinese Academy of Sciences, Add: 509 Nanchang Rd., Lanzhou**,** 730000, China
INFN Bologna	National Institute of Nuclear Physics, Viale B. Pichat, 6/2, I-40127 Bologna, Italy
ITE	Instytut Technologii Elektronowej, Al. Lotników 32/46 02-668 Warszawa, Poland
ITG	Isotope Technologies Garching GmbH, Lichtenbergstrasse 1, D - 85748 Garching
IWEP	Institute for Water and Environmental Problems, Siberian Branch of the Russian Academy of Sciences, 105 Papanintsev Str., RU-Barnaul 656099, Russia
KUP	Climate and Environmental Physics, Physics Institute, University of Bern, Sidlerstrasse 5, CH-3012 Bern, Switzerland
LAC	Laboratory of Atmospheric Chemistry, Paul Scherrer Institut, CH-5232 Villigen PSI, Switzerland
LBNL	Lawrence Berkeley National Laboratory, Berkeley, CA 94720, USA
MPIC	Max-Planck-Institut für Chemie (Otto-Hahn-Institut), Joh.-Joachim-Becher-Weg 27, 55128 Mainz, Germany
NES	Nuclear Energy and Safety Research Department, Paul Scherrer Institut, CH-5232 Villigen PSI, Switzerland
NPI	Norwegian Polar Institute, N-9296 Tromsø, Norway
PSI	Paul Scherrer Institut, CH-232 Villigen PSI, Switzerland

PSI FoKo	Forschung Kommission, (Research Commission), Paul Scherrer Institut, CH-232 Villigen PSI, Switzerland
SCK CEN	Belgian Nuclear Research Centre, Boeretang 200, BE-2400 MOL, Belgium
SLF	Institut für Schnee- und Lawinenforschung, Flüelastr. 11, CH-7260 Davos, Switzerland
SLS	Swiss Light Source, Paul Scherrer Institut, CH-5232 Villigen PSI, Switzerland
SNF	Schweizerischer Nationalfonds SNF, Wildhainweg 3, CH-3001 Bern, Switzerland
SYN	Synchrotron Radiation and Nanotechnology Research Department (SYN), Paul Scherrer Institut, CH-5232 Villigen PSI, Switzerland
Univ. Bern	Departement für Chemie und Biochemie, Universität Bern, Freiestr. 3, CH-3012 Bern, Switzerland
Univ. Bremen	Universität Bremen, Bibliothekstraße 1, 28359 Bremen
Univ. D`Orlèans	Université d'Orléans, 6 Avenue du Parc Floral, 45100 Orléans, France
Univ. Gothenburg	University of Gothenburg, PO Box 100, SE-405 30 Gothenburg, Sweden
Univ. Tallinn	Institute of Geology, Tallinn University of Technology, 10143 Tallinn, Estonia
Univ. Zürich	University of Zurich, Winterthurerstr. 190, CH-8057 Zürich, Switzerland
ZRW	Center for Radiopharmaceutical Sciences, Paul Scherrer Institut, CH-5232 Villigen PSI, Switzerland